DEUTSCHES ELEKTRONEN – SYNCHROTRON DESY

DESY 88-093
July 1988

COHERENCE AND PHYSICS OF QCD JETS

by

Yu.L. Dokshitzer, V.A. Khoze, S.I. Troyan

Leningrad Nuclear Physics Institute, Gatchina, Leningrad

ISSN 0418-9833

NOTKESTRASSE 85 · 2 HAMBURG 52

To be sure that your preprints are promptly included in the
HIGH ENERGY PHYSICS INDEX,
send them to the following address (if possible by air mail):

DESY
Bibliothek
Notkestrasse 85
2 Hamburg 52
Germany

DESY 88-093
July 1988

ISSN 0418-9833

COHERENCE AND PHYSICS OF QCD JETS*)

Yu.L.Dokshitzer, V.A.Khoze,**) S.I.Troyan

Leningrad Nuclear Physics Institute

Gatchina, Leningrad 188350, USSR

This paper presents a review of analytical perturbative approach to QCD jet physics. The role of coherent phenomena reflecting the collective character of multiple hadroproduction is emphasized.

*) To be published in "Perturbative QCD"; A. Mueller, Editor; World Scientific, Singapore

**) presently at DESY

TABLE OF CONTENTS

1. INTRODUCTION

The aim of this paper is to review the perturbative approach to multiple hadroproduction which we consider to be an important tool for gaining information about the colour confinement. By the word 'confinement' we mean here not the formal proof of the desired property of gauge theory with unbroken non-Abelian symmetry, but the meaning of concrete knowledge about how the 'device' transforming colour fields into white hadrons operates in real processes.

1.1. Perturbative Approach to Hard Processes and Jets

Clearly it is the Hard Process (HP) to serve as the base for scrutinizing this know-how. Here one can unambiguously use the language of quarks and gluons to give a detailed description of the small-distance stage of the evolution by means of the Perturbation Theory (PT) [1-8].

Recent experiments [9-15] have presented the solid evidence for the jet structure of final states in HPs. These jets are now being intensively studied both at e^+e^- and hadronic machines. Hadronic jet physics will be one of the central problems of investigation for the e^+e^-, $p\bar{p}$ and ep colliders of the future.

Detailed studies of jets is of importance for better understanding and testing both PT and non-PT QCD, for designing experiments of the present and of the future, and for finding manifestations of new physics.

It would be impossible to be complete in covering the field, announced in the title, so we must apologize in advance for being selective in topics discussed and references cited.

One of the main objects of this paper was to give an introduction to the analytical PT approach which has not

been presented so far in English systematically [16-20].

1.2. Petrurbation Theory and Shower Picture

In current high energy accelerators a collision between two particles may typically lead to the production of ten to hundred offsprings. Exact calculations of QCD matrix elements for multipartonic systems are difficult to use even in the cases where they can be obtained. Therefore, one meets the problem of developing an appropriate PT technique to describe, at least approximately, the properties of such systems.

The desired PT approximation has to be:

1. complete in accounting for main physical ingredients (colour dynamics of parton multiplication processes, asymptotic freedom, energy-momentum conservation etc.),
2. asymptotically exact,
3. powerful in giving testable quantitative predictions with controllable accuracy,
4. physically transparent and
5. systematic in improving the accuracy.

The key idea is to invoke the parton shower picture [4,17,21-26] where one views the evolution, say, of a jet as a sequence of parton branchings. Generally speaking, using a shower picture does not necessarily lead to a loss of accuracy in describing multiparton phenomena. The main idea of the shower picture is to reorganize the perturbative expansion in such a way that its zero order approximation is systematic and involves an arbitrary number of produced particles. This zero order approximation can be achieved through an iteration of basic, $A \rightarrow B+C$, parton branchings. In principle, it should be possible to include higher correction to

the basic branching along with higher point branching vertices $A \to B+C+D...$ in order to systematically improve the accuracy of a calculation. This procedure [17] is closely related to a renormalization group approach [27] where the branchings are not so visible and where higher order corrections can be systematically calculated.

1.3. Leading Logs, Coherence and Hadronization Schemes

The above mentioned zero order approximation is the Modified Leading Logarithmic Approximation (MLLA) taking care of both double logarithmic (DL) and single logarithmic (SL) effects [17,28] which proves to be necessary to predict quantitatively properties of multiparticle systems with reasonable accuracy.

Constructing the MLLA we shall pay special attention to maintaining the probabilistic interpretation of jet evolution. An existence of such interpretation is far from trivial in the problems connected with description of soft particle distributions ($x \ll 1$). Here interference contributions play an important role and prove to be unavoidable, unlike the case of the familiar PT problems dealt with $x \sim 1$ particle spectra (deep inelastic scattering and e^+e^- annihilation structure functions, Drell-Yan and related semiinclusive processes, etc., see [1,5] and refs. therein) where it was the matter of skillful choice of a gauge to approve the straightforward probabilistic picture.

Nevertheless it appears to be possible, by choosing an appropriate evolution parameter (jet opening angle) and accounting for specific angular dependence of soft emission probabilities to maintain probabilistic interpretation of the dynamics of soft partonic cascades [24,25,17].

This not only helps one's physical intuition but provides the base for Monte Carlo simulations of jet physics.

The most elaborated MC schemes [29-35], basing on the concept of well-developed QCD cascade, becoming better and better at building in realistic fragmentation and proper QCD evolution, successfully describe the wealth of experimental data. It is important to notice, however, that the use of MC generators for describing the development of multipartonic systems in terms of classical Markov chains proves to be of limited value, in principal. For example, the collective QCD phenomena in multijet ensembles could be reproduced by MC simulations only in the large-N_c limit.

We shall focus specially on manifestations of coherent phenomena. The rediscovery of coherence in QCD context in early eighties [36,37] has led to dramatic revision of theoretical expectations about the structure of soft particle distributions [4-8].

Thus the coherent effects in the intrajet partonic cascades, resulting, on average, in the angular ordering of sequential branching, gave rise to the hump-backed plateau - one of the most striking PT QCD predictions [38-42,28].

Due to the interjet coherence, responsible for the drag effects in multijet events [43,7,8], the very important physical phenomenon can be said to be experimentally verified, namely the fact that it is the dynamics of the colour which governs the particle production in accordance with the QCD radiophysics of hadron flows.

Surely, tha main lesson of the observations is not the proof of coherence: it would be inexcusable to check quantum mechanics at modern accelerators. Of real importance is that the PT-coherence has revealed itself in

hadron spectra, i.e. confinement has not disturbed the PT -picture of particle generation. The fact that non-PT effects do not radically rearrange a parton system at the confinement stage provides evidence in favour of locality of parton blanching and hadronization processes in configuration space [44,16], thus, supporting the hypothesis of Local Parton-Hadron Duality (LPHD) [17,41].

The phenomenological fragmentation schemes reflect, one way or another, the coherent phenomena. Thus the cluster Webber-Marchesini model [29-31] naturally incorporates the angular ordering; the Lund string picture [45], on the other hand, appears to be suitable for a qualitative reproducing the drag phenomena. Moreover, in the modern versions of MC algorithms both types of QCD coherence might be built in [32]. Such schemes seem to be well suitable for reproducing the bulk of interference phenomena, excluding some subtle effects.

This paper is organized as follows.

In Sec. 2 we shall sketch the space-time picture of the partonic system evolution, the role of PT bremsstrahlung in the soft confinement scenario for foundation the concept of the Local Parton-Hadron Duality (LPHD).

In Sec. 3 the physical origin of QCD coherence phenomena are discussed. One can find here the qualitative guide to the Angular Ordering (AO) in both time-like and space-like partonic cascades, of the $q\bar{q}$/$q\bar{q}g$ drag effect.

In Sec. 4 we briefly discuss the main steps of the formal proof of AO in the Double Logarithmic Approximation (DLA) and present the most important DLA results.

In Sec. 5 the Modified Leading Logarithmic Approximation (MLLA) - asymptotically exact zero order approximation of PT, which corectly keeps leading and next to

leading logarithms, is constructed. Specially emphasized is the possibility to provide the probabilistic interpretation of the partonic system evolution in MLLA and the failure of a naive classical branching picture beyond the MLLA due to soft 'colour monster' contributions.

In Sec. 6 the MLLA evolution equations for generating functionals are used to predict the shape of inclusive energy spectra of particles and to calculate the corrections to asymptotic KNO multiplicity distributions.

In Sec. 7 we consider the gross features of the QCD event portrait, describe the angular collimation of energy and multiplicity flows with the increase of jet energy. The problem of experimental selection rules is also discussed here. It is pointed out that forcing each hard scattering event to correspond to a definite number of jets is seemingly not a good procedure. We emphasize the use of infrared stable criteria for jets and suggest that the purely inclusive determinations of jet characteristics are probably the best way to make sharp connections between theory and experiment.

In Sec. 8 the interference drag phenomena in the interjet soft particle distributions in $e^+e^- \to$ hadrons, high-$p_\perp$ $\gamma(Z,W,H,\ldots)$ and other jet production processes are studied. The azimuthal jet asymmetries prove to be of interest for checking subtle QCD effects.

In Sec. 9 we consider the manifestations of QCD coherence in the structure of final states in Deep Inelastic Scattering (DIS) processes in the small-x region. The QCD solution of the old-famous Feynman-Gribov paradox is discussed.

2. SPACE-TIME PICTURE OF QCD BREMSSTRAHLUNG AND LOCAL PARTON-HADRON DUALITY [16]

2.1. Radiation of Partons

The weakness of colour interaction at small space-time distances does not imply a poverty of dynamics. Indeed, each HP is followed by cascades of parton (gluons and $q\bar{q}$ pairs) production. For example, at, say, W = 20+20 GeV e^+e^- annihilation energy parton population runs to a dozen of bremsstrahlung gluons accompanying the parent $q\bar{q}$ system.

Radiation of a secondary parton does not lead normally to appearance of an additional resolvable jet since this quantum is quasi-collinear to the direction of original q and prefer to have relatively small energy. This is the characteristic property of the bremsstrahlung gluon spectrum

$$d w^{g}_{q(g)} \simeq C_{F(V)} \frac{\alpha_s(k_\perp^2)}{\pi} \frac{dk_\perp^2}{k_\perp^2} \frac{dk}{k} \qquad (2.1)$$

$(C_V = N_c, \quad C_F = (N_c^2-1)/2N_c)$,

which is referred to as Double Logarithmic (DL).The broad distribution over transverse momentum $k_\perp$ ('collinear' or 'transverse' logs) occurs in any field theory with dimensionless coupling (= 'logarithmic theory'); the dK/k spectrum is typical for the vector offspring ('soft', 'infrared' or 'longitudinal' logs).

The DL spectrum (2.1) corresponds to the wide region of gluon momenta

$$Q_0 \ll k_\perp \ll k \ll Q \,, \qquad (2.2)$$

which results in the large total emission probability increasing logarithmically with the 'hardness' of the process Q.

Notice that eq. (2.1) describes gluon radiation in the improved Born approximation: the account of high order effects makes the effective coupling α_s run with $k_\perp$

(2.3)

$$\alpha_s(k_\perp^2) \simeq \frac{4\pi}{b \ln k_\perp^2/\Lambda} \,, \quad b = 11/3\cdot N_c - 2/3\cdot n_f .$$

This can explain, formally, the appearance of the collinear cut-off Q_0 in (2.2): splitting of a parton into two with the small relative transverse momentum

$$k_\perp \lesssim R^{-1} \sim \text{few hundred MeV}$$

proves to be beyond the scope of PT (large α_s).

2.2. Formation and Hadronization Times

To approach the problem of coexisting PT and non-PT physics we have to look at the space-time picture of the $q\bar{q}$ system evolution in e^+e^- annihilation.

From QED experience two phenomena are well known to be closely connected with each other, namely, the bremsstrahlung of real quanta and the regeneration of the classic field attached to a free charged particle. Just after the hard interaction one meets an accelerated charge as a bare particle which will be accompanied by the normal Lorentz contracted disk of Coulomb field only at large distance from the interaction point. The time needed to regenerate the field component with fixed longitudinal and transverse momentum projections can be estimated as

$$t_{regen.} \sim k/k_\perp^2 . \qquad (2.4)$$

The same is true for the formation time of real bremsstrahlung . Applying the uncertainty relation to the virtual state p in the Feynman amplitude for photon radiation (Fig. 1) one has

$$t_{form.} \simeq \frac{p_0}{M^2_{virt.}} = \frac{p_0}{(k+p')^2} \simeq \frac{p}{pk\theta^2} \simeq \frac{k}{k_\perp^2} \,. \qquad (2.5)$$

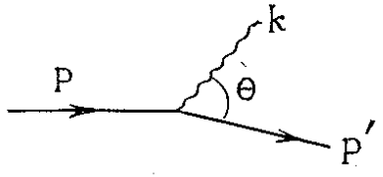

Fig.1. Bremsstrahlung from a charged particle.

The fact that in relativistic situation formation (regeneration) time may become macroscopic leads to a number of well-known peculiar QED phenomena.

These considerations in the QCD context clear up the fortune of quarks created in $e^+e^- \to q\bar{q}$. In the rest frame of a hadron the gluon field confining quarks has typical momenta

$$k_x \sim k_y \sim k_z \sim R^{-1} \sim (1\ \text{fm})^{-1}.$$

For the case of relativistic quarks with $p \approx W/2$ such confining field has the momentum components

$$k_x \sim k_y \sim R^{-1}; \quad k_z \sim R^{-1}\cdot(pR) = p$$

and due to eq. (2.4) needs some time

$$t_{regen} \sim pR^2 \qquad (2.6)$$

to be regenerated.

Thus, starting from the annihilation time $t_{an.} \sim 1/p \sim 10^{-3}$ fm up to hadronization time $t_{hadr.} \sim pR^2 \sim 100^3$ fm, the 200 GeV-quark behaves as a true colour particle radiating gluons perturbatively. An instructive lesson comes from the case of ultraheavy quark Q with mass $m_Q > 100$ GeV [7,46]. Due to the semiweak decay ($Q \to W + q$) its lifetime τ_Q becomes shorter than the hadronization time

$$\tau_Q \sim 1\ \text{fm}\cdot\left(\frac{M_W}{m_Q}\right)^3 \cdot p_Q/m_Q < t_{hadr.} \sim 1\ \text{fm} \cdot p_Q/m_Q \qquad (2.7)$$

and all the bremsstrahlung processes prove to be under the jurisdiction of PT QCD. One can say that such quark in all aspects behaves as if it were a free coloured object.

Applying the same arguments to a secondary parton k one concludes that its lifetime as a coloured object is restricted by

$$t < t_{hadr.} \sim kR^2. \qquad (2.8)$$

Clearly one can say that an additional gluon is emitted really only if its formation time (2.5) is smaller than the hadronization time (2.8)

$$k/k_\perp^2 < t < kR^2. \qquad (2.9)$$

We come to the conclusion that the requirement

$$k_\perp R > 1 \qquad (2.10)$$

not only approves the applicability of PT, keeping α_s formally small, but justifies the very opportunity to use the quark-gluon language for describing the process.

The parameter $(k_\perp R)$ regulates, so to say, the lifetime of a secondary parton. The gluons with momenta satisfying the strong inequality

$$k_\perp R \gg 1, \qquad (2.11)$$

which are the main personages of the DL kinematics (2.2), will live for long, radiating, in their turn, new offsprings thus leading to the cascade multiplication of partons.

2.3. Gluons and 'Gluers': Soft Confinement Scenario

What will be the final hadronic state for such a complex partonic system ? In attemping to answer this question let us turn before to the role of more dangerous - from the PT point of view - kinematic region, namely, radiation at the lower edge of PT phase space - with finite transverse momenta.

It should be 'Something' which is radiated strongly ($\alpha_s \sim 1$) and even could be hardly treated as a gluon since due to (2.9) this 'Something' is forced to 'hadronize' just immediately after being formed. For a sake of definiteness let us call such an object

$$\text{Gluer}: \quad k_\perp R \sim 1, \tag{2.12}$$

stressing the point that it is the prerogative of Gluers and not of Gluons to glue.

Appearance of gluers is a signal of switching on the real strong interactions in a coloured system. According to (2.5) first gluers (with $k \sim k_\perp \sim R^{-1}$) are formed at $t \approx R$ after annihilation. It is the moment when the distance between q and $\bar{q}$ starts to exceed 1 fm.

What a non-PT phenomenon has to happen at this moment? The answer should be the separation of two jets as globally blanched subsystems. Such a blanching is needed (pragmatically) to dump the unstability which manifests itself in the PT framework as the catastrophic increase of interaction strength and, thus, restrains the gluer radiation probability.

Though up to now we have no quantitative description of blanching process, the plausible picture of what is going on can be extracted from the Gribov's confinement scenario [47], where the crucial restructuring of the Dirac sea of light quarks is forced by the strong external colour field created by outgoing quarks and leads to phenomenon qualitatively similar to the QED physics of supercharged ions with $Z > 137$.

With time increasing gluers with larger and larger energies are formed. Their resulting energy spectrum, according to (2.1),

$$k \frac{dN}{dk} \sim \int_{k_\perp \sim R^{-1}} \frac{dk_\perp^2}{k_\perp^2} \frac{\alpha_s(k_\perp^2)}{\pi} = \text{const}, \tag{2.13}$$

can be said to represent the famous uniform hadronic plateau of the old partonic picture. Thus, the plateau of relatively soft hadrons $k \ll p$ appears due to sequential blancing of spreading colour fields in the $q\bar{q}$ system.

How will additional PT gluons (2.11) contribute to the hadronic yield? We have met already with two characteristic time scales in the evolution of a secondary gluon: $t_{form.}$ (2.5) and $t_{hadr.}$ (2.8).

Let us introduce one more scale, namely, the moment when the bremsstrahlung particle and its parent will be separated by the critical 'confinement' distance R in the transverse plane

$$t_{separ.} \sim R/\theta \simeq kR/k_\perp . \tag{2.14}$$

Notice that the three time scales characterizing the gluon's being are parametrically ordered due to (2.11)

$$t_{hadr.}/t_{separ.} \approx t_{separ.}/t_{form.} \approx k_\perp R \gg 1. \tag{2.15}$$

At $t_{separ.}$ some new specific non-PT interaction must take place to blanch the total colour charge of the outgoing gluon (e.g., with the help of light $q\bar{q}$ pair in the octet state). Our qualitative estimates do support this need: at this moment appropriate gluers $\tilde{\kappa}$ are formed which follow the gluon

$$\tilde{\theta} \approx \theta \quad , \quad \tilde{k} \sim 1/R\theta \quad , \quad \tilde{k}_\perp \sim R^{-1}; \tag{2.16}$$

$$\tilde{t}_{form} \sim \tilde{t}_{hadr.} \approx \tilde{k}/\tilde{k}_\perp^2 = R/\theta = t_{separ.}$$

Starting from $t = t_{separ.}$ the gluon becomes an independent source of hadrons with energies

$$1/R\theta \lesssim \omega_{hadr} \lesssim k . \tag{2.17}$$

This additional plateau, from the PT point of view, seems to be $C_V/C_F = 9/4 \approx 2$ times higher than that of original quark (cf. eq.(2.1)). It looks like a jet produced in

some HP with the effective hardness $Q \sim k_\perp$ but boosted with the Lorentz-factor $\gamma = 1/\theta \gg 1$.

At first glance it might seem strange that the new subjet did not contribute to the yield of softest hadrons with

$$R^{-1} \lesssim \omega_{hadr.} < R^{-1}/\theta \quad (\gg R^{-1}). \quad (2.18)$$

This is, in fact, an interesting phenomenon which stems from the very nature of QCD as gauge theory. The reason for this is the conservation of colour current plus coherence: soft hadrons in the energy interval (2.18) are formed early ($t < t_{separ.}$), when the quark and the gluon k appear to be close to each other in the transverse plane. Therefore, they act with respect to gluers ($\lambda\!\!\!^{-} \sim R$) as a single emitter with total colour charge equal to that of the original q (for more details see Subsec. 3.2).

The same arguments work when one considers the first blanching (and hadronization) acts at $t \sim R$. In the previous discussion we spoke about the colour field in the $q\bar{q}$ system. In fact, the quarks here are not in solo flight, being accompanied by narrow bunches of secondary PT partons (gluons) with $t_{form.} < R$. Indeed, the probability to meet two original quarks without any accompaniment can be evaluated as

$$P_0 \backsim \exp\left(-2\omega_q\right), \quad (2.19)$$

where

$$\omega_q = 4C_F \int_\epsilon^P \frac{dk}{k} \int^{k^2} \frac{dk_\perp^2}{k_\perp^2} \frac{\alpha_s(k_\perp^2)}{4\pi} \vartheta\left(t - \frac{k}{k_\perp^2}\right) = \quad (2.20)$$

$$4C_F \int_\epsilon^P \frac{dk}{k} \left(\xi(k^2) - \xi(k/t)\right)$$

is the total quark radiation probability (2.1) restricted by $t_{form.} < t$. Here ϵ stands for the energy resolution,

$$\xi(Q^2) \equiv \int^{Q^2} \frac{d\varkappa^2}{\varkappa^2} \frac{\alpha_s(\varkappa^2)}{4\pi} = \frac{1}{b} \ln\ln \frac{Q^2}{\Lambda^2} + \text{const} \quad (2.21)$$

Substituting $t \sim R \sim \Lambda^{-1}$ one obtains

$$\xi(k^2) - \xi\left(\frac{k}{t}\right) = \frac{1}{b} \ln \frac{\ln k^2/\Lambda^2}{\ln kR^{-1}/\Lambda^2} \approx \frac{1}{b} \ln 2$$

which leads to the power form factor dumping the bare $q\bar{q}$ state

$$P_0 \backsim (W)^{-\frac{8C_F}{b}\ln 2} \quad (2.22)$$

This means that normally the multipartonic 'coats' have already appeared nearly q and $\bar{q}$ at $t \lesssim R$. However, it is the coherence that makes the long-wave field insensitive to the internal structure of fraying parton jets and, thus, makes the yield of hadrons with finite energies ($\omega_{hadr.} \sim R^{-1}$) independent of W.

The latter conclusion is among the brightest predictions of the PT approach and will be discussed in details later in Sec. 6. It was based on qualitative considerations with use of semiclassical space-time description of radiative processes. The coherent phenomena which can be analysed in the PT framework strongly affect the evolution of pure partonic systems as well.

2.4. Angular Ordering and 'Partonic Gas'

Later on we shall sketch the formal proof and give the qualitative explanation of the Angular Ordering (AO) discovered by Fadin, Ermolayev and Mueller [36,37]. AO states that the structure of partonic system representing the jet development can be treated (in the leading DL approximation) as a tree of independent soft gluon emissions into sequentially shrinking angular cones.

Now let us use this fact to justify an important

property of the AO partonic sceletons, namely, that the partons produced in QCD cascades have to hadronize independently. To do this consider a pair of partons with the same hadronization time

$$t_h = \varepsilon R^2 \sim \varepsilon_1 R^2 \sim \varepsilon_2 R^2 \qquad (2.23)$$

(see Fig. 2).

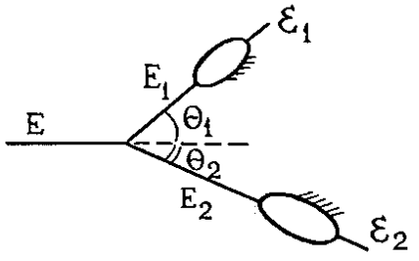

Fig.2 Partonic branching in QCD cascade.

Spatial separation between partons at this moment can be estimated as

$$\Delta\rho_\perp \simeq t_h\cdot(\theta_1+\theta_2) = t_h\cdot\theta \qquad (2.24)$$

$$\Delta z_\parallel \simeq t_h\cdot|v_1^\parallel - v_2^\parallel| \simeq t_h\cdot\frac{1}{2}|\theta_1^2-\theta_2^2|\ , \qquad (2.25)$$

where we have substituted t_h instead of the total evolution time of two partonic branches as the largest contributor due to strong time ordering (2.15). The relative angle θ can be expressed through the time scale of the decay of their common 'grandpa'

$$1/t_{split} \simeq \theta^2\cdot \min\{E_1,E_2\} = E_{min}\cdot\theta^2 \sim \frac{k_\perp^2}{E_{min}}. \qquad (2.26)$$

For the longitudinal distance (2.25) one easily derives

$$|\Delta\theta^2| = \frac{k_\perp^2}{E_0^2}\cdot\left|\frac{1}{z_1^2}-\frac{1}{z_2^2}\right| \sim \frac{k_\perp^2}{E_{min}^2}\ , \qquad (2.27)$$

where $z_{1(2)} = E_{1(2)}/E_0$ - energy (longitudinal momentum)

fractions in the decay.

Combining eqs. (2.24)-(2.27), we have

$$\Delta\rho_\perp \simeq t_h\cdot\left(t_{split}\cdot E_{min}\right)^{-\frac{1}{2}} \simeq R\left(z\cdot\frac{t_h}{t_{split}}\right)^{\frac{1}{2}}$$
$$\Delta z_\parallel \simeq \frac{t_h}{t_{split}}\cdot\frac{1}{E_{min}}\left\langle\frac{|z_1-z_2|}{2}\right\rangle \simeq \frac{1}{\varepsilon R}R\left(z\,\frac{t_h}{t_{split}}\right) \qquad (2.28)$$

where

$$z \equiv \frac{\varepsilon}{E_{min}} = \max\left\{\frac{\varepsilon_1}{E_1}\ ,\ \frac{\varepsilon_2}{E_2}\right\} \qquad (2.29)$$

characterizes the 'softeness' of the partons ε_1 , ε_2 relatively to their parents (E_1,E_2). Now

$$t_h > t_{form.}^{(\varepsilon)} \simeq 1/\varepsilon\theta_\varepsilon^2\ , \qquad (2.30)$$

where θ_ε stands for the emission angle of the parton with respect to its subjet ;

$$\frac{1}{z}t_{split} = \frac{E_{min}}{\varepsilon}\cdot\frac{1}{E_{min}\theta^2} = \frac{1}{\varepsilon\theta^2} \qquad (2.31)$$

Therefore, it is the AO restriction $\theta_\varepsilon \ll \theta$

that forces the $(z\cdot t_h/t_{split})$ parameter in (2.28) to be large and thus providing the partons to be involved in strong interactions (non-PT hadronization) at relative distances larger than the typical size of a relativistic hadron:

$$\Delta\rho_\perp \gg R\ ,\ \Delta z_\parallel \gg \gamma_\varepsilon^{-1}\cdot R\ . \qquad (2.32)$$

We conclude that in spite of intensive multiplication of partons in the main DL kinematical region their density in the configuration space appears to remain small: PT cascading produces 'the partonic gas'. Noteworthy to mention, in the deep inelastic scattering very

different situation takes place. There one faces with the partonic systems which become dense with decreasing Bjorken x and look like liquid rather than gas [5].

In this Section we tried to advocate the view that the PT radiative processes (including gluon emissions and $g \to q\bar{q}$ splittings) are likely to prepare comfortable conditions for the so-called soft confinement. Some non-PT physics must surely be there but to our feeling it reduces to nothing but soft independent hadronization of partons already prepared (in a controllable way) at the PT stage.

2.5. LPHD Concept [17,41]

First evidence in favour of the role of PT bremsstrahlung in hadroproduction, based on the QCD form factor dumping the colour correlations between partons, has become the cornerstone for the 'preconfinement' idea [44].

If colour confinement acts, indeed, locally in the phase space, providing the global blanching of separating pieces of a partonic system, then there remains no place for long-range uncontrollable strong interaction effects which might be pictured as long strings or colour tubes, lightening bolts etc. Therefore confinement would have nothing to do with multiplicities, energy and angular distributions of particles produced in HPs. Obviously, π/K or, say, Meson/Baryon ratio lies beyond the scope of PT. It is the challenge to future qualitative theory of hadroformation to describe the mass and the quantum number dependencies of hadron yield. However, in the soft confinement picture distributions of different hadrons must be similar and proportional to the calculable spectrum of PT partons (at least asymptotically, outside the domain of influence of phase space boundaries and kinematical mass effects). Moreover, these similarity

coefficients have to be universal constants independent of the kind of the process, of particle energies and the total hardness Q.

This is the essence of the Local Parton Hadron Duality (LPHD) concept. The LPHD approach attempts to describe the general features of the hadronic systems produced in HPs, such as the mean multiplicities and multiplicity distributions, angular patterns of energy and multiplicity flow, inclusive energy spectra and correlations of particles etc. without invoking any hadronization scheme at all. This makes predictions very restrictive and, therefore, simply testable since there are few parameters to vary in connecting PT QCD results to experiment. One of the main purposes of the LPHD approach is to look for phenomena where PT disagrees with experiment, in order to deduce some actual knowledge about the physics of confinement.

3. ESSENCE OF QCD COHERENCE [16,18,8]

This Section is intended to an elementary introduction to the basic ideas of coherence phenomena. The purpose is to provide the reader with the essential qualitative background helpful for better understanding the material covered below.

Roughly speaking, there are two types of coherence effects which occur. The first manifestation of coherence is the angular ordering (AO) of the sequential parton decays. Coherence of the second type deals with the angular structure of particle flows when three or more partons are involved in a hard process. Here the particle angular distributions depend on the geometry and colour topology of the whole jet ensemble (radiophysics of particle flows, see Sec. 8).

3.1. Angular Ordering of Successive Parton Branching

To elucidate the physical origin of AO let us consider a simple model of the jet cascade, namely, the radiation pattern of soft photons produced by a relativistic e^+e^- pair in a QED shower. (See Fig.3). The question is to what extent the e^+ and e^- independently emit γ's. To answer this question one has to estimate the formation time, the time interval needed for the γ-quantum to be radiated from, say, e^- leg. According to eq.(2.5) one has

$$t_{form} = \frac{1}{k\cdot\theta^2_{\gamma e}} , \qquad (3.1)$$

where $\theta_{\gamma e}$ is the angle between the emitted photon and the electron. Now $k\cdot\theta_{\gamma e} = k_\perp = \lambda_\perp^{-1}$ with $\lambda_\perp$ the transverse wavelength of the radiated photon. Thus,

$$t_{form} = \lambda_\perp / \theta_{\gamma e} .$$

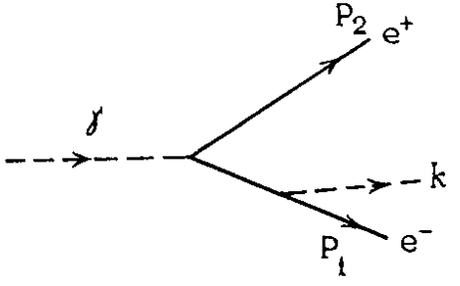

Fig. 3. Emission of soft photon, k, after e^+e^- pair production.

During this period of time the e^+e^- pair separate, transversely, a distance

$$\rho_\perp^{e^+e^-} \approx \theta_{e^+e^-}\cdot t_{form.} \approx \lambda_\perp \frac{\theta_{e^+e^-}}{\theta_{\gamma e}} . \qquad (3.2)$$

One concludes that for large angle photon emissions,

$$\theta_{\gamma e^-} \approx \theta_{\gamma e^+} \gg \theta_{e^+e^-} ,$$

the separation of the two emitters, e^+ and e^-, is smaller than $\lambda_\perp$. In this case the emitted photon cannot resolve the internal structure of the e^+e^- pair and probes only its total electric charge, which is zero. Thus for $\theta_{\gamma e} \gg \theta_{e^+e^-}$ we expect photon emission to be strongly suppressed. This is the Chudakov effect [48], well known in the physics of the QED shower *). The e^+ and e^- can be said to emit photons independently only when $\rho_\perp^{e^+e^-} \gg \lambda_\perp$, that is when $\theta_{\gamma e^+}, \theta_{\gamma e^-} < \theta_{e^+e^-}$.

The same discussion can be given for QCD cascades where soft gluon radiation is governed by the conserved (colour) currents. The only difference is that the coherent radiation of soft gluons by an unresolved pair of gluons, or quarks, is no longer zero but the radiation acts <u>as if</u> it were emitted from the parent gluon <u>imagined</u> to be on shell, as is illustrated in Fig.4a. The remarkable fact is that one gets all double log and single logarithmic effects correctly, for angular averaged observables, by emitting the gluon, independently, off line 1 when $\theta_{1k} < \theta_{12}$, off line 2 when $\theta_{2k} < \theta_{12}$ and off the parent, line g, when $\theta_{kg} > \theta_{12}$, see Sec. 5.

In the general case of large angle soft gluon emission off the multiparton jet (see Fig.4b) the intrajet partons p_i can be considered as collimated. As the result this gluon can be treated as the classical probe testing the total colour charge of the jet, i.e. of the original parton p.

*) In the middle of fifties in cosmic ray physics it was observed that in high energy γ-pair conversion the ionization is diminished as long as the e^+e^- spatial separation is below the diameter of an atom.

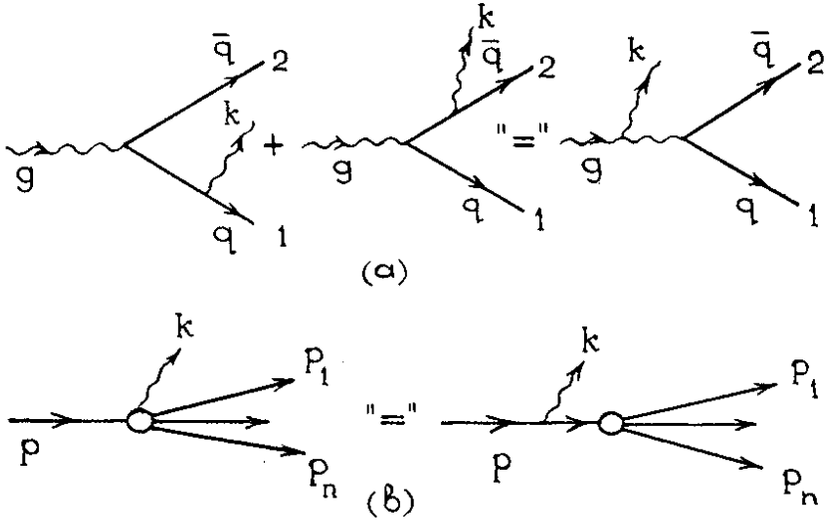

Fig. 4. An illustration of coherence were wide angle emission of soft gluon, k, acts as if the emission came off the parent parton: a) gluon conversion into the quark-antiquark pair; b) parton jet emission off a hard parton p.

The AO occurs not only for the time-like jet evolution but also for the space-like partonic cascades.

Consider, firstly, the soft gluon radiation in the case of high-$p_\perp$ scattering of an energetic parton, when in the t-channel colour is not transferred (e.g., electroweak quark scattering). As well known one should observe here two bremsstrahlung cones with opening angles $\Delta\theta \approx \theta_s$ centered in the directions of incoming and scattered partons ($\theta_{1k} < \theta_s$, $\theta_{2k} < \theta_s$, θ_s -scattering angle, see Figs. 5 a, b). Soft emission at larger angles $\theta_{1k} \sim \theta_{2k} > \theta_s$ is absent since during the time t_{form} the transverse displacement of the charge proves to be small: $\Delta\rho_\perp < \lambda_\perp$, and the situation looks like there were no current change

at all.

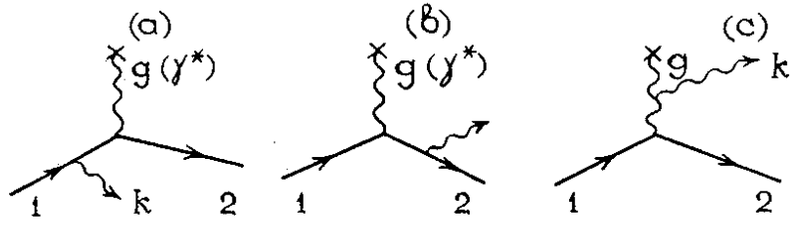

Fig. 5. Soft gluon radiation in the process of parton scattering with (and without) colour transfer in t-channel.

However, in the case of scattering with colour transfer (that is of importance, e.g., for deeply inelastic scattering, see Sec. 9) the additional bremsstrahlung contribution appears, which corresponds effectively to the emission off the t-channel gluon g, when $\theta_{1k} \sim \theta_{2k} > \theta_s$, see Fig. 5c).

3.2. Hump-Backed QCD Plateau in Particle Spectra [42)]

The depletion of emission of soft particles inside a jet (hump-backed plateau) in the inclusive energy spectrum, remains one of the most striking predictions of perturbative QCD. The suppression of soft radiation follows from the angular ordering of partonic cascade in going from greater to lesser virtuality and is a direct manifestation of coherence in QCD. This can be understood on kinematical ground as the result of two conflicting tendencies: on one hand due to the restriction $k_\perp > 1/R$ a slow particle is 'forced out' at large emission angle $\theta > 1/kR$, and on the other hand the allowed decaying angle, after a few successive branching, is shrunk to small values.

Let us illustrate the influence of the colour coherence

on particle spectra with the help of the toy model for parton branching, based on the first order QCD. We start with an old-fashioned plateau of particles with limited transverse momenta $k\Theta = k_\perp \sim R^{-1}$ for a quark jet with energy E. Here the structure of energy (ln k) and angular (ln $1/\Theta$) spectra appeared roughly the same

$$\rho(K) = \rho(\Theta) \ , \qquad \rho(K) \equiv \frac{dn}{d\ln k} \ , \quad \rho(\Theta) \equiv \frac{dn}{d\ln \gamma_{\parallel}} \simeq \frac{dn}{d\ln 1/\Theta} \ , \tag{3.3}$$

for $R^{-1} \ll k \ll E$, $(ER)^{-1} \ll \Theta \ll 1$ (see shaded areas in Fig.6 a-c). In eq. (3.3), $\gamma_{\parallel}$ is the rapidity

$$\gamma_{\parallel} = \frac{1}{2} \ln \frac{E + p_{\parallel}}{E - p_{\parallel}} \ ,$$

$p_{\parallel}$ is the component of momentum of an outgoing particle, measured along the parent quark direction.

Accounting for a gluon with energy ε and emission angle θ_o, let us use a double-log expression for the radiation probability

$$dw_g \backsim \alpha_s \frac{d\varepsilon}{\varepsilon} \frac{d\theta_o}{\theta_o} \vartheta(\varepsilon\theta_o - R^{-1}) \ . \tag{3.4}$$

The step function ϑ restricts here the transverse momentum $p_\perp \approx \varepsilon\theta_o > R^{-1}$ to ensure the gluon's existence $\left[t_{rad.} \sim \varepsilon/p_\perp^2 < t_{hadr.} \sim \varepsilon R^2\right]$.

How does the gluon contribute to the particle yield ? From the standpoint of the orthodox parton model one might expect the gluon to give rise to a subjet of hadrons with $k\theta' \sim R^{-1}$ (θ' being the angle between the registered hadron and the gluon) and an energy plateau as wide as

$$R^{-1} < k < \varepsilon \ . \tag{3.5}$$

The reduction of this additional plateau to

$$(R\cdot\theta_o)^{-1} < k < \varepsilon \tag{3.6}$$

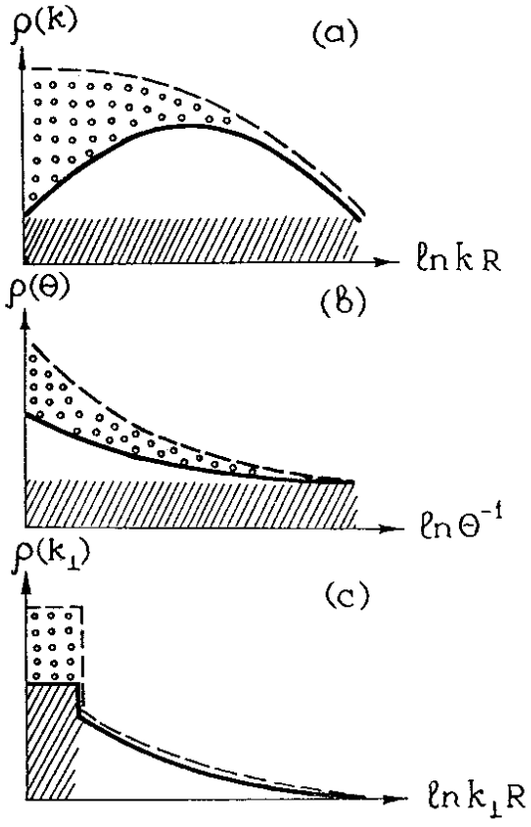

Fig. 6. The effect of coherence on energy, angular and $k_\perp$ distributions. Dotted areas correspond to the contribution which is removed when turning from the incoherent model (dashed) to the coherent one (solid curve). Shaded areas show the old-fashioned plateau (without taking account of bremsstrahlung).

proves to be the major consequence of the coherence.

To verify that the restriction (3.6) is intimately connected with QCD coherence, let us represent the plateau

distribution of particles from a gluon jet symbolically as follows:

$$dn = \frac{dk}{k}\,\frac{d\theta'}{\theta'}\,\delta(k\theta' - R^{-1}) \qquad (3.7)$$

This expression can be thought of as a DL spectrum of bremsstrahlung (k,θ') from the gluon (ε, θ_0), 'projected' onto the domain of the most intensive radiation $(\alpha_s(k\theta')/\pi \sim 1)$. As it follows from the AO in cascade, the off-spring particles are independently emitted by the gluon only inside the cone with the opening angle

$$\theta' < \theta_0 \quad .$$

Applying this inequality to eq. (3.7), one obtains restriction (3.6) at once.

The condition (3.6) reflects the fact that the particle yield from bremsstrahlung depends rather on $p_\perp \approx \varepsilon \cdot \theta_0$ of a parent gluon than on its energy. Finally, the particle multiplicity can be written schematically as follows:

$$n = \int^{E} \frac{dk}{k} \int^{1} \frac{d\theta}{\theta}\,\delta(k\theta - R^{-1}) + \qquad (3.8)$$

$$\alpha_s \int^{E} \frac{d\varepsilon}{\varepsilon} \int^{1} \frac{d\theta_0}{\theta_0}\,\gamma(\varepsilon\theta_0 - R^{-1}) \int^{\varepsilon} \frac{dk}{k} \int^{\theta_{max}} \frac{d\theta'}{\theta'}\,\delta(k\theta' - R^{-1}) .$$

Here the first term stands for the background quark plateau, the second one is constructed from the gluon emission (3.4) and fragmentation (3.7). The difference between the coherent and incoherent approaches has been encoded in eq.(3.8) with the help of θ_{max}:

$$\theta_{max}^{incoh} = 1 \qquad \text{for the incoherent case}$$
$$\theta_{max}^{coh} = \theta_0 \qquad \text{for the coherent one.} \qquad (3.9)$$

Now we are ready to deduce various differential

distributions ρ, inserting appropriate δ function to fix k, $\theta = \theta_0 + \theta'$ or $k_\perp = k\theta$ of the registered particle. For the density of the energy 'plateau' $\rho(k)$ our naive model gives:

$$\rho^{incoh.}(k) = 1 + \frac{\alpha_s}{2}\left(\ln^2 ER - \ln^2 kR\right) \qquad (3.10a)$$

$$\rho^{coh.}(k) = 1 + \alpha_s \cdot \ln\frac{E}{k} \cdot \ln kR \quad . \qquad (3.10b)$$

The additional multiplicity $\int d \ln k\,(\rho(k)-1)$ appears to be twice as large for the incoherent case (this factor '2' exponentiates with account of multiple branching [36, 37]). Expressions (3.10) illustrate qualitatively the well-known fact that the coherence substantially depletes the soft part of the <u>energy</u> spectrum giving rise to a hump (see Fig.6a). For the rapidity (angular) distribution one obtains

$$\rho^{incoh.}(\theta) = 1 + \alpha_s \ln^2(E\theta R) \qquad (3.11a)$$

$$\rho^{coh.}(\theta) = 1 + \frac{\alpha_s}{2} \ln^2(E\theta R) \qquad (3.11b)$$

Thus the <u>rapidity</u> spectra happen to be qualitatively similar, both demonstrating maxima at $y_\parallel \approx 0$ (see Fig. 6b).

Higher order analysis maintains this conclusion. Therefore for a purpose of finding the clear manifestations of QCD coherence $y_\parallel$ is not a good variable.

The essential difference in the structure of particle distributions over $\ln k$ and the rapidity $y_\parallel$ turns out to be an important lesson. The understanding of this fact will help to overcome prejudices originated from the old theory of strong interactions with limited transverse momenta.

3.3. Soft Gluon Emission from Colourless 'Quark-Antiquark Antenna' [43,49]

Let us examine soft emission associated with $q\bar{q}$ pair produced in a colour-singlet state in some hard subprocess, see Fig. 7. This radiation pattern is interesting in its own right, e.g., in connection with two-jet physics in the process $e^+e^- \to q\bar{q}$. Furthermore, neglecting the terms of order $1/N_c^2$, one can represent the radiation pattern in the case of complex hard partonic system as a sum of terms in which each external quark line is uniquely connected to an external antiquark line of the same colour (colourless '$q\bar{q}$-antennae').

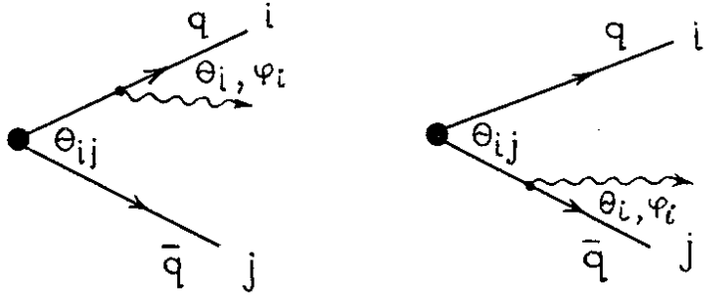

Fig.7. Soft gluon emission from a hard colourless $q\bar{q}$ pair.

In the lowest order the soft gluon distribution takes the familiar form, cf. eq. (2.1):

$$d w_{q\bar{q}} = \frac{d^3k}{(2\pi)^3\, 2k} \cdot \alpha_s \cdot 8\pi \cdot C_F \cdot \frac{(p_i p_j)}{(p_i k)(p_j k)} = \frac{dk}{k}\, d\Omega_k \, \frac{\alpha_s \cdot 2C_F}{4\pi^2} \cdot (\hat{ij}) \quad . \tag{3.12}$$

Here

$$\hat{ij} = a_{ij}/a_i a_j; \quad a_{ij} = (1 - \vec{n}_i \vec{n}_j); \; a_i = (1 - \vec{n}\,\vec{n}_i), \tag{3.13}$$

$\vec{n}_i, \vec{n}_j$ denote the directions of $q, \bar{q}$ momenta respectively, $\vec{n}$ - direction of the emitted gluon.

Let us call the distribution $\hat{ij}$, describing the radiation pattern of the colourless $q\bar{q}$ pair, '$q\bar{q}$-antenna'. Antenna $\hat{ij}$ may be represented in the form

$$\hat{ij} = P_{ij} + P_{ji},$$

where

$$P_{ij} = 1/2 \cdot \left[1/a_i + \frac{a_{ij} - a_i}{a_i a_j} \right] \quad . \tag{3.14}$$

The point about splitting the radiation pattern into two terms P_{ij} and P_{ji} is that only the former (latter) has the pole at $\theta_i = 0$ ($\theta_j = 0$), so this term can be treated as 'belonging to' quark i (j). Notice that after averaging with respect to the azimuthal angle φ_i around the direction $\vec{n}_i$ we get

$$\langle P_{ij} \rangle \equiv \int \frac{d\varphi_i}{2\pi} P_{ij} = \frac{1}{a_i} \, \theta(\theta_{ij} - \theta_i) \quad . \tag{3.15}$$

In other words, $\langle P_{ij} \rangle$ is just the incoherent radiation from quark i, confined to the cone $\theta_i < \theta_{ij}$. Similarly P_{ij} azimuthally averaged around $\vec{n}_j$ describes the radiation from j into the cone $\theta_j < \theta_{ij}$.

This result allows one to incorporate some of the soft gluon interference effects into the MC programs in a probabilistic fashion. By restricting the phase space for soft emission using the angular ordering criterion interference effects are included - on the average - as a sum probabilities.

3.4. Physical Origin of Drag Effect [8]

The drag (or string) effect in the $q\bar{q}g$ events of e^+e^- annihilation is the best example of QCD coherence of the second kind. In Sec. 8 we shall have much more to say

about this coherence, however, our purpose here is simply to explain the basic idea. So far, the most striking experimental test (see Refs. [9,12,13] and references therein) of this idea is the comparison of associated hadron production in $q\bar{q}g$ three jet events with that of $q\bar{q}\gamma$ events with the g and γ having similar kinematics [43]. In the plane of the three jets, counting the photon as a jet, one finds a suppression of associated hadrons in the region between the q and $\bar{q}$ in $q\bar{q}g$ events as compared to $q\bar{q}\gamma$ events.

To illustrate the physical origin of the destructive interference one can use the simple QED model with the q and $\bar{q}$ replaced by e^-'s and the gluon by a collinear e^+e^- pair, 'recharging' electrons, see Fig. 8a.

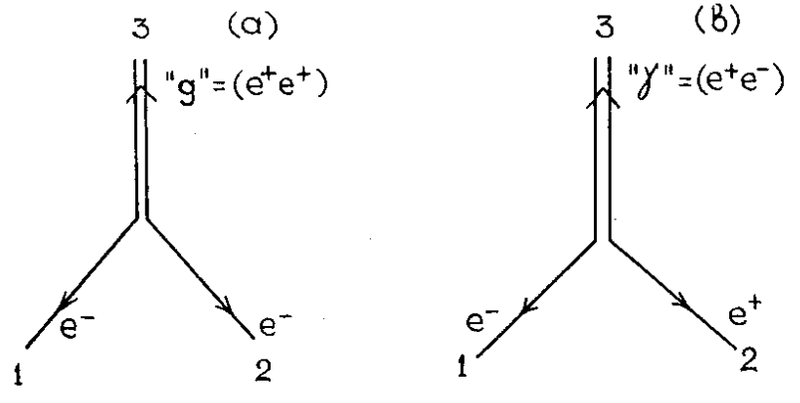

Fig.8. QED model for illustrating drag effect. The 'gluon' is represented as having double electric charge as compared to the electron. The 'photon' is replaced by a collinear e^+e^- pair.

The $q\bar{q}\gamma$ event is illustrated in this model by Fig.8b. The corresponding radiation pattern is

$$dw_{(q\bar{q}\gamma)} = \frac{dk}{k}\, d\Omega_\kappa \frac{\alpha}{2\pi^2}(\hat{12}) \quad . \qquad (3.16a)$$

The soft radiation spectrum in the $q\bar{q}'g'$ case is determined by the standard classical currents and may be written as *)

$$dw_{(q\bar{q}'g')} = \frac{dk}{k}\, d\Omega_\kappa \frac{\alpha}{\pi^2}\left(\hat{13} + \hat{23} - 1/2\cdot\hat{12}\right). \qquad (3.16b)$$

Let us pay attention to the negative contribution of the antenna $\hat{12}$, connected with the 'repulsion' of e^-'s.

It is easy to see that there is no radiation emitted directly opposite the e^+e^- pair in the symmetric configuration. The depletion of radiation originates from the compensation of electromagnetic fields caused by two e^-'s. Analogously in QCD the opposite colour charges of q and $\bar{q}$ in the $q\bar{q}\gamma$ event are replaced by the effectively equal ones in the $q\bar{q}g$ case, that leads to the destructive interference. Thus, one meets here the colour 'recharging' of the quark pair by a gluon.

4. DOUBLE LOG APPROXIMATION [24-26]

In this Section we shall construct the multigluon amplitudes M_N corresponding to the most probable bremsstrahlung patterns, reformulate the answer for $|M_N|^2$ in terms of the classical shower picture (Markov chain) and discuss briefly the main DLA predictions.

Being too crude to describe quantitatively the evolution of particle spectra with Q^2, DLA predicts correctly the asymptotical shape of the KNO distribution, the position of the hump in energy spectra etc. This asymptotics, however, proves to be 'too academic', since the DLA, accounting for gluon cascading and QCD coherence, ignores the energy conservation (recoil effects).

---

*) Notice that this pattern mimics the $q\bar{q}g$ sample at $N_c = \sqrt{2}$, cf. eq. (8.24).

We shall consider the DLA as the base for formulating the true zero order approximation - the MLLA - in Sec. 5. The DLA analysis splits into three problems: construction of tree amplitudes, proof of the Angular Ordering (AO) and account of virtual corrections.

4.1. Tree Multigluon Amplitudes for $e^+e^- \to q\bar{q} + Ng$

Consider gluon radiation accompanying production of the quark and antiquark with 4-momenta p_-, p_+. Let k_i be the 4-momentum, e_i - the polarization vector and a_i - the colour index of the gluon i. Energies of the final gluons are to be strongly ordered

$$E_{+(-)} \gg \omega_1 \gg \omega_2 \gg \ldots \gg \omega_N \qquad (4.1)$$

to give the dominant contribution to the cross section:

$$\sigma_N \sim \int |M_N|^2 \prod_{i=1}^{N} \frac{d^3k_i}{2\omega_i} \sim \left(g_s^2 \log^2\right)^N . \qquad (4.2)$$

To pick up the angular logs it is useful to choose a physical gauge, where the gluon emission vertex, either $q \to qg$ or $g \to gg$, vanishes at collinear momenta.

Following Ref. [24] we use the planar gauge where the gluon propagator reads

$$G^{ab}_{\mu\nu}(k) = \delta^{ab}\,\frac{d_{\mu\nu}(k)}{k^2 + i\varepsilon}\,, \qquad (4.3)$$

$$d_{\mu\nu}(k) = g_{\mu\nu} - \frac{k_\mu c_\nu + k_\nu c_\mu}{(kc)}\,.$$

It is convenient to take the gauge vector c_μ proportional to the total momentum,

$$c_\mu = (1, \vec{c}\,)\,; \quad \vec{c} = 0 \text{ in the } e^+e^- \text{ cms.}$$

In this gauge q and $\bar{q}$ emit soft gluons independently since the interference between them vanishes due to

$$p_{+\mu}\, d_{\mu\nu}(k)\, p_{-\nu} = 0. \qquad (4.4)$$

The resulting amplitude will be explicitly gauge invariant and it is natural to use only two physical polarizations $e_\mu^{(1,2)}$ for the final ('real') gluons:

$$(e_i^{(1,2)}\, k_i) = 0, \quad (e_i\, c) = 0. \qquad (4.5)$$

The planar gauge has the advantage of diminishing the contributions from two nonphysical polarizations in virtual gluon propagators:

$$d_{\mu\nu}(k) = -\sum_{\lambda=0}^{3} e_\mu^{(\lambda)}(k)\, e_\nu^{(\lambda)}(k)\,, \qquad (4.6)$$

$$e_\mu^{(0,3)}(k) = \frac{k_\mu \pm \sqrt{k^2}\cdot c_\mu}{\left(2\omega(\omega \pm \sqrt{k^2})\right)^{1/2}}\,,$$

where $\omega = (kc)$ is the gluon energy ($c^2 = 1$).

4.1.1. Two gluon emission off a quark p_-

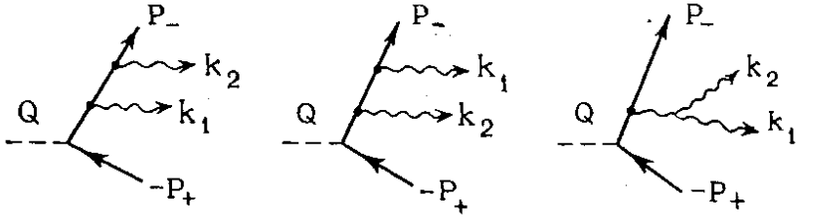

Fig. 9. Feynman amplitudes for $e^+e^- \to q\bar{q}g_1g_2$.

Feynman amplitude corresponding to graphs of Fig. 9 can be written as

$$M_a = g_s^2\, \frac{e_2 p_-}{k_2 p_-} \cdot \frac{e_1 p_-}{(k_1 + k_2) p_-} \cdot t^{a_2}\, t^{a_1}\,, \qquad (4.7a)$$

$$M_b = g_s^2 \frac{e_1 p_-}{k_1 p_-} \cdot \frac{e_2 p_-}{(k_1+k_2)p} \cdot t^{a_1} t^{a_2} . \qquad (4.7b)$$

$$M_c = g_s^2 e_1^\mu e_2^\nu \gamma_{\mu\nu\rho}(k_1,k_2,-k) \frac{d^{\rho\sigma}(k)}{k^2} \cdot \frac{p_{-\sigma}}{k\, p_-} \cdot i f^{a_1 a_2 c} \cdot t^c , \qquad (4.7c)$$

where $k = k_1 + k_2$,

$$\gamma_{\mu\nu\rho}(k_1,k_2,k_3) = g_{\mu\nu}(k_2-k_1)_\rho + g_{\mu\rho}(k_1-k_3)_\nu + g_{\nu\rho}(k_3-k_2)_\mu . \qquad (4.8)$$

Singular dependence on the directions of gluon momenta $\vec{n}_i$ may come only from Feynman denominators ($d^{\rho\sigma}(k)$ contains no angular dependence in denominator), and thus the kinematical regions where both $d\vec{n}_1$ and $d\vec{n}_2$ integrations are logarithmic can be easily shown to be the following:

$$\theta_1^2 \gg \frac{\omega_2}{\omega_1}\theta_2^2 , \qquad (4.9a)$$

$$\theta_2^2 \gg \frac{\omega_1}{\omega_2}\theta_1^2 , \qquad (4.9b)$$

$$\frac{\omega_1}{\omega_2}\theta_1^2 \gg \theta_2^2 \gtrsim \theta_1^2 . \qquad (4.9c)$$

Diagrams of Fig.9 a,b are of the QED type, so let us concentrate on the third amplitude Fig.9 c:

$$2kp_- \simeq E_-(\omega_1\theta_1^2 + \omega_2\theta_2^2) , \quad k^2 \simeq \omega_1\omega_2\theta_{12}^2 . \qquad (4.10)$$

Here θ_1 (θ_2) - the angle between $\vec{p}_-$ and $\vec{k}_1$ ($\vec{k}_2$); θ_{12} - the angle between k_1, k_2. Making use of Eq.(4.9c) one has

$$e_1^\mu e_2^\nu \gamma_{\mu\nu\rho}(k_1,k_2,-k)\, e_\rho^{(1,2)}(k) \sim \omega_1\theta_{12} \gg$$

$$\sqrt{\omega_1\omega_2\theta_{12}^2} \approx \sqrt{k^2} \sim e_1^\mu e_2^\nu \gamma_{\mu\nu\rho}\, e_\rho^{(0,3)}(k) , \qquad (4.11)$$

$$e_\sigma^{(1,2)}(k)\cdot p_-^\sigma \sim \frac{E_-}{\omega_1}(\omega_1\theta_1 + \omega_2\theta_2) \gg$$

$$\frac{E_-}{\omega_1}(\omega_1\theta_1^2 + \omega_2\theta_2^2 + \sqrt{\omega_1\omega_2\theta_{12}^2}) \sim \frac{p_-k + \sqrt{k^2}\cdot p_-c}{\omega} \sim$$

$$\sim e_\sigma^{(0,3)} \cdot p_-^\sigma$$

These inequalities show that nonphysical polarizations $e^{(0,3)}(k)$ prove to be negligible indeed. Therefore, the $d_{\rho\sigma}(k)$ factor in eq. (4.7c) can be replaced by the transversal tensor

$$g^\perp_{\rho\sigma} = -\sum_{\lambda=1,2} e_\rho^{(\lambda)}(k)\, e_\sigma^{(\lambda)}(k) , \qquad (4.12)$$

and the gluon vertex (4.8) - by the dominant term $g_{\mu\rho}\cdot(2k_1+k_2)_\nu$:

$$e_1^\mu e_2^\nu \gamma_{\mu\nu\rho}(k_1,k_2,-k)\, d_{\rho\sigma}(k)\, p_-^\sigma \simeq 2(e_2k_1)e_1^\mu g^\perp_{\mu\sigma}(k)\, p_-^\sigma . \qquad (4.13)$$

Finally, one can replace $g^\perp_{\mu\sigma}$ in eq.(4.13) by the unit tensor $g_{\mu\sigma}$:

$$e_1^\mu g^\perp_{\mu\sigma}(k)\, p_-^\sigma = -(\vec{e}_1\vec{p}_-) + \frac{(\vec{e}_1\vec{k})(\vec{k}\vec{p}_-)}{\vec{k}^2} \simeq \qquad (4.14)$$

$$-(\vec{e}_1\vec{p}_-) = e_1^\mu g_{\mu\sigma}\, p_-^\sigma$$

where we have used eq. (4.9c) to estimate

$$\vec{e}_1\vec{p}_- \sim E_-\theta_1 \gg \frac{(\vec{e}_1\vec{k})(\vec{k}\vec{p}_-)}{\vec{k}^2} \sim E_-\frac{\omega_2}{\omega_1}\theta_{12} .$$

The resulting DL expression for the gluonic amplitude (4.7c) of Fig.9 c looks very much alike eqs.(4.7a) and (4.7b):

$$M_c = g_s^2 \frac{e_2k_1}{k_2k_1} \cdot \frac{e_1p_-}{(k_1+k_2)p_-} \cdot i f^{a_1a_2c} t^c . \qquad (4.15)$$

4.1.2. Angular ordering (N=2). Further simplification of DL amplitudes (4.7a), (4.7b) and (4.15) is connected with formulation of a shower picture.

From the kinematical restrictions (4.9) one concludes that the DL regions a) and c) overlap, and, thus, the corresponding amplitudes interfere. It proves to be possible, however, to avoid the examination of an interference. To do this let us consider the three non-overlapping angular regions

$$\begin{aligned} &\text{I.} \quad \theta_1 \gg \theta_2 \\ &\text{II.} \quad \theta_2 \gg \theta_1 \\ &\text{III.} \quad \theta_{12} \ll \theta_1 \approx \theta_2 \end{aligned} \tag{4.16}$$

and show that the matrix element in each of these regions takes the form of a product of trivial independent radiation factors.

Indeed, in region I the only contribution comes from the amplitude of Fig. 9a which takes the form ($k_1p_- \gg k_2p_-$)

$$M_I = g_s^2 \cdot \frac{e_2p_-}{k_2p_-} \cdot \frac{e_1p_-}{k_1p_-} \cdot t^{a_2}t^{a_1} . \tag{4.17}$$

Kinematical inequality II splits into two subregions:

$$\theta_2^2 \gg \frac{\omega_1}{\omega_2}\theta_1^2 \gg \theta_1^2$$

and

$$\frac{\omega_1}{\omega_2}\theta_1^2 \gg \theta_2^2 \gg \theta_1^2 .$$

In the first case (cf. eq. (4.9b) only graph of fig.9b contributes as ($k_2p_- \gg k_1p_-$)

$$M_{II} = g_s^2 \cdot \frac{e_1p_-}{k_1p_-} \cdot \frac{e_2p_-}{k_2p_-} \cdot t^{a_1}t^{a_2} . \tag{4.18}$$

In the second subregion one has to account for both Figs. 9a and 9c. Here, however, $\theta_{12} \approx \theta_2$, $\frac{e_2k_1}{k_2k_1} \approx \frac{e_2p_-}{k_2p_-}$ and summing (4.7a) and (4.15), with account of commutation relation $[t^{a_2}\, t^{a_1}] = i f_{a_2a_1c} t^c$ and inequality (4.9a) one simply arrives at eq.(4.18), which, thus, proves to be correct all over the region II (4.16).

Finally, the diagram of Fig. 9c dominates in the region III of a quasi-collinear g_1g_2 pair. Here $k_1p_- \gg k_2p_-$ and the amplitude reads

$$M_{III} = g_s^2 \cdot \frac{e_2k_1}{k_2k_1} \cdot \frac{e_1p_-}{k_1p_-} \cdot i f^{a_1a_2c} t^c . \tag{4.19}$$

The tree amplitudes (4.19) in the angular regions (4.16) represent the final result of the N=2 sample.

To make the degeneralization transparent let us formulate the answer in terms of a classical chain of sequential branching processes.

Fig. 9a (b): quark with momentum p_- emits first the gluon k_1 (k_2) and then k_2 (k_1); we attribute the angular region I (II) to this diagram.

Fig. 9c: quark emits the gluon k_1 which, in turn, emits the k_2; the region III. Elementary radiation contributes to the matrix element by the classical bremsstrahlung factor; emission angles strongly decrease along each chain; the colour factor corresponds directly to the classical graph describing genealogy of the process.

4.2. Proof of Angular Ordering

Now we are ready to formulate the rules of constructing the tree multigluon amplitudes in the DLA.

(i) Draw a Feynman diagram D without 4-gluon vertices. Strong energy ordering (4.1) makes it possible to group gluon propagators into N 'gluon lines' - sets of virtual g states with (approximately) the same energies (straight lines in Fig. 10). A vertex $i \to ij$ ($j > i$) we shall treat as an emission of j by the gluon line i (parent particle).

(ii) Now define the region Γ_D in the space of emission angles, corresponding to D: angles decrease along each

path in the tree, starting from $\gamma^* \longrightarrow q\bar{q}$ vertex. Along the quark (antiquark) line emitting sequentially $i_1, i_2, \ldots i_n$ gluons

$$1 \gg \hat{k}_{i_1}\hat{p}_{(\mp)} \gg \ldots \gg \hat{k}_{i_n}\hat{p}_{(\mp)} \; ; \qquad (4.20a)$$

along the gluon line j

$$\hat{k}_j\hat{\mathcal{P}}_j \gg \hat{k}_{j_1}\hat{k}_j \gg \ldots \gg \hat{k}_{j_m}\hat{k}_j \; , \qquad (4.20b)$$

where $j_1, j_2, \ldots j_m$ denote the momenta of its offsprings, $\mathcal{P}_j$ - momentum of its parent ($p_{(\mp)}$ or k_i of a harder gluon $i < j$). Inequalities (4.20) define the strong AO (Γ_D). Notice, that the sequential offsprings here are not ordered in their energies.

(iii) The diagram D in the angular region Γ_D is described by the matrix element

$$M_N = g_s^N \cdot (-1)^m \cdot \prod_{i=1}^{N} \frac{(e_i \mathcal{P}_i)}{(k_i \mathcal{P}_i)} \cdot G \qquad (4.21)$$

where m is the number of gluons emitted by $\bar{q}$, $\mathcal{P}_i$ - 4--momentum of the parent. Noteworthy to mention, $\mathcal{P}_i$ is the momentum of one of the final ('real') partons and not that of any virtual state.

The colour factor G is built up according to the usual Feynman rules for D: $t^a = \lambda^a/2$ for any $q(\bar{q}) \longrightarrow$ $\longrightarrow q(\bar{q})g$ vertex, i f_{abc} for a 3g-vertex, where a(b) marks the gluon with the lowest (highest) energy.

Eq.(4.21) represents the so-called QCD 'soft insertion' rules (see, e.g., Ref. [4]).

The proof follows, in fact, the logic line we have met with in the N=2 case. Let us enumerate and briefly discuss the main steps of the proof (for details see Ref. [24]).

1. Simplify the denominators of the virtual propagators:

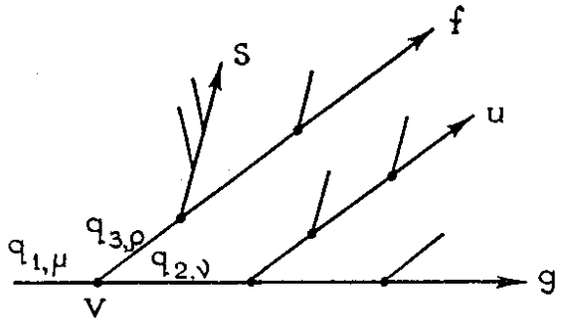

Fig.10. The scheme of a gluon cascade.

$$q_i^2 = (\sum_t k_t)^2 \approx 2\, k_i \cdot \sum_{t \neq i} k_t \; , \qquad (4.22)$$

where sum runs over all the final decay products k_t of a given virtual particle q_i, k_i being the most energetic among them. Eq. (4.22) follows from the

$$k_i(k_j + k_\ell) \sim \omega_i(\omega_j\theta_{ij}^2 + \omega_\ell\theta_{i\ell}^2) \gg \omega_j\omega_\ell(\theta_{ij}^2+\theta_{i\ell}^2) \gtrsim \qquad (4.23)$$

$$\omega_j\omega_\ell\,\theta_{j\ell}^2 \sim k_j k_\ell \qquad (\omega_i \gg \omega_j, \omega_\ell) \; .$$

2. For each vertex (V) in the tree impose the following angular restrictions (to pick up all the necessary θ-logs)

$$\omega_f\,\theta_{fg}^2 \gg \omega_s\,\theta_{sf}^2 \qquad (4.24a)$$

$$\omega_f\,\theta_{fg}^2 \gg \omega_u\,\theta_{ug}^2 \qquad (4.24b)$$

where s marks the eldest 'son' of f ('father'), u - its the eldest uncle (among the young brothers of f); see Fig. 10.

3. Show that due to eq.(4.24) virtual propagators between V and the $q\bar{q}$ creation point prove to be independent of k_s, k_u.

4. Prove that the DL contribution may come only from the angular region where the inequalities (4.24) are fulfilled for each vertex (by showing that the violation of

this restriction somewhere in the tree will lead to a loss of at least one angular logarithm).

5. Simplify the numerators using the planar gauge and physical polarizations for the final gluons and proving the dominance of physical polarizations $\lambda_i = 1, 2$ for each virtual vertex V (Fig.10)

$$\gamma = e_\mu^{(\lambda_1)}(q_1)\cdot e_\nu^{(\lambda_2)}(q_2)\cdot e_\rho^{(\lambda_3)}(q_3)\cdot \gamma^{\mu\nu\rho}(-q_1,q_2,q_3) \approx \tag{4.25}$$

$$2\,(e_\mu^{(\lambda_3)}(q_3)\cdot K_g^\mu)\cdot(e^{(\lambda_1)}(q_1)\cdot e^{(\lambda_2)}(q_2)),$$

where $q_{10}\approx q_{20}\approx\omega_g$; $q_{30}\approx\omega_f$. Considering then the chain of vertices along the line f and estimating (similarly to the N=2 case)

$$d_{\mu\nu}(q_i)\simeq -\sum_{\lambda=1,2} e_\mu^{(\lambda)}(q_i)\,e_\nu^{(\lambda)}(q_i) = g^\perp_{\mu\nu}\approx g_{\mu\nu} \tag{4.26}$$

one finally arrives at eq. (4.21).

6. The last statement to be proved is the possibility to replace the DL angular regions (4.24), which might coincide partially for different diagrams, by the non-overlapping AO regions Γ_D (4.20). One can do this by induction.

4.3. Virtual Corrections

In refs. [36,24] it was supposed that the account of virtual corrections results in the multiplication of the matrix element (4.21) by the factor

$$F = \exp\left\{-\frac{1}{2}\left(w^F(p_-,1) + w^F(p_+,1) + \sum_{i=1}^N w(k_i,\theta_i)\right)\right\} \tag{4.27}$$

where θ_i is the angle between gluon i and its parent:

$$\theta_i = \widehat{\vec{k}_i\vec{p}_i}\,.$$

Here

$$w(p,\theta) = C_V\int_{\Gamma(p,\theta)}\frac{d^3k}{2\omega}\,\frac{g_s^2}{(2\pi)^3}\cdot\frac{\vec{p}^{\,2}\theta_k^2}{(pk)^2} \approx$$

$$\approx C_V\int_p^P\frac{d\omega}{\omega}\int_\theta^\theta\frac{d\theta_k}{\theta_k}\,4\,\frac{\alpha_s(k_\perp^2)}{2\pi} \tag{4.28}$$

is the Born probability for a gluon to decay $g(p)\to g(p)+g(k\ll p)$ inside a cone of half-angle θ,

$$\Gamma(p,\theta):\left\{k^0\equiv\omega<p^0;\ \theta_{k\hat{p}}\equiv\theta_k<\theta;\ k_\perp\approx\omega\theta_k>Q_0\right\}. \tag{4.29}$$

In eq.(4.27) w^F denotes the quark emission probability:

$$w^F(p,\theta)\simeq\frac{C_F}{C_V}\,w(p,\theta) \tag{4.30}$$

with the DL accuracy.

F^2, thus, is the product of two quark and N gluonic DL formfactors [50].

The ansatz (4.27) was based on the low order PT calculations and the physical intuition. The formal proof was given in the recent paper [51] where Gribov bremsstrahlung theorem based on the dispersional considerations [52] and the Kirshner-Lipatov method of constructing the Bethe-Salpeter-type equations for PT amplitudes [53] had been exploited.

4.4. Cross Section. Method of Generating Functionals [22, 24-26]

The cross section of N-gluon production according to eqs. (4.21),(4.27) reads

$$d\sigma = d\sigma_0\,F^2\prod_{i=1}^N\frac{g_s^2}{(2\pi)^3}\,C_i\,\frac{d^3k_i}{2\omega_i}\,\frac{\vec{p}_i^{\,2}\theta_{k_i}^2}{(k_ip_i)^2} \tag{4.31}$$

(where $d\sigma_0$ denotes the Born annihilation cross section). It can be written as a product of the generating functionals (GF) describing the evolution of two quark jets as follows:

$$d\sigma\{u\} = d\sigma_0\, Z_u^{(q)}(p_-,1)\, Z_u^{(\bar{q})}(p_+,1) \quad , \qquad (4.32)$$

$$d\sigma_{excl.}^{(N)} = \left(\prod_{i=1}^{N} d^3k_i \, \frac{\delta}{\delta u(k_i)} \right) d\sigma\{u\} \Big|_{u=0} \quad . \qquad (4.33)$$

Generating functional $Z_u(p,\theta)$ for a gluon jet with the total momentum p and the opening angle θ

$$\left[Z_u(p,\theta) \right]^{C_F/C_V} = Z_u^{(q)}(p,\theta) \qquad (4.34)$$

satisfies the Master equation (4.35)

$$Z(p,\theta) = \exp\left\{ \int_{\Gamma(p,\theta)} \frac{d^3k}{\omega^2}\, C_V\, \frac{\alpha_s}{2\pi^2} \frac{p^0}{(pk)} \left[u(k) Z_u(k,\theta_{\hat{kp}}) - 1 \right] \right\} .$$

Differentiating Z over the probing function $u(k_i)$ near the 'point' u=0 one can obtain multi-particle exclusive probabilities for the production of any number of soft gluons with momenta k_i from the g-jet.

Using eqs. (4.35), (4.34) one can check directly the correspondence between the exclusive cross section (4.31) and the functional derivative (4.33).

When studying inclusive N-particle cross sections one has to apply to $d\sigma\{u\}$ the operator (4.36)

$$d\sigma_{incl.}^{(N)} = \left(\prod_{i=1}^{N} d^3k_i \frac{\delta}{\delta u(k_i)} \right) \cdot \sum_{m=0}^{\infty} \frac{1}{m!} \prod_{j=1}^{m} \left(\int d^3k_j \frac{\delta}{\delta u(k_j)} \right) \cdot d\sigma\{u\} \Big|_{u=0} =$$

$$\left(\prod_{i=1}^{N} d^3k_i \frac{\delta}{\delta u(k_i)} \right) \cdot \exp\left\{ \int d^3k \frac{\delta}{\delta u(k)} \right\} \cdot d\sigma\{u\} \Big|_{u=0} =$$

$$\left(\prod_{i=1}^{N} d^3k_i \frac{\delta}{\delta u(k_i)} \right) \cdot d\sigma\{u\} \Big|_{u=1} \quad ,$$

which proves to be equivalent to the expansion of

the functional $d\sigma\{u\}$ near the 'point' u=1. As an example,

$$d\sigma_{tot} = d\sigma_{incl.}^{(N=0)} = d\sigma_0 \qquad (4.37)$$

(no logs in the total cross section); this follows from eq. (4.35) which gives

$$Z_u(p,\theta) \Big|_{u(k)\equiv 1} = 1 \quad . \qquad (4.38)$$

Note, that the GF similar to eq.(4.32) can be constructed for any other initial state (ϱ) consisting of a number of quarks and hard gluons with energies of the same order and relative angles $\theta_{ij} \sim 1$. (4.39)

$$d\sigma\{u\} = d\sigma_0 \cdot \left[Z_u(p,\theta) \right]^{\varrho}, \quad \varrho = \frac{C_F}{C_V} N_q + N_g \ ,$$

where N_q, N_g are the numbers of primary $q(\bar{q})$ and g - prajets ($e^+e^- \to q\bar{q}$, $\varrho = 8/9$; $e^+e^- \to q\bar{q}g$, $\varrho = 17/9$; $\gamma \to 3g$, $\varrho = 3$, etc.).

4.5. Multiplicity Distributions in DLA [26]

In this Subsection we apply the GF technique to derive the asymptotic behaviour of the KNO-multiplicity distributions [54] in HPs, starting with a single g-jet.

Calculating the multiplicity distribution $P_n = \sigma^{(n)}/\sigma_{jet}$ one has to integrate over the whole phase volume of each gluon emitted, applying to the functional $Z_{u(k)}$ the following operator

$$\frac{1}{n!} \prod_{i=1}^{N} \left(\int d^3k_i \frac{\delta}{\delta u(k_i)} \right) \Big|_{u=0} \quad . \qquad (4.40)$$

This procedure however proves equivalent to the simple differentiation of function Z_u ($u(k) \equiv u = \text{const}$):

$$P_n = \frac{1}{n!} \left(\frac{d}{du} \right)^n Z_u \Big|_{u=0} ; \quad \sum_{n=0}^{\infty} P_n = Z \Big|_{u=1} = 1 \ . \qquad (4.41)$$

Replacing a probing function u in the Master equation (4.35) by a constant, one can simply check up that its solution appears to depend only on the product of jet variables, i.e. on the 'transverse momentum' of a jet:

$$Z_u(p,\theta) = Z(\ln p\theta/Q_0;\ u) \equiv Z(y,u). \qquad (4.42)$$

Here Q_0 stands for an infrared regulator (gluon 'mass') to fix the starting point for the perturbative development of a parton system:

$$Z(y = 0;\ u) = 1. \qquad (4.43)$$

Equation (4.35) then takes finally the form

$$\ln Z(y;u) = \int_0^y dy'(y-y')\, a^2(y')\left[u\, Z(y';u) - 1\right], \qquad (4.44)$$

where

$$a^2 = \frac{2C_v\, \alpha_s(\kappa_\perp^2)}{\pi} = \frac{4C_v}{b(y+\lambda)}, \quad \lambda = \ln\frac{Q_0}{\Lambda}. \qquad (4.45)$$

Running coupling α_s (which we suppose to depend on the transverse momentum of the offspring parton) should be sufficiently small all over the region under consideration, even at $k_\perp^2 \sim Q_0^2$. Thus, the condition $\lambda \gg 1$ has to be imposed to justify formally the perturbative approach.

As it is well known an asymptotic KNO distribution exists with the limit [54]

$$\lim_{y\to\infty}\left[\bar n(y)\, P_n(y)\right] = f(x), \quad x \equiv n/\bar n(y) = \text{fixed}.$$

In terms of GF this is equivalent to the existence of the limit

$$\lim_{y\to\infty} Z(y;u) = \exp(-\beta/\bar n(y)) = Z(\beta). \qquad (4.46)$$

Indeed, replacing a sum over n by an integral in the Tailor expansion for Z (dominant $n \sim \bar n(y) \to \infty$ with $y \to \infty$) one obtains

$$Z(y;u=e^{-\beta/\bar n}) = \sum_{n=0}^{\infty} P_n u^n \simeq \int_0^\infty \frac{dn}{\bar n}\left[\bar n P_n\right]\exp\left(-\beta\frac{n}{\bar n}\right) = \int_0^\infty dx\left[\bar n P_n(y)\right] e^{-\beta x}, \qquad (4.47)$$

and applying 'lim' operation,

$$Z(\beta) = \int_0^\infty dx\, f(x)\, e^{-\beta x}. \qquad (4.48)$$

This equation shows that the asymptotic KNO distribution function f(x) can be obtained using an inverse Mellin transformation

$$f(x) = \int_{-i\infty+\gamma}^{i\infty+\gamma} \frac{d\beta}{2\pi i}\, Z(\beta)\, e^{\beta x} \qquad (4.49)$$

(here Re γ > Re β_0, where β_0 - the position of the rightest singularity of $Z(\beta)$ in the β-plane; as we shall see later, $\beta_0 < 0$).

Another way of studying the KNO function f(x) is connected with the multiplicity correlator

$$n_k(y) \equiv \langle n(n-1)\ldots(n-k+1)\rangle = \sum_{n=k}^{\infty} n(n-1)\ldots(n-k+1)P_n$$

$$= (d/du)^k\left[\sum_{n=0}^{\infty} u^n P_n\right]\Big|_{u=1} = (d/du)^k\, Z(y;u)\Big|_{u=1}, \qquad (4.50)$$

$n_0 = 1$; $n_1 = \bar n(y)$.

Writing down an alternative Tailor expansion of GF near u=1

$$Z(y;u) = \sum_{k=0}^{\infty} \frac{(u-1)^k}{k!}\, n_k(y), \quad (n_0 \equiv 1), \qquad (4.51)$$

and constructing $Z(\beta)$, one obtains

$$Z(\beta) \equiv \lim_{y\to\infty} Z(y;u=e^{-\beta/\bar n}) = \lim \sum_{k=0}^{\infty} \frac{n_k(y)}{k!}\left(e^{-\beta/\bar n} - 1\right)^k =$$

$$\sum_{k=0}^{\infty} \frac{(-\beta)^k}{k!} \lim_{y\to\infty}\left[\frac{n_k(y)}{(\bar n(y))^k}\right] \qquad (4.52)$$

Comparing eqs. (4.52), (4.48) one concludes that the normalized multiplicity correlators

$$f_k \equiv \lim \frac{n_k(y)}{(\bar n(y))^k} \qquad (4.53)$$

are nothing but the moments of the KNO function

$$f_k = \int_0^\infty dx\, x^k\, f(x). \qquad (4.54)$$

Let us differentiate eq. (4.44) over y to obtain

$$Z'(y;u) = Z(y;u) \int_0^y dy'\, a^2(y') \left[uZ(y';u) - 1\right] . \quad (4.55)$$

Then substituting expansion (4.51) for Z and making the ansatz $n_k(y) \approx (\bar{n})^k \cdot f_k$, collect terms proportional to $(u-1)^k$. The result will be for k=1:

$$(d/dy)\,\bar{n}(y) = \int_0^y dy'\, a^2(y')(\bar{n}(y') + 1) \approx \int_0^y dy' a^2(y')\bar{n}(y'), \quad (4.56a)$$

for $k > 1$:

$$\frac{k}{k!} f_k\, \bar{n}^{(k-1)}(y) \frac{d}{dy} \bar{n}(y) = \sum_{m=1}^{k} \frac{f_{k-m}\, f_m}{(k-m)!\;\; m!} \bar{n}(y)^{k-m} \times \cdot \int_0^y dy'\, a^2(y')\, \bar{n}^m(y') \left[1 + O(1/\bar{n})\right] . \quad (4.56b)$$

Eq. (4.56a) describes the energy behaviour of the total multiplicity. For large y one has

$$\bar{n}(y) \sim \exp\Big(\int_0^y dy' \sqrt{a^2(y')}\, \Big) \sim \exp \sqrt{\frac{16 C_v}{b}} (y + \lambda). \quad (4.57)$$

The rate of multiplicity growth certainly depends on the coupling a^2.

This, however, is not the case for the KNO distribution. Indeed, estimating the integral term in eq.(4.56b) as

$$\int_0^y dy' a^2(y') \left(\bar{n}(y')\right)^m = \frac{(\bar{n}(y))^{m-1}}{m} \int_0^y dy' a^2(y') \bar{n}(y') \left[1 + O\left(\frac{1}{\ln \bar{n}}\right)\right]$$

and using eq. (4.56a) we come to the reccurency relations

$$\frac{k}{k!} f_k = \sum_{m=1}^{k} \frac{f_m \cdot f_{k-m}}{m!(k-m)!\, m} = \frac{f_k}{k \cdot k!} + \sum_{m=1}^{k-1} \frac{f_m\, f_{k-m}}{m!(k-m)!\, m}$$

or

$$f_k = \frac{k}{k^2-1} \sum_{m=1}^{k-1} \frac{k!}{m!(k-m)!} \frac{f_m f_{k-m}}{m} = \frac{k^2}{2(k^2-1)} \sum_{m=1}^{k-1} \frac{k!}{m!(k-m)!} \frac{f_m f_{k-m}}{m(k-m)} \quad (4.58)$$

$(f_0 = f_1 = 1)$.

Following the same lines for a general case $\rho \neq 1$ one obtains

$$f_k^{(\rho)} = \frac{\rho^{1-k}}{k^2} f_k + \sum_{m=1}^{k-1} \frac{(k-1)!}{(k-m)!\, m!} \frac{\rho^{1-m}}{m} f_m f_{k-m}^{(\rho)} , \quad (4.59)$$

$f_0^{(\rho)} = f_1^{(\rho)} = 1$.

These relations contain no memory about the coupling at all. This means that the QCD KNO function f(x) appears to be insensitive to α_s being moving or fixed, a^2 being smaller or larger. This amusing phenomenon had been noted by Bassetto et al. in ref. [23].

Account for the abovementioned coherent effects which modifies multiplicity behaviour from refs. [22,23] through

$$(a^2)_{\text{true}} = (1/2 \cdot a^2)_{\text{without coherence}}$$

consequently does not affect f(x) (moments f_k satisfy eq. (4.59) which coincides with those obtained by Konishi in ref.[22] in the framework of the old approach).

We can now simplify the problem keeping a^2 fixed ($\alpha_s(y') = \alpha_s = \text{const}$). This allows one to find the first integral of the differential equation

$$(\ln Z)'' = a^2(uZ-1); \quad Z(0) = 1, \; Z'(0) = 0;$$

following from eq. (4.55); namely,

$$Z'^2 = 2a^2 Z^2 \left[u(Z-1) - \ln Z\right] . \quad (4.60)$$

Writing down the solution

$$\int_Z^1 \frac{dx}{x\sqrt{2\left[u(x-1) - \ln x\right]}} = a\,y \quad (4.61)$$

one has to substitute $u = \exp(-\beta/\bar{n}(y))$ and consider the limit $y \to \infty$. This leads to the connection ($\beta > 0$)

$$\int_Z^1 \frac{dx}{x} \left(\frac{1}{\sqrt{2(x-1-\ln x)}} - \frac{1}{1-x} \right) + \ln\left[\frac{1-Z}{Z} \frac{2\bar{n}(y)}{\beta} \right] = a\,y \quad (4.62)$$

Then, making use of the asymptotic relation $\bar{n}(y) \approx \frac{1}{2} \cdot e^{ay}$, we finally obtain the following representation for $Z(\beta)$:

$$\int_z^{1/2} \frac{dx}{x\sqrt{2(x-1-\ln x)}} = \ln\frac{\beta}{\beta_1} \quad \text{for } \beta>0 \qquad (4.63a)$$

and

$$\int_z^{\infty} \frac{dx}{x\sqrt{2(x-1-\ln x)}} = \ln\frac{\beta_0}{\beta} \quad \text{for } \beta<0 \ . \qquad (4.63b)$$

Here we denoted by $\beta_1>0$ and $\beta_0<0$ the numbers

$$\ln\beta_1 \equiv \int_{1/2}^{1}\frac{dx}{x}\left(\frac{1}{\sqrt{2(x-1-\ln x)}} - \frac{1}{1-x}\right)$$

$$\ln|\beta_0| \equiv \int_{1}^{\infty}\frac{dx}{x}\left(\frac{1}{\sqrt{2(x-1-\ln x)}} - \frac{1}{x-1}\right) \approx 0.937 \ .$$

The rightest singularity of $Z(\beta)$ in the complex β-plane lies at $\beta \simeq \beta_0 \simeq -2.552$ ($\beta=0$ where $Z(\beta) = 1-\beta+ O(\beta^2)$ is an analyticity point). Expanding $Z(\beta)$ near the singularity one obtains using eq.(4.63b)

$$Z(\beta) \simeq 2\beta_0^2/(\beta-\beta_0)^2 + 2\beta_0/(\beta-\beta_0) - \frac{2}{3}\ln\frac{\beta-\beta_0}{|\beta_0|} + (\text{nonsingular terms}).$$

Substituting this expansion into the Mellin integral (4.49), we derive an asymptotic formulae for $f(x)$ at $x \gg 1$ (the tail of the KNO distribution) which has the form

$$f(x) = e^{\beta_0 x}\cdot 2\beta_0\left(\beta_0 x + 1 + \frac{1}{3\beta_0 x} + \ldots\right). \qquad (4.64)$$

In the opposite limit $x \to 0$ ($n \ll \bar{n}$) large β dominate where due to eq. (4.63a)

$$Z(\beta)_{|\beta|\gg 1} \approx \exp(-1/2\ \ln^2\beta/c).$$

Evaluating Mellin integral (4.49) one has roughly

$$f(x)_{x\to 0} \sim 1/x\cdot\exp(-1/2\ \ln^2 x), \qquad (4.65)$$

which reflects the form factor damping of the low multiplicity events.

There exists another way of dealing with the KNO distribution which does not appeal to the Mellin

representation and might appear to be useful for the future more delicate analysis of the KNO phenomenon with account of nonleading corrections. The idea is to accumulate an information about discrete moments f_k (i.e. normalized multiplicity correlators) into the compact nonlinear equation for the distribution $f(x)$ itself. This equation reads

$$x\,f(x) = \int_0^x dy\ f(x-y)\int_y^{\infty} dt\ f(t)\ \ln t/y. \qquad (4.66a)$$

Different methods can be used to derive it. We shall restrict ourselves here by noticing that one can simply check its validity applying $\left[\int_0^{\infty} dx\ x^{k-1}\right]$ operation, which results in the known recurrency relations (4.58).

Let us remind the reader that $f(x)$ corresponds to the KNO distribution in a single gluon jet. For a general case ($\varrho \neq 1$) the function $f^{(\varrho)}(x)$ can be found from the subsequent equation analogous to (4.66a)

$$x\,f^{(\varrho)}(x) = \int_0^{\varrho x} dy\ f^{(\varrho)}(x-y/\varrho)\int_y^{\infty} dt\ f(t)\cdot\ln t/y. \qquad (4.66b)$$

Concluding the discussion of the QCD KNO phenomena let us emphasize once more that one should not be 'too optimistic' to apply the DL formulae to the direct comparison with experimental data. The point here is that except the standard long-lived problem with non-PT hadronization dynamics the purely PT Single Logarithmic(SL) corrections appear to be of crucial importance for the quantitative QCD predictions.

As we shall see in the next Sec., the SL contributions coming mainly from an account of the recoil effects give sizable preasymptotic corrections to the KNO distributims

$$f^{DLA}(x) = \lim_{Q^2\to\infty} f^{MLLA}(x, \sqrt{\alpha_s(Q^2)}). \qquad (4.67)$$

The Q^2-dependence appears to be too weak to lead to any testable violation of the KNO scaling, however the shape

of real multiplicity distributions in HPs, due to the SL effects, will remain to be far from its true asymptotical DL limit 'forever'.

Concluding this Subsec. let us draw the reader attention to the point that the Fadin equation (4.66) (nonlinear integral selfcontained equation for f(x)) seems to be too nice to have no direct clear physical explanation basing on the theory of Markov processes.

4.6. Inclusive Particle Spectra in DLA [25]

Applying the operator (4.36) to the product of the jet functionals (4.39) one can obtain and solve the integral equations for inclusive spectra (N=1) and correlations ($N \geqslant 2$) of the bremsstrahlung particles, following from the Master equation (4.35).

Here we list for illustration the DL formulae for the spectrum of gluons with rapidity

$$y = \ln \omega/Q_0, \qquad 0 \leqslant y \leqslant Y = \ln E_{jet}/Q_0$$

from the q-jet (for g-jet $C_F/C_V \mapsto 1$), keeping α_s fixed which makes it possible to derive simple analytical expressions ($a^2 = 2C_V \alpha_s/\pi = \text{const}$, I_ν stands for the modified Bessel functions).

1) Energy distribution (hump-backed plateau)

$$\frac{dn(y,Y)}{dy} = C_F/C_V \cdot a \cdot \left(\frac{y}{Y-y}\right)^{1/2} \cdot I_1\left(2a\sqrt{(Y-y)y}\right). \quad (4.68)$$

2) Double-differential distribution can be presented as

$$\frac{dn}{dy\, d\ln\theta} = d/d\ln\theta \left(\frac{dn(y_\theta, Y_\theta)}{dy}\right), \quad (4.69)$$

where $y_\theta = y - \ln 1/\theta > 0$, $Y_\theta = Y - \ln 1/\theta$: (4.70)

$$\frac{dn}{dy\, d\ln\theta} = C_F/C_V \cdot a^2 \cdot I_0\left(2a\sqrt{(Y-y)y_\theta}\right). \quad (4.71)$$

3) Angular distribution one derives integrating eq.(4.71)

over y:

$$dn/d\ln\theta = C_F/C_V \cdot a\ sh\ (a\ Y_\theta). \quad (4.72)$$

The total multiplicity of bremsstrahlung gluons, as it follows trivially from eq. (4.72), reads

$$n^{tot}(Y) = \varsigma \cdot (ch\ (a\ Y) - 1). \quad (4.73)$$

This expression solves the differential equation

$$\left(d^2/dY^2\right) n(Y) = a^2\ (1 + n\ (Y)) \quad (4.74)$$

with the boundary conditions $n(0) = n'(0) = 0$ (cf.(4.56a)).

4.7. ς -Scaling [26]

It is interesting to notice that certain characteristics of final states exhibit a kind of new scaling behaviour when one arrives at the well-developed partonic cascades with increase of the hardness of HP. Let us illustrate this statement by two examples starting with the study of the shape of the inclusive energy spectrum.

The DLA energy distribution of gluons, with account of the running coupling $\alpha_s(k^2) = 2\pi/b\ln k_\perp/\Lambda$, can be shown to have the following Mellin representation:

$$\bar{D}(y,Y) = \iint \frac{d\alpha\, d\beta}{(2\pi i)^2} e^{\alpha(Y-y)+\beta Y} \cdot (Y+\lambda) \int_0^\infty \frac{ds}{\beta+s} \left(\frac{\alpha}{\beta}\cdot\frac{\beta+s}{\alpha+s}\right)^{\frac{A^2}{4(\alpha-\beta)}} \cdot e^{-\lambda s} \quad (4.75)$$

where $A^2 = 16C_V/b$ (= 16/3 for $n_f = 3$), $\lambda = \ln Q_0/\Lambda$. Evaluating the integrals by the steepest descent method and neglecting for the sake of simplicity a preexponential factor one obtains

$$\bar{D}(y,Y) \simeq \exp f(y,Y) = \exp \varphi(\alpha_0(y,Y), \beta_0(y,Y), y, Y), \quad (4.76)$$

where

$$\varphi(\alpha,\beta,y,Y) = \alpha(Y-y) + \beta y + \frac{A^2}{4(\alpha-\beta)} \ln \frac{\alpha(\beta+s_0)}{(\alpha+s_0)\beta} - \lambda s_0, \quad (4.76a)$$

$$s_0 = \frac{1}{2}\left(\sqrt{A^2/\lambda + (\alpha-\beta)^2} - (\alpha+\beta)\right).$$

Functions $\alpha_0(y,Y)$, $\beta_0(y,Y)$ must be found from

$$\frac{\partial\varphi}{\partial\alpha} = \frac{\partial\varphi}{\partial\beta} = 0 . \qquad (4.77)$$

Introducing new convenient variables μ, ν through

$$\alpha_0 = \frac{1}{2}\frac{A}{\sqrt{Y+\lambda}} e^{\mu} \quad , \quad \beta_0 = \frac{1}{2}\frac{A}{\sqrt{Y+\lambda}} e^{-\mu} ,$$
$$\alpha_0 + s_0 = \frac{1}{2}\frac{A}{\sqrt{\lambda}} e^{\nu} \quad , \quad \beta_0 + s_0 = \frac{1}{2}\frac{A}{\sqrt{\lambda}} e^{-\nu} , \qquad (4.78)$$

one can resolve eqs. (4.77) to obtain (4.79)

$$\ln \bar{D}(y,Y) \approx f(y,Y) = A\,(\sqrt{Y+\lambda} - \sqrt{\lambda}\,)\,\frac{\mu-\nu}{sh\mu - sh\nu},$$

where μ,ν obey the following equations

$$\frac{2y-Y}{Y} = \frac{(sh2\mu - 2\mu) - (sh2\nu - 2\nu)}{2(sh^2\mu - sh^2\nu)} , \qquad (4.79a)$$

$$\frac{sh\,\nu}{\sqrt{\lambda}} = \frac{sh\mu}{\sqrt{Y+\lambda}} .$$

It can be easily seen that the maximum of $\bar{D}$ corresponds to $y = 1/2\cdot Y$ ($\nu = \sqrt{\frac{\lambda}{Y+\lambda}}\,\mu$ = 0). Expanding (4.79) near this point one can reproduce the known formule for the shape of the hump

$$\bar{D}(y,Y) \underset{y\approx Y/2}{\sim} \exp\Big(-\frac{3}{2} A \frac{(y - Y/2)^2}{(Y+\lambda)^{3/2} - \lambda^{3/2}}\Big), \qquad (4.80)$$

$A = 4\sqrt{C_V/b}$.

It is interesting to note that the general expression (4.79) exhibits a kind of a new asymptotical 'scaling law'[55], namely

$$\frac{\ln \bar{D}(y,Y)}{\ln \bar{D}_{max}} \approx \frac{\ln \bar{D}(y,Y)}{\ln \bar{n}(Y)} \underset{Y\gg\lambda}{\approx} F(y/Y). \qquad (4.81)$$

Indeed, keeping $\zeta \equiv y/Y$ fixed we have $\nu \ll \mu$ for $Y \gg \lambda$ so that $F(\zeta)$ reduces to

$$F(\zeta) = \frac{\mu}{sh\mu} \quad , \quad \text{where} \quad 2\zeta - 1 = \frac{sh2\mu - 2\mu}{2sh^2\mu}. \qquad (4.82)$$

As we have already mentioned above, the restriction

$\lambda = \ln Q_0/\Lambda \gg 1$ had to be imposed for the formal applicability of the PT considerations. For this reason the inequality $Y \gg \lambda$ might seem to be too 'academic'. However the shape of the inclusive spectrum according to the approximate relation (4.79) turns out to be 'infrared stable' in a sense, i.e. it has a final limit with $\lambda \to 0$ ($\alpha_s(Q_0) \to \infty$ formally!).

Later we shall discuss this property in detail in the context of the MLLA. Here let us notice that the insensitivity of the spectrum to the Q_0 value at large Y makes it reasonable to compare spectra of different hadrons in the ζ-scale. For such an attempt see ref. [41].

The second example illustrating ζ-scaling concerns the two-particle energy correlator:

$$\frac{\omega_1\omega_2}{\sigma}\frac{d^2\sigma}{d\omega_1 d\omega_2} = \Big(\frac{\omega_1}{\sigma}\frac{d\sigma}{d\omega_1}\Big)\Big(\frac{\omega_2}{\sigma}\frac{d\sigma}{d\omega_2}\Big)\times$$
$$\Big[1 + \frac{C_V}{2C_F}\cdot\frac{1}{1+2ch(\mu_1-\mu_2)}\Big] , \qquad (4.83)$$

where $\mu_i = \mu(y_i,Y)$ are determined by eq. (4.79a). The dispersion of the correlator should exhibit therefore ζ-dependence

$$D^2 = \frac{C_V}{6C_F}\cdot\frac{1}{1 + \frac{4}{3}\,sh^2\Big(\frac{\mu(\zeta_1)-\mu(\zeta_2)}{2}\Big)} \qquad (4.84)$$

in high energy limit $Y \gg \lambda$.

5. MODIFIED LEADING LOG APPROXIMATION [17]

This Section is devoted to the description of the PT approach which has been designed to describe quantitatively soft particle spectra ($x \ll 1$), following the logic of the famous Gribov-Lipatov-Altarelli-Parisi(GLAP) approach

to DIS and e^+e^- structure functions in hard momenta region ($x \sim 1$) [1-3]. The standard LLA being equivalent in fact to the renorm-group (RG) approach, is known to maintain a clear probabilistic picture of the jet development via the chain of elementary parton branchings $A \to B(z) + C(1-z)$

$$dw_A^{BC} = \frac{\alpha_s(k_\perp^2)}{2\pi} \Phi_A^{BC}(z)\, dz\, \frac{d\theta}{\theta} \quad . \qquad (5.1)$$

Within the LLA accuracy the evolution parameter which separates sequential partonic decays could be chosen in different ways. So, at $x \sim 1$ ($z_i \sim 1$) the strong ordering of parton virtualities k_i^2 or of transverse momenta of products $k_{\perp i}$ or of decay angles θ_i worked equally well. As we know now from the DLA experience, the <u>angular</u> ordering proves to be correct for soft gluon cascades.

Constructing the probabilistic scheme with account of both the DL and the essential SL effects one has to pay for better accuracy of the approximation by the tremendous growth of the number of interference contributions which must be analysed and interpreted. The interference graphs contain soft gluon lines connecting harder partons of quite different generations. Meanwhile, the very idea of a classical shower picture implies that the structure of elementary parton decays, i.e. the blocks for building up the partonic cascade, should depend on just the nearest 'forefathers' of a considered parton. Thus the possibility to absorb all essential interference terms into the local probabilistic scheme is far from being obvious.

Even much more striking, therefore, looks the fact that such a scheme not only exists but proves to be (a posteriori!) a simple generalization of the standard LLA scheme. That is the reason to refer to this 'zero order' approximation (at $x \ll 1$) as the Modified LLA (MLLA).

To obtain the soft particle content of a jet within the MLLA one has to use the GLAP chains of two particle decays eq. (5.1) with

1) the LLA splitting functions $\Phi_A^{BC}(z)$ describing $g \to gg$, $q \to qg$ and $g \to q\bar{q}$ subprocesses [1],

2) $\alpha_s(k_\perp^2)$ prescription for a decay vertex, and

3) the <u>exact AO</u> $\theta_{i+1} \leq \theta_i$ (instead of the <u>strong AO</u> $\theta_{i+1} \ll \theta_i$ we have learned from the DLA).

Now let us concentrate on the last point.

5.1. Exact Angular Ordering

The basic idea of the shower approach is to 'exponentiate' sequential partonic decays separated by an appropriately chosen evolution parameter t

$$Z = C(\alpha_s(t)) \cdot \exp\left\{ \int^t \gamma(\alpha_s(t'))\, dt' \right\} \qquad (5.2)$$

and to study PT expansions for the 'coefficient function' $C(\alpha_s)$ and for the 'anomalous dimension' $\gamma(\alpha_s)$ in terms of probabilities of elementary partonic processes. Starting from the DLA probabilistic picture, where an account of QCD coherence has led to the strong AO, it seems natural to link the evolution parameter with the jet opening angle:

$$dt = \frac{d\theta}{\theta} \quad . \qquad (5.3)$$

This means that all the contributions, which are singular in the relative angle between partons, should be attributed to the evolution of a jet and must be absorbed in the exponential factor of eq.(5.2), whereas the regular residue factor C, being free of collinear ('mass') singularities, could be said to describe wide-angle partonic configurations ('multijet' contributions).

Successive terms of PT series for $\gamma(\alpha_s)$

$$\gamma = \sqrt{\alpha_s} + \alpha_s + \alpha_s^{3/2} + \alpha_s^2 + \ldots \qquad (5.4)$$

correspond to the increasing accuracy in description of

elementary partonic decays ($\theta_{ij} \ll 1$) and thus of the jet evolution; iterating the coefficient function

$$C = 1 + \sqrt{\alpha_s} + \alpha_s + \dots \qquad (5.5)$$

one would account for ensembles of increasing number of such jets with $\theta_{ij} \sim 1$ (some of which could be soft g--jets).

Structure of symbolical series (5.4), (5.5) might seem strange ($\sqrt{\alpha_s}$ as an expansion parameter!), but it is inherent in soft particle spectra and, as we shall see below, has clear mathematical basis.

The leading term in eq.(5.4) corresponds to the DLA for γ and originates from $g \to gg'$ decay as

$$\gamma_{DLA} = \int \alpha_s \cdot dz/z = \alpha_s \cdot l = \sqrt{\alpha_s}\,, \qquad (5.6)$$

where l denotes the 'longitudinal' log coming from the soft gluon emission. Eq. (5.6) shows, thus, that the soft log compensates one power of $\sqrt{\alpha_s}$ smallness in the expression for $\gamma(\alpha_s)$, effectively. Bearing in mind this rule we are ready now to estimate how do different partonic decays contribute to $\gamma(\alpha_s)$, in order to extract MLLA effects and analyse higher corrections.

a) Hard two-parton decays $A \to BC$ $(z \sim (1-z) \sim 1)$

$$\Delta\gamma = \int \alpha_s\, dz = \alpha_s\,. \qquad (5.7a)$$

b) Z-dependence of coupling in a soft radiation

$$A \to A\,g' \quad \left(\Delta\alpha_s = \alpha_s(Q^2) - \alpha_s(Q^2 z) \backsim \alpha_s^2 \ln z\right)$$
$$\Delta\gamma = \int \Delta\alpha_s \frac{dz}{z} = \int (\alpha_s^2 \ln z)\frac{dz}{z} = \alpha_s^2 l^2 = \alpha_s\,. \qquad (5.7b)$$

c) Three-parton soft decays $A \to Ag'g''$

$$(k'' \ll k' \ll k_A,\ \theta' \sim \theta'')$$
$$\Delta\gamma = \int \alpha_s^2 \frac{dz_1}{z_1}\frac{dz_2}{z_2} = \alpha_s^2 l^2 = \alpha_s\,. \qquad (5.7c)$$

The three contributions (5.7) define the MLLA correction to $\gamma(\alpha_s)$:

$$\gamma_{MLLA} = \sqrt{\alpha_s} + \alpha_s\,. \qquad (5.8)$$

The SL term (5.7a) corresponds to a loss of the energy-log and can be taken into account by the specification of the z-dependence of splitting functions:

$$4C_A\, dz/z \longrightarrow \Phi_A^{BC}(z)\, dz. \qquad (5.9)$$

Similarly, the MLLA correction (5.7c) describes a loss of one angle-log and needs the angular pattern of multiple soft gluon production to be analysed in detail:

$$\{\theta_{i+1} \ll \theta_i\} \longrightarrow V(\vec{n}). \qquad (5.10)$$

This problem will be studied in the Subsec. 5.3 where we shall construct the exact 'angular kernel' $V(\vec{n})$ (an analog of the exact energy kernels $\Phi_A^{BC}(z)$):

$$dW_A^{BC} = \frac{\alpha_s(\kappa_\perp^2)}{2\pi}\, \Phi_A^{BC}(z)\, V(\vec{n})\, dz\, \frac{d\Omega}{8\pi} \qquad (5.11)$$

$$V_{f(g)}^{s}(\vec{n}) = \frac{a_{sg} + a_{fg} - a_{sf}}{a_{sf}\, a_{sg}}, \quad a_{ik} \equiv 1 - (\vec{n}_i\vec{n}_k),$$

where subscripts are referred to the gluon - 'son' (s), its'father' (f) and'grandpa' (g).

Noticing that the integral over S-direction at $\theta_{sf} \ll \theta_{fg}$, $V(\vec{n}) = 2/a_{sf}$ is

$$\int \frac{d\Omega}{8\pi} V(\vec{n}) \simeq \int \frac{d\theta_{sf}}{\theta_{sf}} \qquad (5.12a)$$

and at large emission angles $\theta_{sf} \gg \theta_{fg}$, $V(\vec{n}) \backsim 1/\theta_{sf}^3$

$$\int \frac{d\Omega}{8\pi} V(\vec{n}) \backsim \int \frac{d\theta_{sf}}{\theta_{sf}^2} = const\,, \qquad (5.12b)$$

one concludes that the kernel (5.11) reproduces the AO restriction within the DLA accuracy and gives a definite prescription for account of the $\theta_{sf} \sim \theta_{fg} \sim \theta_{sg}$ region (cf. eq. (5.7c)). To see that this prescription is nothing but the exact AO, the reader is advised to check the following nice property of the V-kernel:

$$\langle V^s_{f(g)}(\vec{n})\rangle_{\substack{\text{azimuth}\\ \text{average}}} \equiv \int_0^{2\pi} \frac{d\varphi_{s(f)}}{2\pi} V^s_{f(g)}(\vec{n}) = \frac{2}{a_{sf}}\,\vartheta(a_{fg}-a_{sf})\ , \tag{5.13}$$

where ϑ denotes the step function. This means that the decay probability (5.11) integrated over the azimuth of 's' (around 'f') results in the logarithmic θ-distribution (5.12a) inside the parent cone $\theta_{sf} \leqslant \theta_{fg}$ and vanishes outside. It is important to emphasize that the 'V-scheme' (5.11) proves to eliminate not only $A \to Ag'g''$ ($\Delta\gamma = \alpha_s$) but also $A \to Ag'g''g'''$ ($\Delta\gamma = \alpha_s^{3/2}$) elementary splitting process, factorizing them into the chains of two-parton decays completely. The first specific soft contribution, arising only in the 4^{th} loop, corresponds to subtle interferences between a parent and its four offsprings ordered in energy (with all emission angles of the same small value), contributes to $\Delta\gamma \sim \alpha_s^2$, happens to have an anomalous ($1/N_c^2$ suppressed) colour factor ('colour monster') and can be interpreted physically in terms of the 'colour polarizability' of a jet (Subsec.5.4).

First soft corrections to $C(\alpha_s)$ eq.(5.5) correspond to '4 jet' $e^+e^- \to q\bar{q} + g'g''$ ($\Delta C = \alpha_s$), '5-jet' $e^+e^- \to q\bar{q} + g'g''g'''$ ($\Delta C = \alpha_s^{3/2}$) events etc. They might be interpreted as multipole interactions between jets: 'colour charge-dipole', 'dipole-dipole' and so on (see Subsec. 5.3).

5.2. MLLA Master Equation

The exact AO makes it possible to construct simple evolution equation for GF. The system of two coupled equations for the quark (Z_F) and gluon (Z_G) functionals reads (A,B,C = F,G)

$$Z_A(E,\theta;u(k)) = e^{-W_A(E\theta)}\,u_A(k^\circ=E) + \tag{5.14}$$

$$\frac{1}{2}\sum_{B,C}\int_0^\theta \frac{d\theta'}{\theta'}\int_0^1 dz\; e^{-W_A(E\theta)+W_A(E\theta')}\,\frac{\alpha_s(k_\perp^2)}{2\pi}\,\Phi_A^{BC}(z)\,Z_B(zE,\theta';u)\,Z_C((1-z)E,\theta';u).$$

The first term in r.h.s. corresponds to the (form factor damped) situation when the A-jet (with energy E and opening angle θ) consists of the parent parton only. The integral term describes the first splitting $A \to BC$ with angle θ' between the products. The exponential factor provides this decay being the first one indeed: it is the probability to emit nothing in the angular interval between θ and $\theta'(\leqslant\theta)$. The two last factors account for the further evolution of produced subjets having smaller energies and θ' as the opening angle. The MLLA form factors W_A are the following (cf.eqs. (4.28) - (4.30)):

$$W_F = \int_0^\theta \frac{d\theta'}{\theta'}\int_0^1 dz\;\frac{\alpha_s(k_\perp^2)}{2\pi}\,\Phi_F^F(z)\quad,\quad (F=q,\bar{q})\ , \tag{5.15}$$

$$W_G = \int_0^\theta \frac{d\theta'}{\theta'}\int_0^1 dz\;\frac{\alpha_s(k_\perp^2)}{2\pi}\left[\frac{1}{2}\Phi_G^G(z) + n_f\Phi_G^F(z)\right].$$

The transverse momentum of partons in eqs. (5.14),(5.15) is bounded from below as usual:

$$k_\perp \approx E\cdot z\cdot(1-z)\theta' > Q_0. \tag{5.16}$$

Differentiating the product $\exp W_A(E\theta)\cdot Z_A(\theta)$ over θ and using eqs.(5.15) one can derive the Master equation which is free from the DL form factors (cf. eq.(4.35)):

$$\frac{d}{d\ln\theta}Z_A(E,\theta) = \frac{1}{2}\sum_{B,C}\int_0^1 dz\,\frac{\alpha_s(k_\perp^2)}{2\pi}\,\Phi_A^{B,C}(z)\,\times$$
$$\left[Z_B(zE,\theta)\,Z_C((1-z)E,\theta) - Z_A(E,\theta)\right]. \tag{5.17}$$

The initial condition for this 'regularized' equation reads

$$Z_A(E,\theta;u(k))\Big|_{\theta=Q_0/E} = u_A(k^0=E) \quad . \qquad (5.18)$$

Readers are welcomed to derive the DLA eq. (4.35) from MLLA eq.(5.17) bearing in mind slightly different normalization: $Z_G^{MLLA} \to u\, Z^{DLA}$.

Notice, that the GFs (5.14) have correct normalization of eq.(4.38).

All the properties of the parton system produced in e^+e^- annihilation with total energy $W = 2E$ are described in the MLLA by the GF

$$Z_{e^+e^-}\{u\} = (Z_F(E,\theta;u(k)))^2\Big|_{\theta=\pi} \quad . \qquad (5.19)$$

When expanding beyond the MLLA range some additional correction terms $\sim Z^3$, Z^4 etc. should appear in r.h.s. of the evolution equation (5.15) as well as in eq.(5.19).

5.3. V-Scheme for Gluon Cascades

Our intention now is to analyse the angular pattern of multiple soft gluon production

$$e^+e^- \to q_+\bar{q}_- + g_1g_2\cdots g_N$$

in order to formulate the probabilistic scheme of cascading (V-scheme, see Subsec. 5.1).

Studying the system of gluons with strongly ordered energies (eq.(4.1)) one can apply successively the factorization property (soft insertion rules) to build up the tree amplitude (5.20)

$$M^{(N)} = \sum_i \frac{(e_N k_i)}{(k_N k_i)}\, g_s T_i \cdot M^{(N-1)}, \quad i = +, -, 1, \ldots (N-1),$$

where T_i is an appropriate colour generator. This amplitude gives rise to the N-particle exclusive cross section

$$d\sigma^{(N)} \sim |M^{(N)}|^2 \prod_{i=1}^N \frac{d^3k_i}{2\omega_i} = \qquad (5.21)$$

$$\sigma^{(N)}(\{\vec{n}_i\}) \prod_{i=1}^N \frac{\alpha_s}{2\pi}\,\frac{d\omega_i}{\omega_i}\,\frac{d\Omega_i}{2\pi}$$

with the maximum power of energy logs. Looking for the same power of θ-logs in the DLA context (Sec. 4) we have proved that the angular factor $\sigma(\{\vec{n}_i\})$ corresponded to probabilistic cascade with strong AO. Now we have to analyse $\sigma(\{\vec{n}_i\})$ more carefully to show that the V--scheme (eq.(5.11)) keeps trace of subleading θ-logs as well.

The amplitude (5.20) is gauge invariant. However it proves to be convenient to make use of the planar gauge connected with the cms of the process (eq.(4.3)) which kills the interference between '+' (q) and '-' ($\bar{q}$) and reduces the number of diagrams contributing to $\sigma(\{\vec{n}_i\})$. The number of topologically nonequivalent Feynman graphs for $\sigma^{(N)}(\{\vec{n}_i\})$ could be estimated as

$$\ell_N \geqslant \frac{1}{2}\prod_{m=1}^N \frac{m(m+3)}{2}$$

$= 1, 5, 45, \sim 700\ldots$ for $N=1,\ldots,4\ldots$

The gluon 'i' connecting two harder lines 'l' and 'm' of A and A^+ introduces the factor (5.22)

$$I^i_{lm} = (k_in)^2\frac{k_{l\mu}\,d_{\mu\nu}(k_i)\,k_{m\nu}}{(k_lk_i)(k_mk_i)} = \frac{a_{il}+a_{im}-a_{lm}}{a_{il}\,a_{im}}$$

for $l \neq m$ (Interference terms), and

$$H^i_l \equiv I^i_{ll} = \frac{(k_in)^2}{(k_lk_i)^2}(k_{l\mu}d_{\mu\nu}(k_i)k_{l\nu}) = \frac{2}{a_{il}} \qquad (5.23)$$

for $l = m$ ('self-energy' graph).

5.3.1. Conditional probability V and 'interference remainder'

N = 1. $\sigma^{(1)} = C_F(H_+^1 + H_-^1)$ (5.24)

can be treated naturally as a sum of probabilities of independent q_1 radiation by q and $\bar{q}$.

N = 2. Let us list all the contributions related to q_1 radiation by q : (5.25)

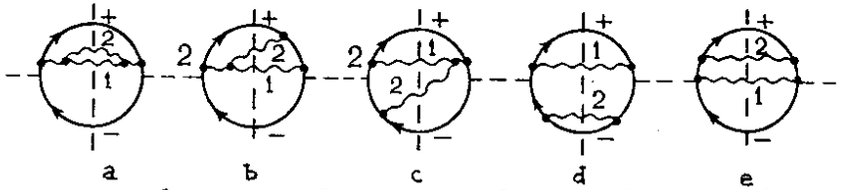

$$C_F C_V H_+^1 H_1^2 + C_F C_V H_+^1 (-I_{1+}^2) + C_F C_V H_+^1 (-I_{1-}^2) + C_F^2 H_+^1 H_-^2 + C_F^2 H_+^1 H_+^2$$

The other part (g_1 off $\bar{q}$) can be obtained via symmetrization $\{'+' \leftrightarrow '-'\}$. Two colour structures C_F^2 and $C_F C_V$ have appeared. The C_F^2 terms (5.25 d, e) describe independent radiation of two gluons by q and $\bar{q}$.

The contributions with $C_F C_V$ factor are the material for constructing the kernel $V(\vec{n}_2)$ determining the cascade '+' $\longrightarrow$ '1' $\longrightarrow$ '2'.

Graphs of eq.(5.25) have essentially different angular behaviour. The item (a) is singular both at $a_{21} \longrightarrow 0$ and at $a_{1+} \longrightarrow 0$. If g_2 is emitted at large angle $a_{2+} \approx a_{21} \gg a_{1+}$ then $I_{1+}^2 \approx H_1^2$ and items (a) and (b) cancel, leading to the AO. Contrary to (a) and (b), the item (c) has no singularity at all. Strictly speaking, the pole in I_{1-}^2 exists when, e.g., $a_{21} \to 0$: $I_{1-}^2 \backsim \sin\theta_{21}/a_{12} \sim 1/\theta_{12}$. But it is reasonable to think of this behaviour as nonsingular because such a pole gives no angle log contribution to the cross section. Cancellation of the singularity at $a_{1+} \longrightarrow 0$ ($H_+^1 - H_2^+$ factor) could be made obvious by rewriting $-I_{1-}^2 = D_{-[+1]}^2$, where

$$D_{l[m,n]}^i \equiv I_{lm}^i - I_{ln}^i \qquad (5.26)$$

could be called naturally the 'angular dipole'.

Such 'nonsingular' dependence on the angles between any pair of particles (i,j) we call in what follows the 'friability' of a contribution.

Less evident is another property of the item (5.25c) - namely the global integrability over directions of all the gluons involved. We shall call this property the 'ideality' of contribution. It means that the term contains no one angle log and corresponds, therefore, to configuration with all the angles being large: $\theta_{ij} \sim 1$. With help of the formula

$$\int \frac{d\Omega_i}{4\pi} I_{lm}^i = \ell n \frac{2}{a_{lm}} \qquad (5.27)$$

one obtains for the item (c)

$$\int \frac{d\Omega_2}{4\pi} \int \frac{d\Omega_1}{4\pi} H_+^1 D_{-[+1]}^2 = \int_0^1 \frac{dx}{1-x} \ell n x = -\zeta(2) = -\frac{\pi^2}{6}. \qquad (5.28)$$

The ideality of (5.25c) is a reason to consider this term as the 'remainder' (R), excluding it from the definition of $V(\vec{n})$ (i.e. V = (5.25a) + (5.25b)):

$$V_{1(+)}^2 = H_1^2 - I_{1+}^2 = \frac{a_{2+} + a_{1+} - a_{21}}{a_{21}\, a_{2+}}. \qquad (5.29)$$

Finally, $\sigma^{(2)}$ has the following representation:

$$\sigma^{(2)} = P^{(2)} + R^{(2)}. \qquad (5.30)$$

The contribution $P^{(2)}$ corresponds to the probabilistic scheme (5.31)

$$P^{(2)} = C_F^2 (H_+^1 + H_-^1)(H_+^2 + H_-^2) + \{C_F H_+^1 C_V V_{1(+)}^2\}_{sym(\pm)}.$$

The remainder reads: (5.32)

$$R^{(2)} = \{C_F C_V H_+^1 D_{-[+1]}^2\}_{sym(\pm)} =$$

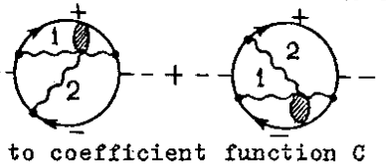

This is the soft correction to coefficient function C we have discussed above in Subsec. 5.1. As we shall show below in Subsec.5.5, this dipole term contributes to

inclusive jet characteristics as $O(\alpha_s)$ and happens to be, therefore, beyond the MLLA scope.

$V^2_{1(+)}$ is the 'conditional probability' of the emission of a 'son' ('2') by a 'father' ('1') up to 'grandpa' ('+'). This saying gets clearness after the azimuthal integration of $\vec{n}_2$ around $\vec{n}_1$:

$$\int \frac{d\varphi_{2(1)}}{2\pi} \frac{1}{a_{2+}} = \frac{1}{|a_{1+} - a_{2+}|} , \qquad (5.33)$$

$$\int \frac{d\varphi_{2(1)}}{2\pi} V^2_{1(+)} = \frac{1}{a_{21}} \left(1 + \frac{a_{1+} - a_{21}}{|a_{1+} - a_{21}|} \right)$$

which leads to the exact AO, see eq. (5.13).

5.3.2. Test of V-scheme in higher orders

N=3. Let us write down the main probabilistic part $P^{(3)}$ accounting for the processes of independent and cascade radiation:

$$P^{(3)} = P^{(3)}_o + P^{(3)}_1 + P^{(3)}_2 \qquad (5.34)$$

$$P^{(3)}_o = C_F^3 (H^1_+ + H^1_-)(H^2_+ + H^2_-)(H^3_+ + H^3_-) ,$$

$$P^{(3)}_1 = C_F^2 C_V H^1_+ \Big[(H^2_+ + H^2_-) V^3_{1(+)} + (H^2_+ V^3_{2(+)} + H^2_- V^3_{2(-)}) + V^2_{1(+)} (H^3_+ + H^3_-) \Big]_{sym(+-)} ,$$

$$P^{(3)}_2 = C_F C_V^2 H^1_+ \Big[V^2_{1(+)} V^3_{1(+)} + V^2_{1(+)} V^3_{2(1)} \Big]_{sym(+-)} .$$

Each of $P_i^{(3)}$ corresponds to a certain number of gluon emissions: $P_i^{(N)} \backsim C_F^{N-i} C_V^i$. $P_o^{(3)}$ is clearly independent radiation of '1', '2', '3' by q_+, $\bar{q}_-$. $P_1^{(3)}$ describes the contribution of the three similar processes ($H^i_{+-} \equiv H^i_+ + H^i_-$):

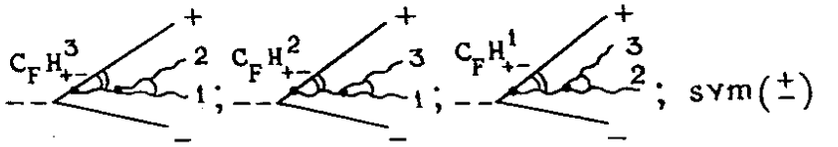

$P^{(3)}_2$ includes the independent radiation of '2' and '3' by '1', which is restricted by direction of their common 'grandpa' '+', as well as the ordered cascade '+' → '1' → '2' → '3' :

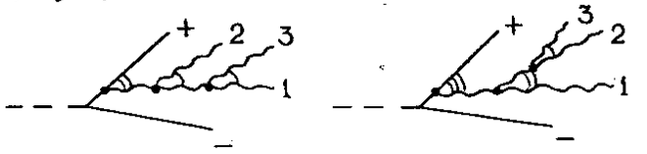

The remainder $R^{(3)}$ contains the two different types of contributions:

$$R^{(3)} = R^{(3)}_\alpha + R^{(3)}_\beta . \qquad (5.35)$$

(α) - the 'winding' g_3 round the remainder $R^{(2)}$ of the previous order ($R^{(3)}_\alpha = (R^{(2)})'$). ($\beta$) - the new irreducible interference structures.

The contributions of Fig.11 contain the collinear divergencies and start the evolution of each of the four jets forming the dipole $R^{(2)}$. The interferences

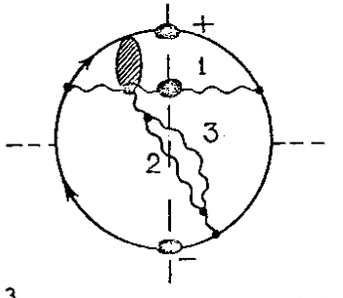

Fig.11. Radiation of g_3 by the 'dipole leg' g_2. Black circles show other possible singular insertions.

I^3_{ik} between partons of the dipole might be absorbed into $R^{(3)}_\alpha$ as well. These interferences do not spoil the 'friability' and 'ideality' of the remainder and lead to

'next-to-next order' correction to coefficient function C.

The evolution picture of the dipole can be finished by extraction from the remainder a few other singular terms which are topologically identical to those of Fig.11, but correspond to different order of gluon energies. Indeed, a gluon, dressing '+', '-' and '1' partons in the final state, could be not only the softest one among the three (as marked by black points in Fig.11), but might have intermediate or even the largest energy (for the emissions off '+' and '-'). E.g., recombining two interference diagrams, not matched by $P^{(3)}$ (eq. (5.34)), one obtains such a contribution:

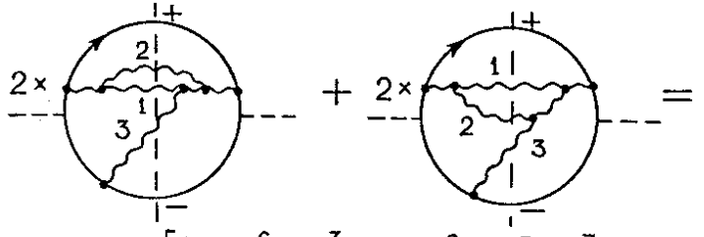

$$C_F H_+^1 C_V H_1^2 \left[\left(C_V - \frac{C_V}{2} \right) D^3_{-[+1]} + \frac{C_V}{2} D^3_{-[+2]} \right] =$$

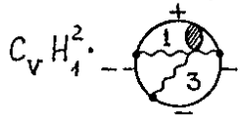

$$+ C_F \frac{C_V^2}{2} H_+^1 H_1^2 D^3_{-[12]} \quad . \qquad (5.36)$$

The first term here is singular at $a_{12} \to 0$ and corresponds to the dressing of the dipole rung ('1') by the gluon ('2'), harder than the 'dipole leg' ('3'). The second term in eq.(5.36) has no a_{12} singularity and has to be combined with a similar one, arising from (5.37)

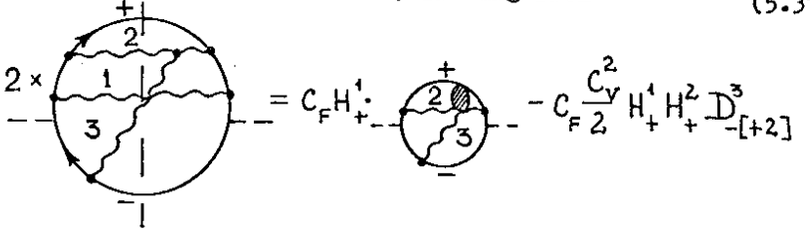

to form a new friable structure:

$$1/2 \cdot C_F C_V^2 H_+^1 \left(H_1^2 D^3_{-[12]} - H_+^2 D^3_{-[+2]} \right). \qquad (5.38)$$

To prove the ideality of this remainder it is convenient to convert eq. (5.38) into the sum of three contributions which might be thought of as dipole interaction of the parton '-' with the AO group '+','1' and '2':

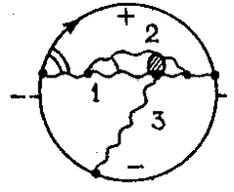

$$= \frac{1}{2} C_F C_V^2 H_+^1 V^2_{1(+)} D^3_{-[12]} \qquad (5.39)$$

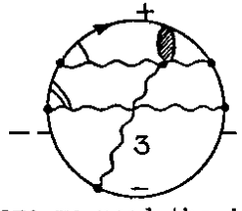

$$= -\frac{1}{2} C_F C_V^2 H_+^1 V^2_{+(1)} D^3_{-[+2]} + \{1 \leftrightarrow 2\}. \qquad (5.40)$$

Here we used the identity

$$H_+^1 I^2_{+1} = H_+^2 V^1_{+(2)} \qquad (5.41)$$

that is easy to check. Notice, the symmetry of eq.(5.40) allows one to remove the energy order between gluons '1' and '2'.

The first term of eq.(5.37) together with (5.42)

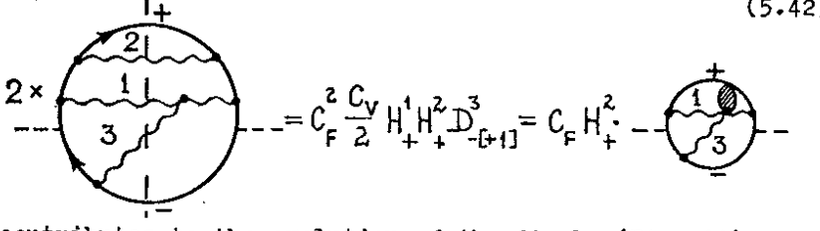

contributes to the evolution of the dipole (Fig. 11).

Dealing analogously with interference diagrams containing the factors $H_+^1 H_-^2$ and $H_-^1 H_+^2$ one singles out

the missing contributions necessary for the total 'dressing' of $R^{(2)}$. The corresponding remainder ($R^{(3)}_\beta$) looks like dipole-dipole interaction between jets (5.43)

$$= C_F \frac{C_V^2}{2} H_+^1 H_-^2 \left(D^3_{2[+1]} - D^3_{-[+1]} \right) + \{1 \leftrightarrow 2\}$$

and proves to be 'ideal' as well.

An additional series of $R^{(3)}_\beta$ comes from the dipole interaction inside jet. It originates after removing the interference terms, necessary for $P^{(3)}$, from the diagrams of the type of Fig.12. This procedure being executed,

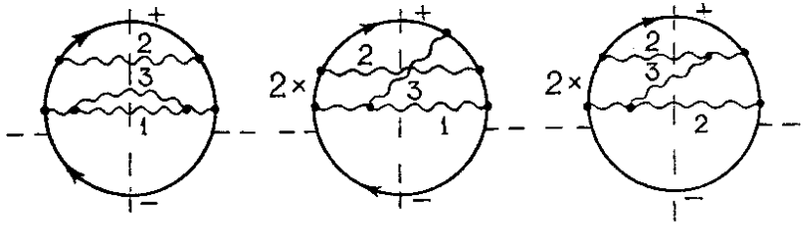

$$C_F^2 C_V H_+^1 H_+^2 H_1^3 \quad -2C_F \left[C_F - \frac{C_V}{2} \right] \frac{C_V}{2} H_+^1 H_+^2 I^3_{1+} \quad -2C_F \left(\frac{C_V}{2} \right)^2 H_+^1 H_+^2 I^3_{12}$$

Fig.12. Extraction of dipole interaction inside quark jet.

one obtains (5.44)

$$\Delta R = 1/2 \cdot C_F C_V^2 H_+^1 (H_+^2 D^3_{1[+2]} + H_1^2 D^3_{+[12]} - 2 \cdot I^2_{+1} D^3_{+[12]}).$$

The expression in brackets vanishes at $a_{1+} \to 0$ ($I^2_{1+} \to H^2_+ \to H_1^2$), so the 'friability' is evident. To prove the 'ideality' of eq.(5.44) let us rewrite it in terms of cascade: (5.45)

$$\Delta R = \frac{1}{2} C_F C_V^2 H_+^1 \left(V^2_{+(1)} D^3_{1[+2]} + V^2_{1(+)} D^3_{+[12]} + I^2_{+1} D^3_{2[+1]} \right)$$

$$= \frac{1}{2} C_F C_V^2 \left[H_+^1 V^2_{1(+)} D^3_{+[12]} + \left(H_+^1 V^2_{+(1)} D^3_{1[+2]} + \{1 \leftrightarrow 2\} \right) \right].$$

On the last step we used the identity (5.41).

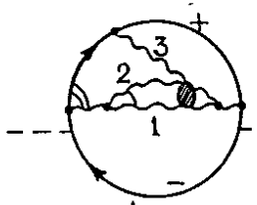

$$= \frac{1}{2} C_F C_V^2 H_+^1 V^2_{1(+)} D^3_{+[12]} \,, \qquad (5.46)$$

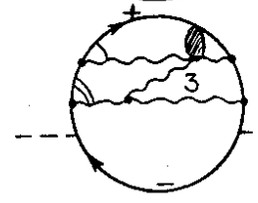

$$= \frac{1}{2} C_F C_V^2 H_+^1 V^2_{+(1)} D^3_{1[+2]} + \{1 \leftrightarrow 2\} \,, \qquad (5.47)$$

the 'ideality' of which is clear now. Notice, the symmetry of eq.(5.47) allows one to remove the energy order between '1' and '2' (compare with eq. (5.40)).

Let us summarize the result for

$$\sigma^{(3)}(\{\vec{n}_i\}) = P^{(3)} + (R^{(2)})' + R^{(3)}_\beta \,. \qquad (5.48)$$

The set of Feynman graphs splits into

1. the probabilistic part $P^{(3)}$ describing independent and cascade radiation of $g_1 g_2 g_3$ (V-scheme),
2. the first expansion term of the product of evolution exponents $Z_F^2 Z_{G'} Z_{G''}$ describing the dipole (5.32) $(R^{(2)})'$,
3. the new irreducible interference remainder (5.49)

$$R^{(3)}_\beta = (\text{Eq.(5.39)} + \text{Eq.(5.40)} + \text{Eq.(5.46)} + \text{Eq.(5.47)})_{\text{sym}(\pm)} + \text{Eq. (5.43)}.$$

The full angle integrals of the items of eq.(5.49) are, the following: (5.50)

$$\left(\prod_{i=1}^{3} \int \frac{d\Omega_i}{4\pi} \right) R^{(3)}_\beta = C_F \frac{C_V^2}{2} \zeta(3) \left[(0; -1; -2; -2)_{\text{sym}(\pm)}; 2 \right],$$

$$\zeta(3) = \frac{1}{2} \int_0^1 \frac{dx}{1-x} \ln^2 x \,.$$

The ideality (total integrability) of the remainder shows

that the V-scheme kept trace of all subleading (as well as leading) angular logs.

When constructing $P^{(N)}$, we dealt with consequtive emissions of gluons by the same 'father' as independent probabilities. For example: $C_F{}^3H_+{}^1H_+{}^2H_+{}^3$, $C_FC_V^2H_+^1V_{1(+)}^2V_{1(+)}^3$ etc. Keeping in mind further integration over azimuths, one could proceed to replace the energy ordering with the strict angular ordering of sequential emissions. For example,

$$H_+{}^1H_+{}^2 = H_+{}^1V_{+(1)}^2 + H_+{}^2V_{+(2)}^1 \qquad (5.51)$$

is a clear identity. Along this way the V-scheme gets natural generalization to incorporate hard partonic decays ($\omega_i \sim \omega_j$) described with use of $\Phi_A^{BC}(z)$ splitting functions. The resultant picture gets symbolical expression

$$\mathrm{EXP}\,(\alpha_s(k_\perp)\cdot\Phi\cdot V)\cdot(1 + R^{(1)}_{hard} + R^{(2)} + R^{(3)}_\beta + \ldots) \qquad (5.52)$$

where EXP denotes the evolution operator 'propagating' both the major $q\bar{q}$ configuration (first item in brackets) and the multijet ensembles $q\bar{q}g$, $q\bar{q}g'g''$, $q\bar{q}g'g'\,g'''$ etc.

Let us remark that the prescription $\alpha_s(k_\perp^2)$ which affects essentially soft g emission (see Subsec. 5.1) had been tested by the direct calculation of renormalization functions in the planar gauge [56] and by the analysis of 2-loop anomalous dimension in a soft limit (see, e.g., ref. [3]).

The first nonasymptotic exponentiating correction is connected with 3-particle hard decays $A \to BCD$ that give a single θ-log for the whole group ($\omega_g \sim \omega_c \sim \omega_D$). It could be extracted from the 2-loop analysis of γ (see, e.g., ref. [57]). The same order correction originates from soft 'colour monsters' mentioned above in Subsec. 5.1, which we are going to describe now.

5.4. Jet Polarizability and Colour Monsters

The V-scheme had been checked in the N=4 case as well. In few words, the procedure of the analysis would be the following. First, the necessary probabilistic part $P^{(4)}$ is constructed. Then the remainder is separated

$$R^{(4)} = R^{(4)}_\alpha + R^{(4)}_\beta, \quad \text{where } R^{(4)}_\alpha = (R^{(2)})'' + (R^{(3)}_\beta)'$$

accounts for evolution of previous remainder terms. Finally, the irreducible $R^{(4)}_\beta$ is 'dipolized' and acquires the 'friability'.

However $R^{(4)}_\beta$ happens to be 'nonideal' owing to specific interferences which have topology of a 'gluonic square' (see Fig. 13).

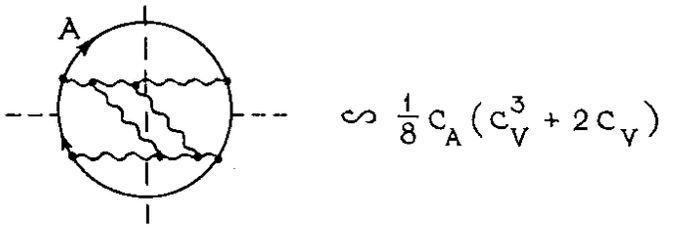

Fig.13. The diagram with nontrivial colour factor (the 'colour monster'). $C_A = C_F = 4/3$ for A=q, $C_A = C_V = 3$ for A=g.

It is only the contributions proportional to $C_A \cdot C_V$ which spoil the ideality.

The total 'monster' contribution to the cross section is clearly gauge-invariant since it has the unique colour structure. Therefore, the axial gauge $n_\mu = (k_-)_\mu$ can be chosen, where there are only 15 'monster' diagrams (lesser than in planar gauge). Three of them are shown in Fig.14. After the 'dipolization' is fulfilled the remainder is reduced to the AO cascade and the trick of eq.(5.41) is used to convert the interference I^2_{1+} to the conditional probability $V^1_{+(2)}$, one arrives at the clear result

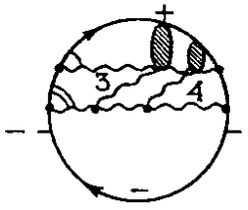

$$= C_F C_V H^1_+ V^2_{+(1)} D^3_{1[+2]} D^4_{1[+2]} + (1 \leftrightarrow 2), \quad (5.53)$$

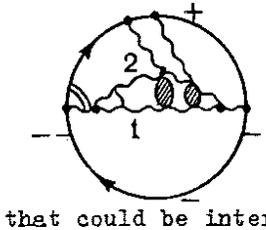

$$= C_F C_V H^1_+ V^2_{1(+)} D^3_{+[12]} D^4_{+[12]} , \quad (5.54)$$

that could be interpreted as the 'double-dipole' interaction inside a jet. Notice, the notations here are to be corresponded to the gauge $n = k_-$, e.g.,

$$I^{\,2}_{1+} \equiv \left\{1^{\,2}_{-}+\right\} = \frac{a_{1-}}{a_{21}a_{2-}} + \frac{a_{+-}}{a_{2+}a_{2-}} - \frac{a_{1+}}{a_{21}a_{2+}} , \quad (5.55)$$

$$V^{\,2}_{1(+)} \equiv \left\{+^{\,2}_{1}-\right\} = \frac{a_{1+}}{a_{21}a_{2+}} + \frac{a_{1-}}{a_{21}a_{2-}} - \frac{a_{+-}}{a_{2+}a_{2-}} . \quad (5.56)$$

Let us recall that in this gauge there is no soft emission off $\bar{q}_-$, and so the graphs of eqs.(5.53),(5.54) contain both the q_+-jet and the $\bar{q}_-$-jet contributions.

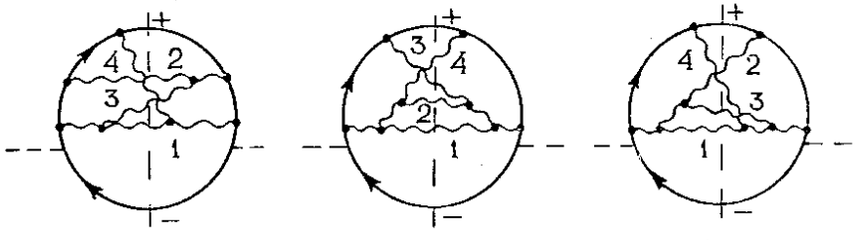

$-\frac{1}{4} C_F C_V$ (a) $\quad +\frac{1}{4} C_F C_V$ (b) $\quad -\frac{1}{4} C_F C_V$ (c)

Fig.14. Some of 'monster' graphs. Colour factor of the graph (c) depends on the position of '3' in interference between '1' and '2'.

Integrating the 'monster' (5.53) over angles one obtains the collinear divergency: (5.57)

$$\int \frac{d\Omega_1}{4\pi} \int \frac{d\Omega_2}{4\pi} \; H^1_+ V^2_{+(1)} \; \ln^2 \frac{a_{1+}}{a_{21}} =$$

$$\int_0^2 \frac{da_{1+}}{a_{1+}} \left[\int_0^1 \frac{dx}{1-x} \ln^2 x + \int_{\frac{a_{1+}}{2}}^1 \frac{dx}{1-x} \ln^2 \frac{1}{x} \right] =$$

$$4\zeta(3) \int_0^2 \frac{da_{1+}}{a_{1+}} + 6\zeta(4) .$$

Here we have used the planar gauge formulae for I and V since in the main contributing region $a_{1+} \sim a_{21} \sim a_{31} \sim a_{41} \ll 1$ Eqs. (5.55) and (5.56) could be reduced to the planar gauge expressions.

In the case of single D-interaction (5.46),(5.47) one would get the first power of log in the square brackets and hence the finite result (5.50). Singular 'monster' contributions of eqs.(5.53),(5.54) to the evolution exponent could be treated physically as an effect of 'polarizability': a parton interacts with the induced 'colour dipole moment' of some parton pair.

5.5. Magnitude of Dipole Corrections to Jet Characteristics

Let us evaluate the 'dipole contribution' of eq.(5.32) to the mean multiplicity of particles in e^+e^-annihilation. This contribution arises when the registered particle comes from the softest of 'dipole' jets (the 'dipole leg' g_2); other cuts are cancelled by corresponding virtual corrections. Hence one gets (5.58)

$$\Delta N_{e^+e^-}\left(E = \frac{W}{2}\right) = 2 C_F C_V \left(-\frac{\pi^2}{6}\right) \int^E \frac{dk_1}{k_1} \frac{\alpha_s}{2\pi} \int^{k_1} \frac{dk_2}{k_2} \frac{\alpha_s}{2\pi} N_G(k_2) ,$$

where $N_G(k_2)$ denotes the multiplicity originated from g_2. Here the integral over the directions of g_1 and g_2 (see eq. (5.28)) and the large opening angle of g_2-jet ($\theta_2 \sim 1$) were taken into account.

Differentiating the DLA equation for multiplicity[25,26]

$$N_G(\kappa\theta) = C_V \int^{\kappa} \frac{d\kappa'}{\kappa'} \int^{\theta} \frac{d\theta'}{\theta'} \frac{\alpha_s}{2\pi} N_G(\kappa'\theta') \qquad (5.59)$$

one gets for the inner integral of eq.(5.58)

$$\int^{\kappa_1} \frac{d\kappa_2}{\kappa_2} \frac{\alpha_s}{2\pi} N_G(\kappa_2) = \frac{1}{C_V} \frac{d}{d\ln\kappa_1} N_G(\kappa_1)$$

that leads to

$$\Delta N_{e^+e^-}(E) = -\frac{\pi^2}{6} 2C_F \frac{\alpha_s}{2\pi} N_G(E)\,(1+O(\alpha_s)) = -\frac{C_V\alpha_s}{2\pi}\frac{\pi^2}{6} N_{e^+e^-}. \qquad (5.60)$$

The result displays the relative smallness $\sim \alpha_s$ of a 'dipole' contribution to average characteristics of a process.

6. MLLA RESULTS FOR JET CHARACTERISTICS [17]

6.1. Correlators of Jet Multiplicity

Let us calculate the multiplicity correlators as the first example of exploiting the MLLA GF-technique.

Here we use the correlators normalized to the mean multiplicity of particles in a gluon jet $\bar n \equiv \langle n\rangle_{g\text{-jet}}$:

$$g_k = \langle n(n-1)\dots(n-k+1)\rangle_g/\bar n^k \quad , \quad g_0 = g_1 = 1, \qquad (6.1a)$$

$$f_k = \langle n(n-1)\dots(n-k+1)\rangle_q/\bar n^k, \qquad f_0 = 1, \qquad (6.1b)$$

where g_k denotes the correlators of a gluon jet, and f_k - of a quark jet. For simplicity, all the particle produced are considered to be identical. These quantities define the coefficients in the series expansion of the functionals $Z_g[u]$ and $Z_q[u]$ on a class of constant probing functions (u = const). For example,

$$Z_q[u] = \sum_{k=0}^{\infty} \frac{(u-1)^k}{k!} \cdot \bar n^k \cdot f_k,$$

$$f_k = \frac{1}{\bar n^k}\left(\frac{\delta}{\delta u}\right)^k Z_q[u]\Big|_{u=1} \quad , \quad \bar n = \frac{\delta}{\delta u} Z_g[u]\Big|_{u=1} . \qquad (6.2)$$

It is convenient to use also the correlators φ_k and ψ_k that are given by the expansion of the functionals

$$\varphi[u] \equiv \ln Z_G[u] \ , \quad \psi[u] \equiv \ln Z_q[u] \ , \qquad (6.3)$$

similar to eq. (6.2). They describe the true k-particle correlations irreducible to the correlations of smaller groups of particles. The correlators φ_k (ψ_k) are related to g_k(f_k) in a following way:

$$g_k = \varphi_k + \sum_{\left(\sum_{j=1}^{i} m_j = k \ ,\ 1 \le m_j \le k-1\right)} Q_{[m_j]}\, \varphi_{m_1}\cdot\varphi_{m_2}\cdot\dots\cdot\varphi_{m_i} \qquad (6.4)$$

where the coefficients $Q_{[m_j]}$ of the polynomial (6.4) are to be extracted from the expression

$$\left(\frac{d}{dx}\right)^k \exp u(x) = \exp u(x)\cdot\Big[u^{(k)} + \sum_{[m_j]} Q_{[m_j]}\, u^{(m_1)}\dots u^{(m_i)}\Big]. \qquad (6.5)$$

For instance:

$$f_2 = \psi_2 + \psi_1^2 \ , \ f_3 = \psi_3 + 3\psi_2\psi_1 + \psi_1^3 \ , \ f_4 = \psi_4 + 4\psi_3\psi_1 + 3\psi_2^2 + 6\psi_2\psi_1 + \psi_1^4 .$$

Notice, the quantity $\psi_1 = f_1 = \langle n\rangle_q/\langle n\rangle_g$ means the multiplicity ratio; $\sqrt{\psi_2}/\psi_1 \equiv d_F$ and $\sqrt{\varphi_2} \equiv d_G$ are the normalized multiplicity dispersions for q- and g-jets.

Let us write down the system of MLLA equations for the GFs, which follows from eq. (5.17):

$$Z_g'(y) = \frac{1}{2}\int_0^1 dz\, \Phi_G^G(z)\, \frac{\alpha_s}{2\pi}\Big[Z_g(y+\ell n(1-z))\, Z_g(y+\ell n z) - Z_g(y)\Big]$$
$$+ n_f \int_0^1 dz\, \Phi_G^F(z)\, \frac{\alpha_s}{2\pi}\Big[Z_q(y+\ell n(1-z))\, Z_q(y+\ell n z) - Z_g(y)\Big] \ , \qquad (6.6a)$$

$$Z_q'(y) = \int_0^1 dz\, \Phi_F^G(z)\, \frac{\alpha_s}{2\pi}\Big[Z_q(y+\ell n(1-z))\, Z_g(y+\ell n z) - Z_q(y)\Big] \ , \qquad (6.6b)$$

where $' \equiv d/dy$, $y = \ln E\theta/\Lambda$ (E - jet energy, θ - angle of a first decay in a jet). Using the symmetry $z \leftrightarrow (1-z)$ in (6.6a) one could change $\frac{1}{2}\Phi_G^G(z) \to (1-z)\Phi_G^G(z)$ to remove the singularity of the kernel at Z=1:

$$(1-z)\,\Phi_G^G(z) = 4N_c\Big\{\frac{1}{z} - 2(1-z) + z(1-z)^2\Big\} \ . \qquad (6.7)$$

Other kernels are regular at Z=1 also:

$$\Phi_G^F(z) = z^2 + (1-z)^2, \qquad (6.8)$$

$$\Phi_F^g(z) = 4C_F\left\{\frac{1}{z} - 1 + \frac{z}{2}\right\} \quad . \qquad (6.9)$$

Thus, eqs. (6.7) - (6.9) imply the mean value of $\ln(1-z)^{-1} \sim 1 \ll y$, and so one may use the approximation

$$z\,(y + \ln\cdot(1-z)) \simeq z(y) \qquad (6.10)$$

in eqs. (6.6).

In the DLA case the account of the singular parts of the kernels (6.7),(6.9) was quite sufficient. The non-singular parts as well as the entire kernel (6.8) are therefore the source of MLLA corrections. Neglecting the dependence of $z(y+\ln z)$ and α_s on z in nonsingular integrands, analogously to eq.(6.10), one simplifies the system (6.6) substantially:

$$Z_g'(y) = Z_g(y)\cdot\int^y dy'\,\gamma_o^2(y')\left[Z_g(y')-1\right] - \frac{11}{12}\gamma_o^2(y)Z_g(y)\left(Z_g(y)-1\right)$$
$$+ \frac{2}{3}n_f\frac{\alpha_s}{2\pi}\left[\left(Z_q(y)\right)^2 - Z_g(y)\right] \quad , \qquad (6.11a)$$

$$Z_q'(y) = Z_q(y)\left(\int^y dy'\,\gamma_o^2(y')\left[Z_g(y')-1\right] - \frac{3}{4}\gamma_o^2(y)\left[Z_g(y)-1\right]\right)\frac{C_F}{N_c} \quad . \qquad (6.11b)$$

Here $\gamma_o(y) \equiv \sqrt{4N_c\alpha_s(y)/2\pi}$ is the anomalous dimension that determines the rate of the multiplicity growth in DLA (see Sec. 4).

Now let us rewrite the system (6.11) in terms of the GFs φ and Ψ defined by eq. (6.3). Subtracting eq. (6.11b) from eq.(6.11a) one obtains the relation between multiplicity correlators for q- and g-jets:

$$\left(\frac{N_c}{C_F}\Psi - \varphi\right)' = \frac{\gamma_o^2}{4N_c}\left\{\left(\frac{11}{3}N_c - 3N_c\right)\left[Z_g - 1\right] - \frac{2}{3}n_f\left[Z_g^{\frac{2C_F}{N_c}} - 1\right]\right\} . \qquad (6.12)$$

Here we used the DLA relation

$$Z_q = Z_g^{C_F/N_c} \qquad (6.13)$$

in the correlation term of eq.(6.11a).

Dividing eq. (6.11a) by Z_g and taking the derivative of the result one comes with the account of eq.(6.13) to the following equation (6.14)

$$\varphi''(y) = \gamma_o^2(y)\left[Z_g(y)-1\right] + \frac{\gamma_o^2}{4N_c}\left\{-\frac{11}{3}N_c Z_g(y) + \frac{2}{3}n_f Z_g^{\frac{2C_F}{N_c}-1}\right\}' .$$

It is useful to introduce the 'anomalous dimension' γ -

$$\bar{n} = \exp\int^y dy'\,\gamma(y') \qquad (6.15)$$

and reduce eq. (6.14) with the help of eqs.(6.2)-(6.4) to the series of recurrent relations for φ_k :

$$\left[k^2\gamma^2 - \gamma_o^2 + k\left(\gamma' + \gamma a\frac{\gamma_o^2}{4N_c}\right)\right]\varphi_k =$$
$$\gamma_o^2\sum_{[m_j]_{1;i}} Q_{[m_j]}\cdot\varphi_{m_1}\cdot\ldots\varphi_{m_i}\cdot\left\{1 + \frac{k\gamma}{4N_c}\left[-\frac{11}{3}N_c + \frac{2}{3}n_f\left(\frac{2C_F}{N_c}-1\right)^i\right\}\right. , \qquad (6.16)$$

where $a = 11/3\cdot N_c + 2/3\cdot n_f\cdot(1 - 2C_F/N_c)$.

The r.h.s. of eq.(6.16) equals zero identically at $k = 1$. Hence,

$$\gamma^2 - \gamma_o^2 + \gamma' + \gamma a\frac{\gamma_o^2}{4N_c} = 0 \qquad (6.17)$$

Solving this equation by substitution

$$\gamma' \simeq \gamma_o' = -\frac{b}{2}\cdot\frac{\gamma_o^3}{4N_c} + O(\gamma_o^4) \quad , \quad \left(b = \frac{11}{3}N_c - \frac{2}{3}n_f\right) \qquad (6.18)$$

with account of smallness of γ_o ($\gamma_o^2 \sim \alpha_s$) , one gets the MLLA-corrected rate of the multiplicity growth [28,17]:

$$\gamma \simeq \gamma_o - \frac{\gamma_o^2}{4N_c}\frac{1}{2}\left(a - \frac{b}{2}\right) + O(\gamma_o^3) \quad . \qquad (6.19)$$

For $k > 1$ let us insert eqs.(6.18),(6.19) in eq.(6.16) to obtain (6.20)

$$\left(k^2-1\right)\left(1 + k\frac{\gamma_o}{4N_c}\left[\frac{11}{3}N_c - \frac{a-\frac{b}{2}}{k+1}\right]\right)\varphi_k = \sum Q_{[m_j]}\varphi_{m_1}\cdot\ldots\varphi_{m_i} + k\frac{\gamma_o}{4N_c}\frac{2}{3}n_f\left(\frac{2C_F}{N_c}-1\right)^2\tilde{Q}_k$$

where the symbol $\tilde{Q}$ denotes the series

$$\tilde{Q}_k \equiv \sum Q_{[m_j]}\varphi_{m_1}\cdot\ldots\varphi_{m_i}\left(\frac{2C_F}{N_c}-1\right)^{i-2}, \quad \text{i.e.} \qquad (6.21)$$

$\tilde{Q}_1 = 0$, $\tilde{Q}_2 = 1$, $\tilde{Q}_3 = 2C_F/N_c = \frac{8}{9}$, $\tilde{Q}_4 = 1/3 + (2C_F/N_c)^2 = 91/81, \ldots$

The recurrence (6.16) allows one to calculate φ_k consequtively. The limit $\gamma_0 \to 0$ corresponds to DLA: $\varphi_2 = 1/3$, $\varphi_3 = 1/4$, etc.

For the dispersion of the g-jet one gets the MLLA correction

$$d_g^2 = \varphi_2 = \frac{1}{3}\left(1 + \frac{\gamma_0}{4N_c}\left[-\frac{55}{9}N_c + \frac{2}{3}n_f + \frac{4}{9}\frac{n_f}{N_c^2} + \frac{4}{3}\frac{n_f}{N_c^4}\right]\right) + O(\gamma_0^2). \qquad (6.22)$$

Similar to eq.(6.14), the relation (6.12) can be reduced to

$$\Psi_k = \frac{C_F}{N_c}\left\{\varphi_k\left(1 + \frac{\gamma_0}{4N_c}\left[(a - 3N_c)k + \frac{2}{3}n_f\left(\frac{2C_F}{N_c} - 1\right)\frac{k^2-1}{k}\right]\right) - \frac{\gamma_0}{4N_c}\frac{2}{3}n_f\frac{1}{k}\left(\frac{2C_F}{N_c} - 1\right)^2\tilde{Q}_k\right\} \qquad (6.23)$$

that expresses the q-jet correlators through the g-jet ones. For instance, eq.(6.23) gives the ratio of q-jet to g-jet multiplicities [58,59]:

$$\Psi_1 = \frac{C_F}{N_c}\left(1 + \frac{\gamma_0}{4N_c}\left[a - 3N_c\right]\right) = \frac{C_F}{N_c}\left(1 + \frac{\gamma_0}{4N_c}\left[\frac{2}{3}N_c + \frac{2}{3}\frac{n_f}{N_c^2}\right]\right). \qquad (6.24)$$

For the normalized quantity Ψ_k / Ψ_1^k one gets, therefore,

$$\frac{\Psi_k}{\Psi_1^k} = \left(\frac{N_c}{C_F}\right)^{k-1}\left[\varphi_k\left(1 + \frac{\gamma_0}{4N_c}\frac{2}{3}n_f\left(\frac{2C_F}{N_c} - 1\right)\frac{k^2-1}{k}\right) - \frac{\gamma_0}{4N_c}\frac{2}{3}n_f\left(\frac{2C_F}{N_c} - 1\right)^2\frac{\tilde{Q}_k}{k}\right]. \qquad (6.25)$$

The dispersion of q-jet, e.g., reads

$$d_q^2 \equiv \frac{\Psi_2}{\Psi_1^2} = \frac{N_c}{3C_F}\left(1 + \frac{\gamma_0}{4N_c}\left[-\frac{55}{9}N_c + \frac{2}{9}n_f - \frac{2}{9}\frac{n_f}{N_c^2} + \frac{1}{3}\frac{n_f}{N_c^4}\right]\right). \qquad (6.26)$$

Notice that MLLA corrections to the dispersion of q- and g-jets appear to be approximately equal, as the dominating terms in the square brackets of eqs.(6.22),(6.26) are the same. This is not a casual coincidence. As a matter of fact, it follows from eq.(6.25) that the SL correction to the DL relation

$$\frac{\Psi_k}{\Psi_1^k} = \left(\frac{N_c}{C_F}\right)^{k-1}\frac{\varphi_k}{\varphi_1^k} \qquad (\varphi_1 \equiv 1) \qquad (6.27)$$

vanishes at $n_f = 0$ and is proportional to the small factor $1 - 2C_F/N_c = 1/N_c^2 = 1/9$. Notice, that the smallness of the colour factor $(1 - 2C_F/N_c)$ allows one to omit in eqs.

(6.20),(6.23) the terms with $\tilde{Q}_k$ as being proportional to N_c^{-4} and, thus, to simplify considerably the calculations.

Therefore, the account of the SL effects results in the substantial corrections to φ_k and Ψ_k while the relation (6.27) between them is violated rather weakly (see also ref. [49]).

Using the numerical values $N_c = 3$, $n_f = 3$ one obtains approximately

$$d_q^2 \approx 3/4\cdot(1 - 1.5\,\gamma_0) \approx 3/4\cdot(1 - 2.1\sqrt{\alpha_s(E)}).$$

So far we considered the multiplicity correlations for a single jet. The real events contain several jets. For example, in the case of $e^+e^- \to q_{jet} + \bar{q}_{jet}$

$$z_{e^+e^-} = z_q^2,$$

which implies that

$$d^2_{e^+e^-} = 1/2\cdot d_q^2.$$

Combining these equations one gets the numerically large correction to the DLA-value of $\langle n\rangle/D$, which improves the agreement with experiment. It is of interest to note that last equation was checked experimentally. This gave a clear evidence in favour of the independent evolution and hadronization of the two back-to-back quark jets.

Attention would be paid also to the fact that the true parameter of expansion in the recurrent relations (6.20), (6.23) is the quantity $(k\cdot\gamma_0)$. It means that MLLA corrections to the higher correlators (at $k \gtrsim \alpha_s^{-1/2} \gg 1$) can not be estimated according to eqs.(6.23), (6.25). But this non-uniformity in k is connected just with the crudeness of the chain of transformations leading to eqs. (6.12),(6.14) and does not come from the initial functional eqs. (6.6). As a matter of fact, the dependence of

$z\,(y + \ln(1-z))$ on z in eqs. (6.6) for high value of k could be considered as weak. That is why the reconstruction of the preasymptotic KNO function $f(z)$ especially at large $z \gg 1$ (higher correlators) needs a more detailed analysis of eqs.(6.6) for one to obtain the formulae for g_k and f_k (or φ_κ, ψ_κ), which are uniform in $(\kappa \cdot \gamma_0)$. MC simulation of events corresponding to the evolution eqs. (6.6) is likely to be the straight way to predict the shape of KNO distribution at the realistic energies[29].

6.2. Inclusive Energy Spectrum of Partons in MLLA

The inclusive gluon spectrum of A-jet (A=q,g) with the given 'opening angle' θ,

$$1/k\ \bar{D}_A \equiv \frac{\delta}{\delta u(k)}\ Z_A\,(E,\ \theta;\ [u(k)])\Big|_{u\equiv 1}\ , \qquad (6.28)$$

is determined by the system of two equations following from the eqs. (5.15), (5.17):

$$\bar{\mathcal{D}}_A^g(\ell,Y) = \delta(\ell)\,\delta_A^g + \int_0^Y dy' \int_0^\ell d\ell'\,\frac{\alpha_s}{2\pi}\,\Phi_A^B(\ell-\ell')\,\bar{\mathcal{D}}_B^g(\ell',y') \qquad (6.29)$$

Here Φ_A^B stands for the regularized AP kernels ; $l = \ln\frac{E}{k} = \ln 1/x$, $y = \ln k\theta/Q_0$ ($l' = \ln z/x$, $y' = \ln k\theta'/Q_0$). The running coupling α_s depends on the transverse momentum of soft gluon

$$\frac{\alpha_s(\kappa_\perp)}{2\pi} \simeq \frac{\alpha_s(zE\theta')}{2\pi} = \frac{1}{b(\lambda+y'+\ell')}\ , \quad \lambda = \ln\frac{Q_0}{\Lambda}\ . \qquad (6.30)$$

The energy spectrum for e^+e^- annihilation is the sum of two q-jet contributions:

$$\frac{1}{\sigma_{e^+e^-}}\,\frac{x\,d\sigma_{e^+e^-}}{dx} = 2\,\bar{\mathcal{D}}_q(\ell,Y)\Big|_{\theta\sim 1\ (Y=\ln\frac{k}{Q_0})}\ . \qquad (6.31)$$

Notice, the region $\theta \sim 1$ in the angular integral of eq. (6.29) leads to the negligible correction of order $\sim\sqrt{\alpha_s}$ to eq. (6.31).

Eqs. (6.29) can be solved directly with use of double Mellin transformation similar to eq.(4.75). The resulting integrand proves to have an additional SL factor $\left(\frac{\beta+s}{\beta}\right)^{-a/b}$ as compared to that of eq. (4.75).

We shall follow the way that manifests the relation of eqs. (6.29) to the RG approach. First of all, let us introduce the variable

$$Y \equiv \ln\frac{E\theta}{Q_0} = y + l \qquad (Y>0) \qquad (6.32)$$

that is connected with the largest k available for partons in a jet. Then turn to the moment representation

$$\tilde{D}(\omega,\ Y) = \int_0^\infty dl\ e^{-\omega l}\ \bar{D}(l,\ Y). \qquad (6.33)$$

Owing to the fact that the evolution parameter θ appears, due to strict AO, exclusively in the upper limit of the integral (6.29), one can write down eqs.(6.29) in a symbolic matrix form as

$$\frac{d}{dY}\,\tilde{\mathcal{D}}(\omega,Y) = \int_0^\infty d\bar{\ell}\ e^{-\omega\bar{\ell}}\,\hat{\Phi}(\bar{\ell})\,\frac{\alpha_s(Y-\bar{\ell})}{2\pi}\,\tilde{\mathcal{D}}(\omega,Y-\bar{\ell})\ . \qquad (6.34)$$

Eq. (6.34) generalizes the RG equation for the LLA ($\omega \sim 1$) over the region of parametrically small moments $\omega \sim 1/\sqrt{Y} \ll 1$. Indeed, neglecting $\bar{l} \ll Y$ in the arguments of α_s and $\tilde{D}$ one could transform eq.(6.34) to

$$\frac{d}{dY}\,\tilde{\mathcal{D}}(\omega,Y) = \frac{\alpha_s(Y)}{2\pi}\,\hat{\tilde{\Phi}}(\omega)\,\tilde{\mathcal{D}}(\omega,Y)\ . \qquad (6.35)$$

Diagonalization of the kernel matrix $\hat{\tilde{\Phi}}(\omega)$ results in the two 'trajectories'

$$\gamma_\pm(\omega) = \frac{1}{2}\left[\Phi_g^g + \Phi_F^F \pm \sqrt{(\Phi_g^g-\Phi_F^F)^2 + 8n_f\Phi_F^g\Phi_g^F}\ \right] \qquad (6.36)$$

that determine the anomalous dimensions of the two operators arising from mixing of g and q states in a cascade:

$$\gamma^{\pm}_{LLA}(\omega,\alpha_s) = \frac{d}{dY}\ell n\,\tilde{\mathcal{D}}^{\pm}(\omega,Y) = \frac{\alpha_s(Y)}{2\pi}\nu_{\pm}(\omega) \quad . \tag{6.37}$$

At $x \ll 1$ the trajectory $\nu_+(\omega)$, singular at $\omega = 0$,

$$\nu_+(\omega) = \frac{4N_c}{\omega} - a + O(\omega), \quad a = \frac{11}{3}N_c + \frac{2}{3}\frac{n_f}{N_c^2} \quad , \tag{6.38}$$

gives the main contribution do $\bar{D}(1,y)$.

The 'nonlocal' in Y eq.(6.34) encloses in a compact form the information about the anomalous dimension, which is not easy to reveal by means of the standard RG approach.

Indeed, let us trace the chain of transformations of eq. (6.34):

$$\frac{d}{dY}\tilde{\mathcal{D}}(\omega,Y) = \Big(\int_0^\infty d\bar{\ell}\; e^{-\bar{\ell}(\omega+\frac{d}{dY})}\hat{\Phi}(\bar{\ell})\Big)\frac{\alpha_s(Y)}{2\pi}\tilde{\mathcal{D}}(\omega,Y) \tag{6.39}$$

$$= \hat{\tilde{\Phi}}(\omega+\frac{d}{dY})\frac{\alpha_s(Y)}{2\pi}\;\tilde{\mathcal{D}}(\omega,Y) \quad .$$

The diagonalization leads formally to the known LLA trajectories with the differential operator as an argument (see eq. (6.37)):

$$\frac{d}{dY}\tilde{\mathcal{D}}^{\pm}(\omega,Y) = \nu_{\pm}(\omega+\frac{d}{dY})\frac{\alpha_s(Y)}{2\pi}\;\tilde{\mathcal{D}}^{\pm}(\omega,Y) \quad . \tag{6.40}$$

Using eq. (6.39) one obtains

$$(\omega+\frac{d}{dY})\frac{d}{dY}\tilde{\mathcal{D}}^{+} = 4N_c\frac{\alpha_s}{2\pi}\tilde{\mathcal{D}}^{+} - a(\omega+\frac{d}{dY})\frac{\alpha_s}{2\pi}\tilde{\mathcal{D}}^{+} \quad . \tag{6.41}$$

Introducing γ as follows :

$$\tilde{\mathcal{D}}(\omega,Y) = \tilde{\mathcal{D}}(\omega,Y_0)\exp\int_{Y_0}^{Y} dy\;\gamma(\omega,\alpha_s(Y)) \quad , \tag{6.42}$$

one gets the equation for $\gamma(\omega,\alpha_s)$ which clearly possesses the necessary property of locality

$$(\omega+\gamma)\gamma - \frac{4N_c\alpha_s}{2\pi} = -\beta(\alpha_s)\frac{\partial}{\partial\alpha_s}\gamma - a(\omega+\gamma)\frac{\alpha_s}{2\pi} \quad , \tag{6.43}$$

where $\beta(\alpha_s) \equiv \frac{d}{dY}\alpha_s(Y) \simeq -\frac{b}{2\pi}\alpha_s^2(Y)$.

The r.h.s. of eq. (6.43) proves to be the correction $\sim\alpha_s^{3/2}$ to the l.h.s. ($\sim\alpha_s$). In the DLA case

$$(\omega+\gamma)\gamma = \frac{4N_c\alpha_s}{2\pi} \quad , \quad \gamma = \gamma_{DLA}(\omega,\alpha_s) = \frac{-\omega+\sqrt{\omega^2+4\gamma_0^2}}{2} \quad , \tag{6.44}$$

where $\gamma_0^2 = 4N_c\frac{\alpha_s}{2\pi}$. This result certainly needs neither diagonalizing nor accurate handling with d/dY and follows immediately from eq. (6.39):

$$\frac{d}{dY}\tilde{\mathcal{D}}(\omega,Y) = \Phi^{\mathcal{C}}_{\mathcal{C}}(\omega+\frac{d}{dY})\frac{\alpha_s}{2\pi}\tilde{\mathcal{D}} = \frac{4N_c}{\omega+\gamma}\frac{\alpha_s}{2\pi}\tilde{\mathcal{D}} = \gamma\tilde{\mathcal{D}} \quad . \tag{6.45}$$

Meanwhile, to derive γ_{DLA} in the framework of conventional RG approach one has to sum up the series $\sum_{k=0}^{\infty} c_k(\alpha_s/\omega^2)^k$ representing in fact the square root with c_k to be found from the PT expansion of eqs. (6.29).

Thus, the nonlocal eq. (6.34) reduces the RG series, defining γ_{DLA}, to the shift of the argument of $\tilde{D}$, which is inherent to the evolution equation:

$$\gamma_{DLA}(\omega,\alpha_s)\tilde{\mathcal{D}}(\omega,Y) = \frac{\alpha_s}{\omega}\sum_k\Big(\frac{\alpha_s}{\omega^2}\Big)^k\tilde{\mathcal{D}} = \tag{6.46}$$

$$\int_0^\infty d\bar{\ell}\;e^{-\omega\bar{\ell}}[1+\alpha_s\bar{\ell}^2+(\alpha_s\bar{\ell}^2)^2+\ldots]\frac{\alpha_s}{2\pi}4N_c\,\tilde{\mathcal{D}}(\bar{\ell},Y) =$$

$$\int_0^\infty d\bar{\ell}\;e^{-\omega\bar{\ell}}\frac{\alpha_s}{2\pi}\tilde{\mathcal{D}}(Y-\bar{\ell}) \quad .$$

The SL correction to γ_{DLA} corresponds in terms of the ordinary RG technique to series

$$\gamma^{(1)}(\omega,\alpha_s) = \frac{\alpha_s^2}{\omega^2}\sum_k c_k\Big(\frac{\alpha_s}{\omega^2}\Big)^k + \alpha_s \quad . \tag{6.47}$$

This results from the account of the regions $\theta_i \sim \theta_{i+1}$ and the renormalization of α_s ; the last term $\sim\alpha_s$ in eq. (6.47) is connected with the hard decays $k_i \sim k_{i+1}$ (see eqs.(5.7)). But here eq.(6.34) proves to be very effective once more: it has already accounted for both the angular regions $\theta_i \sim \theta_{i+1}$ (exact AO) and the renormalization effect via the shift of the arguments:

$$[\alpha_s\ell(1+\alpha_s\ell^2+\dots)]\,\alpha_s(Y)\bar{\mathcal{D}}(Y) \longrightarrow [\alpha_s\ell]\alpha_s(Y)\bar{\mathcal{D}}(Y-\ell)$$
$$\longrightarrow \alpha_s(Y-\ell)\,\bar{\mathcal{D}}(Y-\ell) \quad .$$

Therefore, combining eqs. (6.43),(6.44) one gets immediately the SL contribution to $\gamma(\omega,\alpha_s)$:

$$\gamma = \gamma_{DLA} - a\frac{\alpha_s}{2\pi}\cdot\frac{1}{2}\left[1+\frac{\omega}{\sqrt{\omega^2+4\gamma_0^2}}\right] + b\frac{\alpha_s}{2\pi}\cdot\frac{\gamma_0^2}{\omega^2+4\gamma_0^2} + O(\alpha_s^{3/2}) \quad . \tag{6.48}$$

The omitted corrections here are small uniformly in ω. Eq.(6.48) coincides with the result of RG calculations[28].

One can solve the differential eq.(6.41) exactly, reducing it to confluent hypergeometric equation for the function $\alpha_s(Y)\cdot\tilde{D}(Y)$. Accounting for the initial conditions fixed by the integral eqs.(6.29) one obtains the result:

$$\tilde{\mathcal{D}}^+(\omega,Y,\lambda) = \frac{\Gamma(A+1)}{\Gamma(B+2)}\,z_1 z_2^B\left\{\Phi(-A+B+1,B+2,-z_1)\Psi(A,B+1,z_2)\right.$$
$$\left. + e^{-(z_1-z_2)}(B+1)\Psi(A+1,B+2,z_1)\,\Phi(-A+B+1,B+1,-z_2)\right\} \quad , \tag{6.49}$$

where $z_1 \equiv (Y+\lambda)\omega = \omega\ell n\frac{E\theta}{\Lambda}$, $z_2 \equiv \omega\lambda = \omega\ell n\frac{Q_0}{\Lambda}$, $A \equiv \frac{4N_c}{b\omega}$, $B = \frac{a}{b}$.

For the Mellin representation of the spectrum in a physical region ($\Gamma = \ln 1/x < Y$) the second term in eq.(6.49) could be omitted:

$$x\,\bar{\mathcal{D}}^+(x,Y,\lambda) = \frac{4N_c(Y+\lambda)}{bB(B+1)}\,\vartheta(Y-\ell)\int_{(\varepsilon>0)}^{\varepsilon+i\infty}\frac{d\omega}{2\pi i}\,\Phi(-A+B+1,B+2,-\omega(Y+\lambda))\cdot$$
$$\cdot K(\omega,\lambda)\,x^{-\omega} \quad , \tag{6.50}$$
$$K(\omega,\lambda) \equiv \frac{\Gamma(A)}{\Gamma(B)}(\omega\lambda)^B\Psi(A,B+1,\omega\lambda) \quad ,$$

since it decreases exponentially at $Re\,\omega \to +\infty$ and so gives zero contribution to the contour integral. Its role consists in the cancellation of the first term near the poles of $\Gamma\left(\frac{4N_c}{b\omega}+1\right)$ and at the left cut ($Re\,\omega < 0$).

As a result $\tilde{D}(\omega,Y,\lambda)$ has no singularities in ω-plane. The asymptotic behaviour $e^{-\omega Y}$ provides zero value of the spectrum $\tilde{D}(x)$ in a non-physical region $xE < Q_0$ ($\Gamma > Y$).

The integral eqs. (6.29) determine also the relation of q and g-jet momentum functions $\tilde{D}_{g,q}(\omega,Y,\lambda)$:

$$\tilde{\mathcal{D}}_{g(q)}(\omega,Y,\lambda) \approx C^+_{g(q)}\,\tilde{\mathcal{D}}^+(\omega,Y,\lambda) \quad ,$$
$$C^+_g = \frac{\nu_+(j)-\tilde{\Phi}^F_g(j)}{\nu_+(j)-\nu_-(j)} \simeq 1 + O(j) \quad , \tag{6.51}$$
$$C^+_q = \frac{\tilde{\Phi}^F_F(j)}{\nu_+(j)-\nu_-(j)} \simeq \frac{C_F}{N_c} + O(j) \quad ,$$

where $j \equiv \omega + \gamma(\omega,\alpha_s(Y)) \ll 1$ (for derivation of the LLA residues C see ref. [1]). Thus, the asymptotic spectra of q- and g-jets prove to be similar. In the DLA they have the known constant ratio $C_F/C_V = 4/9$. This similarity appears to be slightly violated by $\sqrt{\alpha_s}$ terms which, as it follows from Subsec. 6.1, are under the MLLA control.

For the jet multiplicity, taking $\omega = 0$ in eq.(6.49), one gets:

$$N_g = \tilde{\mathcal{D}}^+(0,Y,\lambda) = x_1\left(\frac{x_2}{x_1}\right)^B\left[I_{B+1}(x_1)K_B(x_2) + K_{B+1}(x_1)I_B(x_2)\right] ,$$
$$x_1 = \sqrt{\frac{16N_c}{b}(Y+\lambda)} \quad , \quad x_2 = \sqrt{\frac{16N_c}{b}\lambda} \quad , \tag{6.52}$$

where I and K are the standard modified Bessel functions. The second term in eq.(6.52) decreases with Y increasing and provides the normalization $\tilde{D}(\omega=0,\ E\sim Q_0) \approx 1$. The asymptotical energy behaviour of the multiplicity reads

$$N \sim \left(\ell n\frac{E}{\Lambda}\right)^{-\frac{B}{2}+\frac{1}{4}}\exp\sqrt{\frac{16N_c}{b}\ell n\frac{E}{\Lambda}} \quad . \tag{6.53}$$

The ratio of parton multiplicities in q- and g-jets follows from eqs. (6.51) (cf. eq. (6.29)):

$$\frac{C_q^+}{C_g^+} = \frac{\tilde{\Phi}_F^F(\gamma_0)}{\gamma_+(\gamma_0)-\tilde{\Phi}_F^F(\gamma_0)} \simeq \frac{\frac{4C_F}{\gamma_0}-3C_F}{\frac{4N_c}{\gamma_0}-a} \approx \frac{C_F}{N_c}\left[1+\gamma_0\frac{a-3N_c}{4N_c}\right], \quad (6.54)$$

where $\omega = 0$ was taken. It is seemingly the simplest way of derivation of the q/g ratio [58,59], which needs in fact no more than the LLA coefficient functions and γ_{DLA}.

6.3. Developed Cascade and LPHD Concept

Besides the jet energy E and the QCD parameter Λ the parton spectrum eq.(6.50) contains one more dimensional quantity Q_0 which regularizes collinear divergencies. This quantity represents the minimal value of the relative $k_\perp$ of decay products in jet evolution. Q_0 also bounds parton energies $E_p = x\,E \gtrsim k_\perp/\theta_0 \gtrsim Q_0/\theta_0$, thus playing the role of effective mass of a parton.

The choice of the Q_0 value sets a formal boundary between two stages of jet evolution: the one of the parton branching process, which is controlled by PT, and then the stage of non-PT transition into hadrons. In essence, partons and hadrons are the complementary languages. So, if the theory of hadronization would exist, the result would be independent of the formal quantity Q_0 separating the two stages. As a matter of fact, for large enough Q_0 (for example, at $Q_0 \approx 3$ GeV) the number of partons produced at recent energies is certainly small. So, one is forced to apply for some 'ad hoc' hadronization model describing the multihadron production as the evolution 'below Q_0' of a partonic system with large invariant masses of parton pairs. Unfortunately, an experimental verification of such results looks rather like a tuning of parameters, which are inevitably present in any phenomenological model, than a test of QCD predictions.

But with the intent look at eq.(6.50) an opportunity

to make a model independent prediction may be found. If PT partons hadronize independently of each other, then the distribution of a hadron h over the energy fraction x_h is given by convolution of the parton x-spectrum with the gluon hadronization function $C_g^h(x_h/x, Q_0, M_h)$. Hence, because of the factorized dependence of the integrand in eq. (6.50) on the jet energy E and Q_0, the hadron spectrum has the same form of eq.(6.50) but with $K(\omega,Q_0)$ replaced by the product

$$K^h(\omega, M_h) = K(\omega,Q_0)C_g^h(\omega,Q_0,M_h). \quad (6.55)$$

Here

$$C_g^h(\omega,Q_0,M_h) = \int_0^1 dz\, z\, C_g^h(z,Q_0,M_h)$$

is a moment of the hadronization function.

What can be said about the ω-dependence of the K^h factor which influences a shape of the hadronic spectrum? We are interested in the kinematical region of relatively soft (though relativistic) particles. In such a case essential values of ω under the integral (6.50) are small: $\omega \ll 1$ (near the maximum of the spectrum they are parametrically small: $\omega \sim \sqrt{\alpha_s}$). Therefore, to understand how hadronization affects the spectrum shape one needs to know behaviour of K^h at $\omega \to 0$.

Let us consider the two qualitatively different variants:

$$K^h(\omega,M_h) \simeq 1/\omega \cdot C(M_h) + \text{const} + O(\omega), \quad (6.56a)$$

$$K^h(\omega,M_h) \simeq \text{const} + O(\omega). \quad (6.56b)$$

The first (singular) case corresponds to the physical picture where each coloured parton produced hadrons with a plateau-like energy distribution: $C_g^h(z) \backsim 1/z$. One can see that in such a case the dip at small x which is characteristic for partonic spectra never will manifest itself in experimental hadron spectra.

The regular behaviour (6.56b) corresponds to <u>local</u> in

the phase space blanching and hadronization of partons (see Sec. 2). It is perhaps surprizing to see the x-dependence of $x\bar{D}_g^h$ being given completely in terms of the PT evolution. Non-PT effects can smear the hadron distribution over a finite interval in ln 1/x. However, such a smearing is, formally, a higher order effect in the framework of MLLA.

Thus, the overall normalization factor K^h is the only phenomenological parameter which remains arbitrary, concerning the PT-LPHD approach. It may be found, e.g., by fitting the average multiplicity.

The parton spectrum (6.50) has another interesting property: for large energy E, when $Y > \lambda^2$ (recall that $Y = \ln E/\Lambda$, $\lambda = \ln Q_0/\Lambda$), the shape of the spectrum becomes independent of Q_0 as far as Q_0 determines then only a constant factor:

$$K(\omega, Q_0) \simeq \frac{2}{\Gamma(B)} (Z_0/2)^B K_B(Z_0) \qquad (6.57)$$

at $\omega\lambda \ll 1$, where $Z_0 = \sqrt{16N_c\lambda/b}$ (recall, that essential values of ω in eq.(6.50) are parametrically small: $\langle\omega\rangle \sim 1/\sqrt{Y} \ll 1$). So, this situation resembles the hadronization function (6.56b). At asymptotically high jet energy E, when only small ω-region is important, the spectrum (6.50) for any $\lambda \sim 1$ has the same shape as in the case $\lambda = 0$, differing just in the numerical factor (6.57).

Thus, when the bremsstrahlung cascade is developed enough, the shape of resulting energy distribution of particles gets insensitive to the processes occurring at the last steps of evolution (at $k_\perp \sim Q_0$). This observation may serve to justify the attempts to provide the developed cascade not with the expensive increase of total energy E, but with the decrease of Q_0, thus enhancing the responsibility of PT for jet evolution at recent

energies.

6.4. On Infrared Stability of Limiting Parton Spectrum

The PT formula (6.50) was based on the smallness of $\alpha_s(k_\perp^2)$, that implied the fulfilment of strong inequality $\lambda = \ln Q_0/\Lambda \gg 1$ even at the last steps of parton cascade. Decreasing λ (and so extending the responsibility of PT) one comes to the finite 'limiting' parton spectrum at $Q_0 = \Lambda$.

Moreover, at $\lambda = 0$ eq. (6.50) simplifies noticeably since in this case $K(\omega, Q_0) = 1$ at all ω. The fact, that PT formula (6.50) leads to finite result in a somewhat senseless limit, may be explained formally by integrability of the anomalous dimension over the region of 'infrared pole':

$$\int_{\Lambda^2} \frac{dk_\perp^2}{k_\perp^2} \sqrt{\alpha_s(k_\perp^2)} < \infty \qquad (6.58)$$

But so fas one is still unaware, in a rigorous sense, of the real behaviour of 'running coupling' $\alpha_s(k_\perp^2)$ at small $k_\perp$. Furthermore, in the region of small $k_\perp$ the variable α_s should disappear from the theory, since new physics turns on and the language of the coloured quarks and gluons ceases to be appropriate. Nevertheless, one might dare to consider the perturbative approach, PT formulae, to be plausible, if the predicted results turn to be independent of the concrete function $\alpha_s(k_\perp^2)$ in the dangerous region.

A characteristic feature of the limiting spectrum is the presence of the maximum. One may find analytically the asymptotic shape of distribution not too far from its peak by saddle-point evolution of the integral (6.50):

$$x\bar{D}(x,Y) \sim \sqrt[4]{\frac{36N_c}{\pi^2 b Y^3}} \exp\left[-\sqrt{\frac{36N_c}{b}}\left(\ln\frac{1}{x} - \frac{Y}{2} - B\sqrt{\frac{b}{16N_c}}Y\right)^2\right], \qquad (6.59)$$

$Y = \ln E/\Lambda$.

It has a broad Gaussian shape with a peak at $Ep = E_0 = x_0 E$,

$$\ln 1/x_o = 1/2 \cdot Y + B\sqrt{\frac{b}{16N_c}\,Y}, \qquad (6.60)$$

that grows rather slowly with the jet energy E:

$$\frac{E\,d\,E_o}{E_o\,d\,E} = 1/2 - B\sqrt{\frac{b}{64N_c\,Y}}\ . \qquad (6.61)$$

The subtracted term here represents a SL correction to DLA, which is asymptotically small. For example, eq. (6.61) gives $d\ln E_o/d\ln E \approx 0.4$ at E = 30 GeV (Λ = 150 MeV).

Thus, inclusion of SL terms shifts the maximum to lower x. This result is quite obvious because these SL terms account for the more complete description of harder parton emissions than the pure DLA does. Therefore, a share of the total jet energy, which is supplied for creation of the soft plateau, somewhat lowers due to the recoil effect, and the spectrum softens.

It is noteworthy to emphasize, that the recent data on inclusive energy distribution of hadrons in e^+e^-annihilation (see refs. [10,12] and references therein) demonstrate the existence of the hump-backed plateau, supporting the concept of LPHD. So far, probably the most convincing evidence for the hump-backed distribution is the growth of the energy, E_{hump}, at which the spectrum reaches its maximum as one increases the jet energy. In refs. [41,42] one may find the discussion of the unexpectedly close correspondence between the limiting spectrum and the observed hadron distributions.

To sharpen the influence of AO on the parton multiplication process, and in attempt to find the dip in jets produced in hadronic collisions, it proves to be important to look at the spectra of particle restricted to lie within a particular

opening angle with respect to the jet (see for detail ref. [8]). Here the hump should be observed for the energetic particles and the influence of the kinematical phase space effects will be reduced.

7. CHROMODYNAMICS OF HADRONIC JETS [61,19]

In this Section we shall discuss the QCD portrait of a jet ensemble and the properties of an individual jet in HPs. The emphasis is on the collective QCD phenomena in the jet dynamics.

7.1. On Experimental Selection Procedures

Traditionally, the final state structure in a hard collision is interpreted in terms of jets of hadrons with kinematics corresponding to those of the energetic quarks and gluons participating in HP. The standard exclusive procedures for jet finding as well as the reconstruction of the jet parameters (energy, angular direction, mass and so on) differ in some details, but all of them are based on the idea of assigning each hadron in an event to a certain jet. This has been a very fruitful approach especially as regards three jet events in e^+e^-collisions, where the gluon was found, and two high $p_\perp$ jet events in hadronic collisions, where the point-like nature of quark and gluon interactions has been best measured. However,

the separation of an event into a certain number of jets is inherently ambiguous, especially as one goes to higher energies. The ambiguity comes from several sources.

(i) In a particular part of an even it may be equally correct to identify a set of particles as belonging to one jet, two jets or even more jets. After all a jet often has an identifiable substructure consisting of further jets.

ii) Such a procedure completely ignores the collective QCD nature of particle production in HPs. In particular, due to colour coherence soft hadrons do not belong to any particular jet, but have emission properties dependent on a jet ensemble. The spectrum of particles associated with 3-jet events in e^+e^- annihilation, especially in the wide angle regions, is of this character (see the next Sec.).

In particular, this collective phenomenon is not the least of the factors explaining the measured in the three-fold-symmetric 3-jet events [60] ratio for hadron multiplicities in g- and q-jets, that turns out to be lower than the famous asymptotic value 9/4, see for details refs. [7,61]. We emphasize, in addition, that the coherent influence of the colour topology of the overall jet ensemble affects not only the flows of interjet particles, but also the particle distributions inside each jet (azimuthal asymmetry of jets, see Subsec. 8.6).

Attempting to force particles to belong to some jet in an event may cause difficulties. This leads, e.g., to the sizable uncertainties in the finding of a 'jet axis', resulting in the bias-effects for the particle distribution relative to such an axis.

It is instructive to recall here the appearance of the artificial two-humped distribution in the rapidity spectrum $dN/dy_{\parallel}$ observed in experiments (e.g., [62]). As it has been demonstrated above in the language of the toy

model (see Sec. 3) the coherence of QCD does not produce a dip in $dN/dy_{\parallel}$ at $y_{\parallel} = 0$. Analysis, accounting for the QCD cascades, maintain this conclusion. So, in the DL expression

$$\frac{dN}{dy_{\parallel}} = \frac{1}{2}\sqrt{\frac{16 N_c}{b \ln\left(\frac{\varepsilon}{\Lambda ch y_{\parallel}}\right)}}\; N$$

(cf. eq. (4.72) there is no hint of a dip as $y_{\parallel}$ decreases.

An important point is, that one produces a dip at $y_{\parallel} = 0$ simply from a bias against choosing the jet axis so that $y_{\parallel} = 0$ (see for details ref. [42]).

The serious shortcoming of some exclusive procedures (e.g., dealing with the sphericity tensor) is the lack of infrared stability of the event characteristics. If the jet algorithms do not use infrared safe quantities, comparison with QCD cannot be carried to higher orders and the whole procedure, though adequate when only crude data and crude calculations are available, may have limited quantitative significance. Even if the jet finding algorithms are infrared stable, the procedure for assigning particles to jets remains, in principle, unjustified.

Especially as higher energies are attained a purely inclusive procedure for quantitatively dealing with hard collisions is preferable to organizing the event according to a certain number of jets. There is in general a rather direct correspondence between jets and energy correlations so that any observable which can be described in terms of jets can also be described in terms of energy correlations [7,63,64]. As the simplest example consider the angular distribution of the multiplicity flow in two-jet events of e^+e^- annihilation. Its study is accessible through an $(\text{energy})^2$ multiplicity correlation (E^2MC) (7.1a)

$$\frac{dN_3}{d\Omega_{\vec{n}}} = \sum_{a,b} \int dE_a dE_b dE_{\vec{k}} \; \frac{E_a E_b \; d\sigma_3}{\sigma_2 \, dE_a dE_b dE_{\vec{k}} d\Omega_a d\Omega_b d\Omega_{\vec{k}}} \;,$$

$$\sigma_2 = \sum_{a,b} \int dE_a\, dE_b\, \frac{E_a E_b\, d\sigma_2}{dE_a\, dE_b\, d\Omega_a\, d\Omega_b} \quad , \quad \vec{n}_b \simeq -\vec{n}_a \, , \tag{7.1b}$$

where the sum is over all particle types. The energy weighted integrals over E_a and E_b, at fixed angular directions $\vec{n}_a$ and $\vec{n}_b \simeq -\vec{n}_a$, specify the 'jet' directions about which one has an associated multiplicity distribution at variable angular direction $\vec{n}(\Omega)$.

The cross section (7.1b), describing the correlation between two back-to-back energy fluxes (EEC), contains the known double logarithmic form factor [63,1]. This reflects the natural disbalance of the jet directions, caused by the gluon bremsstrahlung.

The same angular distribution may be discussed in terms of a more simple double-inclusive correlation between the energy flux and the multiplicity flow (EMC)

$$\frac{dN_2}{d\Omega_{\vec{n}}} = \sum_a \int dE_a\, dE_{\vec{n}}\, \frac{E_a\, d\sigma_2}{\sigma_1\, dE_a\, dE_{\vec{n}}\, d\Omega_a\, d\Omega_{\vec{n}}} \, , \tag{7.2a}$$

$$\sigma_1 = \sum_a \int dE_a\, \frac{E_a\, d\sigma_1}{dE_a\, d\Omega_a} \, . \tag{7.2b}$$

The point is that here the main contribution also comes from the two-jet sample whose kinematics is practically fixed by the choice of the direction $\vec{n}_a$. The difference between the distributions (7.1a) and (7.1b) occurs only when the angular direction $\vec{n}$ is parametrically close to the backward 'jet axis', $\vec{n} \simeq -\vec{n}_a$. In this case the shape of the distribution (7.2a) near $\vec{n} = -\vec{n}_a$ becomes somewhat wider due to the natural for QCD 'shaking' of the non-registered jet [65] ($\theta_{sh} \sim (\Lambda/W)^{\gamma}$, $\gamma \simeq b/(b+4C_F)$ (≈ 0.64 at $n_f = 3$)).

The drag effect physics becomes accessible through

a more complicated correlation, E^3MC, see the next Section.

In the general case multiple correlations between the energy and multiplicity flows could be referred to as $E^{\alpha}M^{\beta}C$.

In the discussions that follow we shall refer to measurements involving determinations of jets and jet axes. To see, qualitatively, the effects we shall be considering even crude determinations of jet axes are probably sufficient. However, in making precise quantitative relation to theory the purely inclusive approach (a use of $E^{\alpha}M^{\beta}C$) seems to be the best way.

7.2. On Structure of Particle Flows in Multijet Events

As it is discussed in detail in the next Subsec., the collimation of the QCD cascade around the parent parton becomes stronger as the parton energy increases. Moreover, the collimation of an energy flux grows much more rapidly as compared to a multiplicity flow. Therefore, at asymptotically high energies each event should possess the clear geometry, that reflects the topology of the partons participating in the hard interaction. Therefore, the best characteristic of the final hadronic system is probably the spatial distribution of the energy fluxes. After some smearing this takes the shape of the closed energy surface with a few comparatively sharp bumps, corresponding to the primary partons. The widths of these bumps determine the angular apertures of each one of the main colour currents (see the next Subsec.). Fixing a jet axis with the accuracy higher than the natural angular width of the corresponding energy flux is unreasonable.

Therefore, the space-energy portrait of events represents a natural partonometer for registration the kinematics of the energetic partons participating in HP.

While the <u>hard component</u> of a hadron system (a few

hadrons with the energy fraction $z \sim 1$) determines the partonic skeleton of an event, the soft component (the other hadrons with $z \ll 1$) forms the bulk of multiplicity.

Closely following the radiation pattern, associated with the partonic skeleton, the soft component is concentrated inside the bremsstrahlung cones of QCD jets. Theoretically, the opening angle of each cone is bounded by the nearest other jet, since at larger angles particles are emitted coherently by the overall colour charge of both jets. Even though the bremsstrahlung cones of the neighbouring jets strongly overlap, the resulting total multiplicity can be presented as the additive sum of the contributions of the individual jets, see for detail Subsec. 8.1.

If one keeps the angle between the two jets fixed, then with increase of the total energy these jets become experimentally distinguishable. This fact stems from the asymptotical collimation of the energy and multiplicity flows within each jet. Shrinkage of the characteristic opening angle permits one to introduce the notions of the 'intrajet' and the 'interjet' hadron flows.

7.3. QCD Portrait of Individual Jet [66]

Let us consider the general inclusive characteristics which may be called, in some sense, the characteristics of an isolated jet (neglecting the mutual influence of jets in their ensemble). One can study the properties of an individual quark jet when measuring the different inclusive distributions in the process $e^+e^- \longrightarrow$ hadrons. The decay into two gluons of the C-even heavy quarkonium states, $\chi_Q = Q\bar{Q}$, might define, by analogy, the individual gluon jets. In spite of the high importance of the coherence phenomena the notion of the isolated jet makes sense, if one does not deal with the azimuthal effects,

but considers only multiplicities, energy spectra and correlations, etc. In this case all the influence of the jet ensemble on a given jet may be encoded in a single parameter θ_o, the jet 'opening angle', this, in essence, being the angle between the considered jet and the nearest other one.

Multiplicity, energy spectra of particles and the other jet characteristics prove to depend not on the jet energy E but on the hardness, Q, of the process producing jet, i.e. on the product of jet energy and its opening angle θ_o, $Q = E\theta_o$ at $\theta_o \ll 1$.

7.3.1. Collimation of energy in jet. Consider a jet with the energy E and the opening angle θ_o. Let us try to answer the question, what is the angular size θ ($Q_0/E \lesssim \theta \lesssim \theta_0$) of the cone, where the definite fraction $z \sim 1$ of the jet energy is deposited (see Fig. 15). The smaller

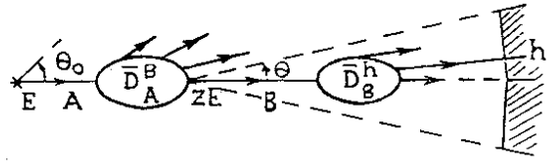

Fig.15. Production of a subjet B being registered by the calorimeter with the angular aperture θ.

is the angle, where the bulk of the energy is concentrated (aperture of the energy flux), the higher is the jet collimation. Experimentally this task would correspond to the calorimetric measurement of the energy flux being deposited within the given cone.

From the point of view of PT the sequential parton decays in a cascade are ordered in angles (the 'hard' decays due to the LLA kinematics and the 'soft' ones due to the QCD coherence). Therefore a calorimeter measures

an energy of a subjet, initiated by a parton B, produced at that stage of the cascade evolution where the characteristic transverse momenta in the decays, $k_\perp$, are of order $z\Sigma\theta$. In other words, a calorimeter with an aperture θ registers the energy spectrum of the intermediate partons at the certain phase of the development of the partonic system. Hence, the probability that the energy fraction z is deposited in a cone with an opening angle θ, should be related to the inclusive spectrum of partons

$$\bar{\mathcal{D}}_A(z,\xi_{\theta_0},\xi_\theta) = \sum_{B=q,g} \bar{\mathcal{D}}_A^B(z,\xi_{\theta_0},\xi_\theta) \quad , \qquad (7.3)$$

where A denotes the incoming parent parton (A = q, g) and $\xi_\theta = 1/b \ln\ln(E\theta/\Lambda)$ at $\theta < \theta_0 \ll 1$. We assume here that the type of the registered parton B is not identified.

To quantify the energy collimation in jet let us suppose that the deposited share of energy is large, $z \to 1$. Then the 'valence' contribution, $D_A^A(1-z)$, dominates in eq. (7.3)

$$\bar{\mathcal{D}}_A^A(z,\xi_{\theta_0},\xi_\theta) \simeq (1-z)^{4C_A\Delta\xi-1} \cdot \frac{\exp[C_A(3-4\gamma_E)\Delta\xi]}{\Gamma(4C_A\Delta\xi)} \quad , \qquad (7.4)$$

where $\Delta\xi = \xi_{\theta_0} - \xi_\theta$ corresponds to the evolution from the incoming parton A to the parton B=A, decaying inside a given cone with opening angle θ ($\gamma_E \simeq 0.5772$, $C_q \equiv C_F = 4/3$, $C_g \equiv N_c = 3$).

At fixed value of z this formula describes the distribution in θ, that has a characteristic maximum at some angle $\theta = \theta_z$. Indeed, when $\theta \to \theta_0$, practically the whole energy should be deposited in the cone. The fact, that only a certain energy fraction z has been registered, means that the fraction (1-z) is carried away by the additional hard partons produced at larger angles (smallness $\sim \alpha_s(E\theta_0)$; $\bar{D}_A^A(z,\Delta\xi) \to (1-z)$ at $\Delta\xi \to 0$).

Therefore, the probability $\bar{D}$ for $z \neq 1$ should rapidly decrease when $\theta \to \theta_0$. On the contrary, with θ decreasing (down to $\theta \gtrsim \Lambda/E$) the share of emission outside the cone grows. The quantity $\Delta\xi$ increases, and so the probability $\bar{D}$, that the energy fraction z is deposited in the cone, decreases again (the effect similar to the Sudakov form factor). To illustrate the energy dependence of the quantity θ_z,

$$\frac{\theta_z}{\theta_0} = \left(\frac{E\theta_0}{\Lambda}\right)^{-\gamma_A(z)} \qquad (7.5)$$

we present the approximate values of $\gamma_A(z)$ at z=0.9 and z=0.5 (see Fig. 16)

$$\gamma_q(0.9) \simeq 0.55, \qquad \gamma_q(0.5) \simeq 0.83;$$
$$\gamma_g(0.9) \simeq 0.30, \qquad \gamma_g(0.5) \simeq 0.54.$$

It follows from eq.(7.5) and Fig. 16 that the energy collimation in a quark jet is stronger than in gluon one, and the collimation grows as energy increases.

7.3.2. Energy spectrum of particles within given cone. Even more subtle proves to be a spectral characteristic of the energy flux registered by a calorimeter with the angular aperture θ. Such a quantity represents a correlation between the energy flux and a particle within this flux. This implies, in essence, the double inclusive cross section: a parton B is registered as well as one of its offstrings, a particle h, as shown in Fig.15. The distribution in x, the energy fraction, of hadrons of type h within the registered energy flux may be presented as the convolution

$$\mathcal{F}_A^h(x,\theta;E,\theta_0) = \sum_{B=q,g} \int_x^1 dz\, \bar{\mathcal{D}}_A^B(z,E\theta_0,zE\theta)\, \bar{\mathcal{D}}_B^h\left(\frac{x}{z},zE\theta,Q_0\right) . \qquad (7.6)$$

In the above $\bar{D}_A^B$ determines the probability to find the parton B, initiating the subjet with the energy E and the opening angle θ, within a jet A, and $\bar{D}_B^h$ describes

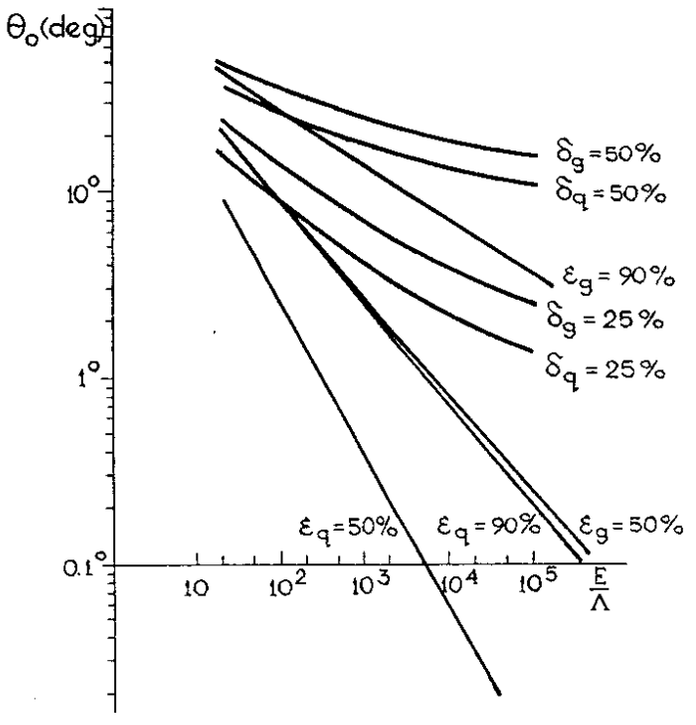

Fig.16. Shrinkage of the cones, in which the fixed shares of multiplicity (δ_A) or energy (ε_A) of a jet A(A=q,g) are concentrated.

the distribution in the energy fraction x/z of hadrons of type h in a subjet B.

Notice, that one can obtain eq. (7.6) by integrating the standard expression for the double-inclusive correlation between particles [1].

An integration over z in eq.(7.6) corresponds to the simplest case when it is known, that an energy flux is deposited within a given solid angle, but the corresponding

energy share is not measured. If one fixes the value of z, the integration in eq.(7.6) should be omitted. To estimate the integral in eq.(7.6) one can neglect z in the arguments of all logs since only the values of $z \sim 1$ are essential. This stéms from the behaviour of the function $\bar{D}_B^h$ at $x \ll 1$

$$\bar{D}_B^h(x, E\theta_o, Q_o) = 1/x \cdot \rho(1/x,\ \ln E\theta_o/\Lambda\ ,\ \ln Q_o/\Lambda), \qquad (7.7)$$

where ρ is a slowly changing logarithmic function that describes the hump-backed plateau (see Sec. 6).

For better understanding the correlative nature of eq. (7.6) one may consider the two limiting cases.

$$\text{(i)}\ \ \theta \to \theta_o\ ,\ \bar{\mathcal{D}}_A^B(z) \to \delta(1-z)\delta_A^B,\ \mathcal{F}_A^h \to \bar{\mathcal{D}}_A^h(x, E\theta_o, Q_o)\ . \qquad (7.8)$$

In this case the whole energy flux of a jet A is deposited in a calorimeter, and the particle spectrum coincides with that in the overall jet.

$$\text{(ii)}\ \ \theta \to \frac{Q_o}{zE}\ ,\ \bar{\mathcal{D}}_B^h \to \delta(1-\frac{x}{z})\delta_B^h\ ,\ \mathcal{F}_A^h \to x\bar{\mathcal{D}}_A^h(x, E\theta_o, Q_o)\ . \qquad (7.9)$$

Here a'subjet' reduces only to one hadron h, the energy flux is predetermined by the value of x. Then the correlation disappear, and the expression (7.6) factorizes into x, the energy flux, and $\bar{D}_A^h$, the probability for finding a hadron h with an energy fraction x inside a jet A.

The correlation, that in a general case (at $x < 1$) is described by eq.(7.6), disappears, in fact, also for soft hadrons h, where $x \ll 1$. Emission of such particles proves to be less sensitive to the energy balance, and it should be determined by the average 'colour current' of hard partons. Substituting eq.(7.7) to eq.(7.6) at $x \ll 1$ one has

$$F_A^h(x, \theta\ ;\ E, \theta_o\ ) \simeq \langle C\rangle_A/N_c \cdot \bar{D}_g^h(x, E\theta, Q_o), \qquad (7.10)$$

where $\bar{D}_g^h$ is the known spectrum of particles h in a gluon

jet having the energy E and the opening angle θ_o, and the quantity $\langle C\rangle_A$ is (7.11)

$$\langle C\rangle_A = \langle z_g\rangle_A C_g + \langle z_q\rangle_A C_q \quad (C_g \equiv N_c,\ C_q \equiv C_F)$$

In the above

$$\langle z_B\rangle_A = \int_0^1 dz\, z\, \bar{\mathcal{D}}_A^B(z, E\theta_o, E\theta) \quad , \quad \langle z_g\rangle_A + \langle z_q\rangle_A = 1 \quad ,$$

represents the average 'colour current' of parton B registered by a calorimeter.

Integrating eq. (7.6) over x one immediately obtains the multiplicity of hadrons of type h in a registered flow

$$N_A^h(\theta; E, \theta_o) = \langle C\rangle_A / N_c \cdot N_g^h(E\theta). \qquad (7.12)$$

Thus, as it is easily seen from eqs.(7.10), (7.12), for a registered part of a jet the energy spectrum of particles as well as their multiplicity are proportional to those in an isolated g-jet with the different hardness $Q = E\theta$. The hardness of a primary A-jet, $E\theta_o$, determines only a proportionality coefficient, that is the average colour current of the parent parton initiating the registered part of a jet (as measured in the units of a gluon charge, $C_V = N_c$).

The value of the mean colour current, originated by a parton A depends on the momentum balance between the quarks and the gluons in evolution of a jet A. The momenta carried away by the quarks ($\langle z_q\rangle_A$) and the gluons ($\langle z_g\rangle_A$) are calculable in the LLA [1]. Substituting them to eq.(7.11) one obtains

$$\begin{aligned} \langle C\rangle_q &= \langle C\rangle_\infty - \alpha(N_c - C_F)\cdot e^{-\gamma\Delta\xi} \quad , \\ \langle C\rangle_g &= \langle C\rangle_\infty + \beta(N_c - C_F)\cdot e^{-\gamma\Delta\xi} \quad , \\ \langle C\rangle_\infty &= \alpha N_c + \beta C_F \quad , \end{aligned} \qquad (7.13)$$

where

$$\Delta\xi = \frac{1}{b}\ln\frac{\ln(E\theta_o/\Lambda)}{\ln(E\theta/\Lambda)} \quad , \quad \gamma = \frac{8}{3}C_F + \frac{2}{3}N_c \quad , \quad \alpha = \frac{8}{3}\frac{C_F}{\gamma} \quad , \quad \beta = \frac{2}{3}\frac{n_f}{\gamma} \quad .$$

Eqs.(7.13) describe, in some sense, the process of losing by a registered parton B the memory of the colour charge of a parent parton A, as the aperture θ decreases. In asymptotics, when $E \to \infty$ and $\theta \to 0$ ($\theta > Q_0/E$), one has $\langle C_q\rangle = \langle C_g\rangle = \langle C\rangle_\infty = 2.4$ for $n_f = 3$ and 2.12 for $n_f = 6$. This mean colour current of a parton in a cascade proves to be, naturally, somewhere in-between the gluon and the quark charges. Therefore, for a gluon jet the 'colour-grasp' of an emitter decreases with θ decreasing, and for a quark jet this quantity increases, as shown in Fig. 17.

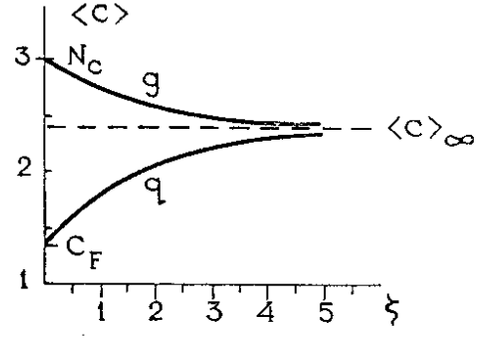

Fig.17. The mean colour current of parton ⟨C⟩ in the q- or g-jet with hardness $Q=E\theta_o$ (E is the jet energy, θ_o is its opening angle) as registered by the calorimeter with an angular aperture θ, $\xi = \ln\ln E\theta_o/\Lambda - \ln\ln E\theta/\Lambda$.

It is of interest that, while the ratio of the total multiplicities in g- and q-jets asymptotically equals to $C_g/C_q = 9/4$, for the case of a narrow cone of observation this ratio tends asymptotically to 1.

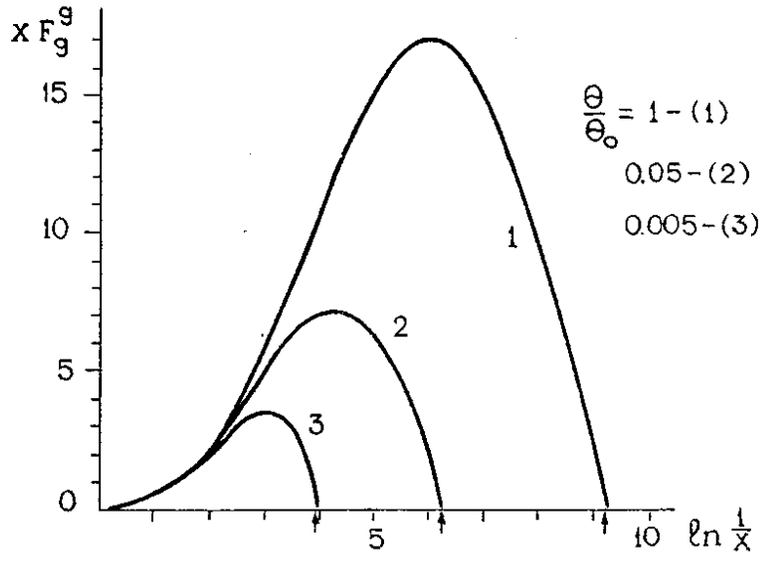

Fig.18. Energy spectrum of partons (versus ln 1/x) in a gluon jet with an opening angle θ_0, registered by the calorimeter with an angular aperture θ: (1) for the whole aperture $\theta/\theta_0 = 1$, (2) - $\theta/\theta_0 = 0.05$, and (3) - $\theta/\theta_0 = 0.05$.

Fig. 18 illustrates the dependence of an energy distribution on the aperture of the registered particle flow, as given by eq. (7.6). The narrower is the registration cone, the harder are the particles within this cone, $x > x_{min} = Q_0/E\theta$. On the other hand, eq.(7.6) describes the average energy flux deposited within a cone θ around the registered hadron h carrying an energy fraction x. As seen in Fig.18, a soft hadron with $x \ll 1$ is 'accompanied' by the energy flux only starting from the sufficiently large values of the calorimeter aperture,

$$\theta > \theta_{min} = Q_0/xE. \qquad (7.14)$$

7.3.3. Collimation of multiplicity inside jet. By analogy with the discussion above, one can ask, what is the angular size θ of the cone, where the main part of jet multiplicity is concentrated, and what is the energy behaviour of this aperture.

To answer this question quantitatively one should solve the equation

$$N_A^h(\theta_\delta; E, \theta_0) = \delta \cdot N_A^h(E\theta_0) \qquad (7.15)$$

and find the value of the angle θ_δ, where the share δ of the total multiplicity is concentrated. Then accounting for the DL relation $N_A(E\theta_0) = C_A/N_C \cdot N_g(E\theta_0)$, from eqs. (7.12),(7.15) one can obtain

$$\langle C \rangle_A N_g^h(E\theta_\delta) = \delta \cdot C_A \cdot N_g^h(E\theta_0) \quad . \qquad (7.16)$$

Using eqs. (7.13) we can rewrite eq.(7.16) in the form

$$\left[a_A + b_A \left(\frac{\ln \frac{E\theta_\delta}{\Lambda}}{\ln \frac{E\theta_0}{\Lambda}} \right)^{\frac{50}{81}} \right] N_g^h(E\theta_\delta) = \delta N_g^h(E\theta_0) \ , \qquad (7.17)$$

where

$a_q \simeq 1.8$, $b_q \simeq 0.8$ and $a_g \simeq 0.8$, $b_g \simeq 0.2$.

Shown in Fig.16, for both q- and g-jets, is the dynamics of shrinkage of the cones θ_δ, where the shares $\delta = 0.25$ and $\delta = 0.5$ of the jet multiplicity are concentrated. As it is easily seen, the multiplicity flow in a q-jet is collimated around the direction of the energy flux much stronger than in a g-jet. With the jet energy increasing the collimation of the multiplicity flow grows much slower than that of the energy flux.

One can obtain a qualitative estimate for the growth of the multiplicity collimation roughly simplifying eq. (7.17),

$$N(E\theta_\delta) = \delta \cdot N(E) \quad \text{at} \quad \theta_0 \sim 1,$$

$$\exp\sqrt{\frac{16N_c}{b}\ln\frac{E\theta_\delta}{\Lambda}} = \delta\cdot\exp\sqrt{\frac{16N_c}{b}\ln\frac{E}{\Lambda}}$$

This leads to

$$\theta_\delta \sim [N(E)]^{\,b/8N_c\cdot\ln 1/\delta}. \qquad (7.18)$$

Thus, the solid angle, where a half of jet multiplicity is concentrated, decreases with the increase of jet hardness ($E\theta_0 \sim E$) approximately as $N^{-1/4}(E)$, i.e. parametrically much slower than in the case of the energy collimation (see eq. (7.5)).

7.3.4. Angular distribution of multiplicity inside jet. Finally, let us consider the angular distribution of a multiplicity flow around the direction of a jet energy flux. This can be obtained by differentiating eq.(7.12) over the variable ln θ.

$$\frac{d}{d\ln\theta}N_A^h(\theta;E,\theta_0) \simeq \frac{\langle C\rangle_A}{N_c}\frac{d}{d\ln\theta}N_g^h(\ln E\theta) + O(\alpha_s N_g^h). \qquad (7.19)$$

Here the main contribution comes from the rapidly rising exponent describing the asymptotical growth of the particle multiplicity in a jet, as given by eqs.(6.52), (6.53)

$$\frac{dN_g^h(\ln(E\theta))}{d\ln\theta} \simeq \sqrt{\frac{4N_c\alpha_s(E\theta)}{2\pi}}\,N_g^h(\ln(E\theta)) + O(\alpha_s N_g^h). \qquad (7.20)$$

8. RADIOPHYSICS OF PARTICLE FLOWS [7,8,19]

In the framework of LPHD the source of multiple hadroproduction in HPs is gluon bremsstrahlung, so one should expect that all of the produced hadrons are the consequences of the colour dynamics. Therefore, the properties of the partonic skeleton, such as the flow of colour quantum numbers, should influence the distribution of colour singlet hadrons in the final state.

The phenomenon of such a kind has been first observed in the experiments (see refs. [9,12,13] and references therein), studying the angular flows of hadrons in three-jet ($q\bar{q}g$) events from e^+e^- annihilation, the so-called string [67] (or drag [43]) effect. The data have strongly supported the predicted drag of the interjet particles in the direction of the gluon jet (net destructive interference in the region between the q and $\bar{q}$), for details see Subsec. 8.2.

Detailed studies of the string-like phenomena are of importance for the high energy HPs. These effects are interesting not only in their own right as tests of QCD. They should be valuable in helping to distinguish new physics signals from the conventional QCD backgrounds.

In this Section we examine the distributions of multiplicity flow accompanying reactions with the complex topology, where three or more hard partons are involved in a HP. Our emphasis is on the QCD coherent drag phenomena and their manifestations in different types of hard interactions. Let us begin with the particle distributions in the gold-plated three-jet events.

8.1. Inclusive QCD Portrait of $q\bar{q}g$ Events of e^+e^- Annihilation

8.1.1. Spatial distribution of multiplicity flow [61]

In terms of the inclusive approach, discussed in the previous Sec. , a proper inclusive characteristic of the spatial distribution of particle flows in the $e^+e^- \to q\bar{q}g$ events is the E^3MC

$$\frac{dN_4}{d\Omega} = \sum_{a,b,c} \int dE_a dE_b dE_c dE_{\vec{n}} \frac{E_a E_b E_c \, d\sigma_4}{\sigma_3 \, dE_a dE_b dE_c dE_{\vec{n}} d\Omega_a d\Omega_b d\Omega_c d\Omega} , \tag{8.1a}$$

$$\sigma_3 = \sum_{a,b,c} \int dE_a dE_b dE_c \frac{E_a E_b E_c \, d\sigma_3}{dE_a dE_b dE_c \, d\Omega_a d\Omega_b d\Omega_c} , \tag{8.1b}$$

where the sum is over all particle types. This represents an angular correlation between the three registered hard particles (a, b, c), moving in the directions $\vec{n}_a$, $\vec{n}_b$ and $\vec{n}_c$ and the multiplicity flow around the direction $\vec{n}$, see Fig.19. When all three vectors $\vec{n}_a$, $\vec{n}_b$ and $\vec{n}_c$ are in the same plane, the main contribution to dN_4 comes from the $q\bar{q}g$ configuration of the primary parton system. In the leading order in α_s the parton kinematics is unambiguously fixed as follows

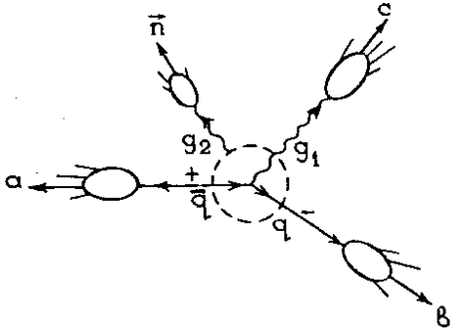

Fig.19. Angular inclusive correlation between three energetic (a,b,c) and one soft particle ($\vec{n}$) in the process of e^+e^- annihilation

$\vec{n}_+ \simeq \vec{n}_a$, $\vec{n}_- \simeq \vec{n}_b$, $\vec{n}_1 \simeq \vec{n}_c$;

$$x_+ = 2\frac{\sin\theta_{1-}}{\sum \sin\theta_{ij}} , \quad x_- = 2\frac{\sin\theta_{1+}}{\sum \sin\theta_{ij}} , \quad x_1 = 2\frac{\sin\theta_{+-}}{\sum \sin\theta_{ij}} \tag{8.2}$$

$(x_+ + x_- + x_1 = 2)$,

where $x_i = 2E_i/W$ are the normalized parton energies, θ_{ij} are the angles between partons i and j (+,- $\equiv q\bar{q}$; $1 \equiv g_1$).

Emphasize here, that owing to coherence, the radiation of a secondary soft gluon g_2 ($k_2 \ll E_i$) at angles higher than the characteristic angular size of each parton jet proves to be insensitive to its internal structure: g_2 is emitted by the colour current which is conserved when the jet splits. That is the reason why one may replace each jet by its parent parton with $p_i^2 \simeq 0$, as, e.g., in eq. (8.2).

Let us turn firstly to the simpler case of two-jet events. Here the particle flow distribution corresponding to the discussed above correlation (7.2a) can be written as

$$\frac{8\pi \, dN_{q\bar{q}}}{d\Omega} = \frac{2}{a_+} N_q'(Y_+, Y) + \frac{2}{a_-} N_q'(Y_-, Y), \tag{8.3}$$

where $N_A'(Y_i,Y) \equiv (d/dY_i) N_A(Y_i,Y)$; $N_A(Y_i, Y)$ stands for the multiplicity in a jet $A(A = q,g)$ of particles, concentrated in the cone with an angular aperture θ_i around the jet direction $\bar{n}_i$. In the above $a_i \equiv 1 - \vec{n}\vec{n}_i$ $(i = +, -)$, $\bar{n}_+ \simeq \bar{n}_a$, $\bar{n}_- \simeq \bar{n}_b = -\bar{n}_a$,

$$Y_i \equiv \ln (E/\Lambda \cdot \sqrt{a_i/2}), \quad Y \equiv \ln E/\Lambda$$

and $E = W/2$ is the jet energy.

To understand the meaning of the quantity $N_A(Y_i,Y)$ it is helpful to represent it as

$$N_A(Y_i,Y) = \sum_{B=q,g} \int_0^1 dz \; z \, \mathcal{D}_A^B(z, \Delta\xi) \, N_B(\bar{Y}_i) , \tag{8.4}$$

$$\Delta\xi = \frac{1}{b}\ln\frac{Y}{\bar{Y}_i} \quad , \quad \bar{Y}_i = Y_i + \ln z = \ln\left(\frac{zE}{\Lambda}\sqrt{\frac{a_i}{2}}\right)$$

(see for details Subsec. 7.3).

In the above N_B is the multiplicity initiated by a parton B within the cone θ_i, and $\bar{D}_A^B$ denotes the structure function for parton fragmentation $A \to B$ (see ref. [1]). Eq. (8.4) accounts for the fact that due to coherence the radiation at small angles $\theta_i \ll 1$ is governed not by the overall colour current of a jet A, but by that of a subjet B, developing inside a much narrower cone θ_i. This formula has a correct limit at $\theta_i \to \pi$,

$Y_i \longrightarrow Y$, $\Delta\xi \to 0$, $\bar{D}_A^B \to \delta(1-z)\,\delta_A^B$, $N_A(Y_i, Y) \to N_A(Y)$.

Eq. (8.2) looks, formally, as the sum of two contributions, accounting for the independent evolution of the q and $\bar{q}$-jets. However, one can see, that this reflects also the collective character of the soft radiation at large angles. Indeed, in this case neglecting relative corrections of order $O(\alpha_s)$ one obtains

$$N_q'(Y_+, Y) \simeq N_q'(Y_-, Y) \simeq N_q'(Y) \sim \sqrt{\alpha_s}\cdot N_q(Y), \qquad (8.5)$$

and eq.(8.2) can be transformed to

$$\frac{8\pi\, dN_{q\bar{q}}}{d\Omega} = \frac{2C_F}{N_c}\,(\hat{+-})\,N_g'\left(\ln\frac{E}{\Lambda}\right) \quad , \qquad (8.6)$$

where the notations of eqs.(7.20) and (3.13) are used ($a_+ + a_- = a_{+-} = 2$). Eq. (8.6) represents, in fact the radiation pattern for the interjet gluon emission by an antenna $(\hat{+-})$, of eq.(3.12), the factor N_g' takes into account that the final gluon is a part of a cascade

$$\int^{E}\frac{dE_g}{E_g}\,4N_c\,\frac{\alpha_s(E_g)}{2\pi}\,N_g\left(\ln\frac{E_g}{\Lambda}\right) = N_g'\left(\ln\frac{E}{\Lambda}\right) \quad .$$

For the so-called radiative two-jet events ($e^+e^- \to q\bar{q}g$) the emission pattern is given by a $q\bar{q}$ sample Lorentz

boosted from the quark cms to the lab.system (i.e. the cms of $q\bar{q}g$), and the corresponding particle multiplicity should surely be equal to that in $e^+e^- \to q\bar{q}$ at $W^2_{q\bar{q}} = (p_q + p_{\bar{q}})^2$. It is useful also to introduce here the Lorentz-invariant generalization of the rapidity $y_{\parallel}$ of an emitted gluon k and its momentum component transverse to the + and - directions, $k_\perp$,

$$y_{\parallel} = \frac{1}{2}\ln\frac{(p_q k)}{(p_{\bar{q}} k)} \quad , \quad k_\perp^2 = \frac{2(p_q k)(p_{\bar{q}} k)}{(p_q p_{\bar{q}})} \qquad (8.7)$$

By analogy with eq.(8.2) the formula for angular distribution of particle flow in $q\bar{q}g$ events can be written as

$$\frac{8\pi\, dN_{q\bar{q}g}}{d\Omega} = \frac{2}{a_+}N_q'(Y_{q+}, Y_q) + \frac{2}{a_-}N_{\bar{q}}'(Y_{\bar{q}-}, Y_{\bar{q}}) + 2I_{+-}\cdot N_g'(Y) \quad , \qquad (8.8)$$

where

$$Y_{q(\bar{q})} = \ln\frac{E_{q(\bar{q})}}{\Lambda}, \quad Y_{q+} = \ln(E_q/\Lambda\cdot\sqrt{a_+/2}), \quad Y_{\bar{q}-} = \ln\left(\frac{E_{\bar{q}}}{\Lambda}\sqrt{\frac{a_-}{2}}\right), \qquad (8.9)$$

$$Y = \ln E/\Lambda \quad , \quad E = W/2,$$

and

$$I_{+-} = (\hat{+-}) - 1/a_- - 1/a_+. \qquad (8.10)$$

For the emission at large angles ($a_+ \sim a_- \sim 1$) when according to eq.(8.5) all the factors N' are approximately the same, eq. (8.8) coincides with eq. (8.6).

We are ready now to deal with the three-jet event sample when a hard radiative photon is replaced by a gluon g_1. For a given $q\bar{q}g_1$ configuration the particle flow can be presented, analogously to eqs. (8.8)-(8.10), as (8.11)

$$\frac{8\pi\, dN_{q\bar{q}g}}{d\Omega} = \frac{2}{a_+}N_q'(Y_{q+}, Y_q) + \frac{2}{a_-}N_{\bar{q}}'(Y_{\bar{q}-}, Y_{\bar{q}}) + \frac{2}{a_1}N_g'(Y_{g1}, Y_g)$$
$$+ \left[I_{1+} + I_{1-} - \left(1 - \frac{2C_F}{N_c}\right)I_{+-}\right]N_g'(Y)$$

with $Y_A = \ln E_A/\Lambda$, $Y_{Ai} = \ln(E_A/\Lambda\cdot\sqrt{a_i/2}\,)$, $Y = \ln E/\Lambda$.

This formula accounts for both types of coherence: the angular ordering inside each of jets and the collective nature of the interjet flows. The first three terms in eq. (8.11) are collinear singular as $\theta_i \to 0$ and contain the factors N', describing the evolution of each of the QCD jet initiated by the hard emitters $q, \bar{q}$ and g_1. The last term in eq.(8.11) accounts for the interference between these jets. It has no collinear singularities and contains the common factor $N'(Y, Y)$ independent of the direction $\vec{n}$.

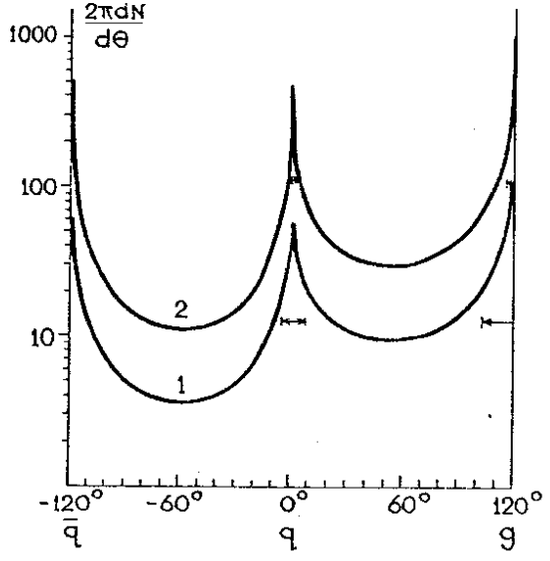

Fig.20. Particle angular flows in the three-fold symmetric $q\bar{q}g$ events on the event plane with respect to the q-jet axis at different values of the parameter E/Λ = 60 (1), 1000 (2). Arrows indicate the mean cone apertures, where the 50% of the energy flow of each jet is concentrated.

Fig. 20 illustrates the predicted distribution of particle flows projected onto the event plane for the three-fold symmetric $q\bar{q}g$ events.

As it follows from eqs. (8.8),(8.11) when replacing a radiative photon by a gluon g_1, with otherwise identical kinematics, an additional particle flow arises

$$\left(\frac{8\pi\, dN}{d\Omega}\right)_g = \frac{8\pi\, dN_{q\bar{q}g}}{d\Omega} - \frac{8\pi\, dN_{q\bar{q}}}{d\Omega} = \tag{8.12}$$

$$= 2/a_1 \cdot N_g'\,(Y_{g_1}\,,\, Y_g) + \left[I_{1+} + I_{1-} - I_{+-}\right] N_g'\,(Y).$$

Note that for the case of large radiation angles both cascading factors N' become approximately equal and one has

$$\left(\frac{8\pi\, dN}{d\Omega}\right)_g = \left(\,(\hat{1+}) + (\hat{1-}) - (\hat{+-})\right)\cdot N_g'\,(Y). \tag{8.13}$$

An interesting point is that this expression which seems to look as a 'true' gluon contribution is not positively definite. One can see clearly, e.g., the net destructive interference in the region between the q- and $\bar{q}$-jets. The soft radiation including the gluon jet proves to be less than that in the absence of the gluon jet [43]! This drag phenomenon is clearly seen in the recent experiments (see refs. [9,12,13]) thus strongly supporting the LPHD concept. The physics of drag effect shall be discussed in more detail in Subsec. 8.1.3.

Finally, let us emphasize that for detailed study of $q\bar{q}g$ events it would be important to identify quark and gluon jets. This could be made in heavy quark events $Q\bar{Q}g$ (Q = c, b) [43]. For example, one may utilize the high rates at the Z^0-factories. If we take the integrated luminosity $\int \mathcal{L}\, dt$ /experiment to be $\sim 2\cdot 10^{38}$ cm^{-2}, we expect $\sim 10^5$ $c\bar{c}g$, $b\bar{b}g$ events produced. Possible taggings of the heavy quark jets include, e.g., secondary vertex tag, triggering on high $p_\perp$ leptons or the specific decay modes

of the heavy particles, etc.

8.1.2. On total particle multiplicity in $q\bar{q}g$ events.

Let us discuss the connection of the particle multiplicities in two-jet and three-jet samples of e^+e^-annihilation. The particle multiplicity in an individual quark (gluon) jet can be defined through that in $e^+e^- \to q\bar{q} \to$ hadrons ($\mathcal{X}_Q \to gg \to$ hadrons) as follows

$$N_{e^+e^-}(W) = 2\, N_q\,(E)\cdot(1 + O(\alpha_s(E))),\ E = W/2, \qquad (8.14a)$$

$$N_{\mathcal{X}_Q}(M_{\mathcal{X}}) = 2\, N_g\,(E)\cdot(1 + O(\alpha_s(E))),\ E = M_{\mathcal{X}}/2. \qquad (8.14b)$$

When three or more partons are involved in a HP, say, $e^+e^- \to q\bar{q}g_1$ the multiplicity can not be interpreted in a similar simple way. The point is that multiplicity becomes depending on the geometry of the whole jet ensemble.

So, the problem arises of describing the multiplicity in three-jet events, $N_{q\bar{q}g}$, in terms of the discussed above characteristics of q- and g-jets. The quantity $N_{q\bar{q}g}$ should depend on the $q\bar{q}g$ geometry in a Lorentz-invariant way and should have a correct limit when the event is transformed to two-jet configuration by decreasing an energy of a gluon g_1 or by decreasing its emission angle.

Note that when deriving the formula for $N_{q\bar{q}g}$ accounting for the interjet contribution, one needs to control systematically the relatively small $\sim\sqrt{\alpha_s}$ terms. Formally, the MLLA analysis does not provide such an accuracy, since the change of scale of parameter Λ, say, $\Lambda \to C\Lambda$ leads to the relative change of N

$$\Delta N/N \sim \sqrt{\alpha_s(E)}\cdot \ln C.$$

The subleading to the MLLA, $\alpha_s^{3/2}$ corrections to the anomalous dimension $\gamma(\alpha_s)$ (see Sec. 6), that generate $\sqrt{\alpha_s}$ terms in the multiplicity, can be calculated if the second

loop contribution to the β function is included. This is interesting, theoretically, in its own right, but for our purposes here it is enough to note, that $\alpha_s^{3/2}$ corrections to γ can be formally absorbed into the definition of parameter Λ, the value of which is determined phenomenologically from connection of the MLLA partonic spectra with the measured ones [41,42].

In the following we shall use the MLLA eqs.(6.52), (6.53)-formulae for particle multiplicities with just that very value of Λ. This permits one to fix the energy dependence of the hadron multiplicities including the terms $\sim\sqrt{\alpha_s}\cdot N$.

One can easily check that integration of eq. (8.2) over the total solid angle reproduces eq.(8.14a). Similarly, with an account of eq.(5.27) the angular integral of eq. (8.8) can be written as (8.15)

$$N_{q\bar{q}g} = \int \frac{dN_{q\bar{q}g}}{d\Omega}\, d\Omega = N_q(Y_q) + N_{\bar{q}}(Y_{\bar{q}}) + 2\ln\sqrt{\frac{a_{+-}}{2}}\cdot N_g'(Y).$$

Now we can transform this formula to the Lorentz-invariant form. For this let us rewrite $Y_{q(\bar{q})}$ as

$$Y_{q(\bar{q})} = Y + \ln x_{+(-)},\ x_{+(-)} \equiv E_{q(\bar{q})}/E \qquad (8.16)$$

and use the expansion

$$N_q(Y_q) = N_q(Y) + \ln x_+ \cdot N_q'(Y) + O(\alpha_s\cdot N_q). \qquad (8.17)$$

Then

$$N_{q\bar{q}g} = 2N_q(Y) + 2\ln\sqrt{\frac{x_+x_-a_{+-}}{2}}\, N_q'(Y) + O(\alpha_s N)$$

$$= 2N_q(Y_{+-}^*)\cdot(1 + o(\sqrt{\alpha_s})), \qquad (8.18)$$

where

$$Y_{+-}^* = Y + \ln\sqrt{\frac{x_+x_-a_{+-}}{2}} = \ln\sqrt{\frac{(P_qP_{\bar{q}})}{2\cdot\Lambda^2}} = \ln\frac{E^*}{\Lambda} \qquad (8.19)$$

and E^* is the quark energy in the cms of $q\bar{q}$, i.e. the Lorentz-invariant generalization of a true parameter of hardness of q ($\bar{q}$)-jet. The multiplicity $N_{q\bar{q}g}$ is, by analogy

$$N_{q\bar{q}g} = \int \frac{dN_{q\bar{q}g}}{d\Omega} d\Omega = N_q(Y_q) + N_{\bar{q}}(Y_{\bar{q}}) + N_g(Y_g) + \left[\ln\sqrt{\frac{a_{1+}a_{1-}}{2a_{+-}}} + \frac{2C_F}{N_c}\ln\sqrt{\frac{a_{+-}}{2}}\right]\cdot N_g'(Y), \quad (8.20)$$

where $Y_{q(\bar{q})} = Y + \ln x_{+(-)}$, $Y_g = Y + \ln x_1$, $Y = \ln E/\Lambda$. Using the expansion analogous to eq. (8.17) for the multiplicity of each of jets one comes to the final Lorentz-invariant result

$$N_{q\bar{q}g} = \left[2N_q(Y^*_{+-}) + N_g(Y^*_g)\right]\cdot(1 + O(\alpha_s)) \quad (8.21)$$

with $Y^*_{+-} = \ln\left(\sqrt{\frac{(P_+P_-)}{2}}/\Lambda\right)$, $Y^*_g = \ln\left(\sqrt{\frac{(P_+P_1)(P_-P_1)}{2(P_+P_-)}}/\Lambda\right) = \ln\frac{P_{1\perp}}{\Lambda}$

where $P_{1\perp}$ stands for the transverse momentum of g_1 in the cms of $q\bar{q}$, cf. eq. (8.7).

As is easily seen from eqs.(8.18),(8.21), the replacement of a photon by a gluon g_1 leads to an additional multiplicity

$$N_g(Y_g^*) = N_{q\bar{q}g}(W) - N_{q\bar{q}\gamma}(W), \quad (8.22)$$

which depends not on the gluon energy but on its transverse momentum, i.e. on the hardness of the primary process. Eq. (8.21) reflects the coherent nature of soft emission and has a correct limit when the event is transformed to two-jet configuration.

Another form of representing $N_{q\bar{q}g}$,

$$N_{q\bar{q}g} = 2N_q(Y^*_{+-}) + N_g(Y^*_{1+}) + N_g(Y^*_{1-}) - N_g(Y^*_{+-}) + O(\alpha_s N), \quad (8.23)$$

where $Y^*_{ij} = \ln\left(\sqrt{\frac{(P_iP_j)}{2}}/\Lambda\right) = \ln E^*_{ij}/\Lambda$, deals with the multiplicities of two-jet events at the appropriate invariant pair energies E^*_{ij}. This formula has also

proper limit, $2N_g$, when $q\bar{q}g$ configuration is transformed to a quasi-two-jet one, $g + q\bar{q}$ with the small angle between q and $\bar{q}$.

8.1.3. Drag effect in three-jet events [43]. Consider now the particle flows at large angles to the jets in $e^+e^- \longrightarrow q\bar{q}g$. Let all the angles between jets, θ_{ij}, and the jet energies, E_i, be large: $\theta_{+-} \sim \theta_{+1} \sim \theta_{-1} \sim 1$, $E_1 \sim E_+ \sim E_- \sim E \sim W/3$. As it was discussed above, the angular distribution of soft interjet hadrons carries information about the coherent gluon radiation off the colour antenna being formed when three emitters (q, $\bar{q}$ and g) separate from one another. The angular distribution of a secondary

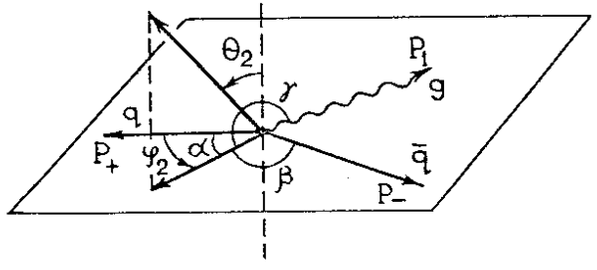

Fig. 21. Kinematics of interjet radiation in three-jet events.

soft gluon g_2 (see Fig. 21) can be written in the notations of eq. (3.13) as

$$\frac{8\pi dN_{q\bar{q}g}}{d\Omega_2} = 1/N_c\cdot W_{\pm 1}(\vec{n}_2)\cdot N_g'(Y_m) = \left((1\hat{}+) + (1\hat{}-) - 1/N_c^2\cdot(+\hat{}-)\right)\cdot N_g'(Y_m), \quad (8.24)$$

cf. eqs. (8.11)-(8.13) and (3.16b). In the above $Y_m = \ln E\theta_m/\Lambda$, $\theta_m = \min\{\theta_+, \theta_-, \theta_1\}$ with $\cos\theta_i = \vec{n}_2\vec{n}_i$.

The radiation pattern, corresponding to the case when a photon γ is emitted instead of a gluon g_1 is, cf.(8.6),

$$\frac{8\pi d N_{q\bar{q}g}}{d\Omega_2} = 1/N_c \cdot W_{+-}(\vec{n}_2) \cdot N'_g(Y_m) = 2C_F/N_c \cdot (\hat{+}-) N'_g(Y_m). \quad (8.25)$$

The dashed line in Fig. 22 displays the corresponding 'directivity diagram', projected onto the $q\bar{q}g$ plane:

$$W_{+-}(\varphi_2) = 2C_F \int \frac{d\cos\theta_2}{2} (\hat{+}-) = 2C_F a_{+-} V(\alpha,\beta) , \quad (8.26)$$

where

$$V(\alpha,\beta) = \frac{2}{\cos\alpha - \cos\beta}\left(\frac{\pi-\alpha}{\sin\alpha} - \frac{\pi-\beta}{\sin\beta}\right) . \quad (8.27)$$

Here $\alpha = \varphi_2$, $\beta = \theta_{+-} - \varphi_2$ (see Fig. 22).

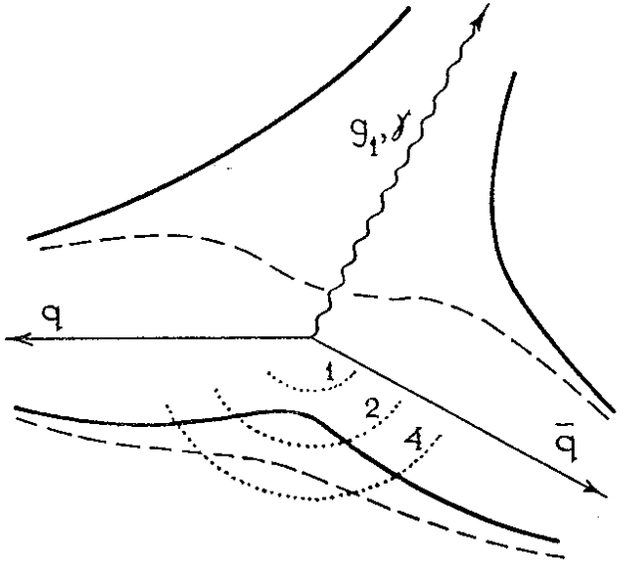

Fig.22. Directivity diagram of soft gluon radiation, projected onto the $q\bar{q}g$ (dashed line) and $q\bar{q}g$ (solid line) event plane. The curves corresponding to expressions (8.26) and (8.28) are drawn in polar coordinates: $\Theta = \varphi_2$, $r = \ln 2W(\varphi_2)$. Dotted circles show the constant levels of density flow $W(\varphi_2) = 1, 2, 4$.

Distribution $W_{+-}(\vec{n}_2)$ is simply related to the particle distribution in the two-jet events $e^+e^- \to q(p_+) + \bar{q}(p_-)$, Lorentz boosted from the quark cms to the lab system (i. e. the cms of $q\bar{q}g$).

Replacing g by g_1 changes the directivity diagram essentially because the antenna element g_1 now participates in the emission as well. However, contrary to intuition, this change does not only lead to the appearance of an additional particle flow in the g_1 direction. Integrating eq.(8.24) over θ_2 one obtains ($\alpha = \varphi_2$, $\beta = \theta_{+-} - \varphi_2$, $\gamma = \theta_{1+} + \varphi_2$):

$$W_{\pm 1}(\varphi_2) = N_c\left[a_{+1} \cdot V(\alpha,\gamma) + a_{-1} \cdot V(\beta,\gamma) - \frac{1}{N_c^2} a_{+-} V(\alpha,\beta)\right]. \quad (8.28)$$

Fig. 22 illustrates that the particle flow in the direction opposite to $\vec{n}_1$ appears to be considerably lower than in the photon case. So the destructive interference cancels radiation in the region between the quark jets. For example, suppose $\vec{n}_+\vec{n}_- = \vec{n}_+\vec{n}_1 = \vec{n}_-\vec{n}_1$ and $\vec{n}_2$ points in a direction exactly opposite to $\vec{n}_1$, that is, midway between the directions $\vec{n}_+$ and $\vec{n}_-$. Then neglecting the weak dependence N'_g on θ one arrives at

$$\frac{dN_{q\bar{q}g}/d\vec{n}_2}{dN_{q\bar{q}g}/d\vec{n}_2} = \frac{N_c^2 - 2}{2(N_c^2 - 1)} = 7/16. \quad (8.29)$$

Due to the constructive interference effects, there is a surplus of radiation in the q-g and g-$\bar{q}$ regions.

Thus, the analysis of soft bremsstrahlung radiation pattern demonstrates particle 'drag' by the g_1 jet. This phenomenon is easy to understand qualitatively. If a term proportional to $1/N_c^2$ is dropped, the two remaining terms in eq.(8.24) may be interpreted as the sum of two independent $(1\hat{+})$ and $(1\hat{-})$ antenna patterns, boosted from their respective rest frames into the overall $q\bar{q}g$ cms. The depletion of the q-$\bar{q}$ region is a direct

consequence of these boosts. This scenario literally repeats the explanation given in the Lund string model.[67] So it appears that the latter provides an excellent picture for mimicking the collective QCD effects.

Experiment [9,12,13] has presented evidence of the drag effect in three-jet events. The depletion of particles was observed in the q-$\bar{q}$ valley relative to the q-g and g-$\bar{q}$ valleys. The strong support of this effect comes from the comparison of $q\bar{q}g$ and $q\bar{q}\gamma$ events, that provides the test of coherence effects in a model independent way [43]. Fig. 23 shows the measured ratio [12] of particle density in the q-$\bar{q}$ region for $q\bar{q}g$ and $q\bar{q}\gamma$ events. This ratio should be 1 if no coherence effects would be present, since kinematical configurations of both event types were similar.

Emphasize that eqs. (8.11) and (8.24) provide not only the planar picture, but also the total three-dimensional pattern of the particle flows in three-jet sample. It is worth noting that the destructive interference proves to be so strong, that the particle flow in the region opposite the gluon jet is smaller than that in the most kinematically 'unfavourable' direction, which is a normal to the event plane. In the asymptotics the ratio of these flows in the case of three-fold symmetric $q\bar{q}g$ events is

$$\frac{N_{<\perp>}}{N_{<q\bar{q}>}} = \frac{N_c + 2C_F}{2(4C_F - N_c)} = 17/14. \qquad (8.30)$$

As we shall see below, in other types of HPs coherence should lead to a rich diversity of the collective drag phenomena. So, let us enumerate the main lessons from studying this phenomenon.

1. The effects of gluon interference do not permit one to formulate, a priori, a probabilistic scheme for the development of partonic cascades. However for each specific

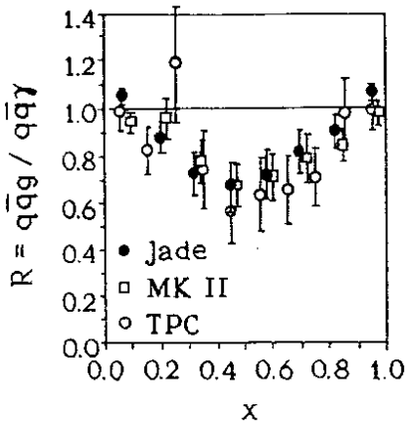

Fig.23. Ratio of the particle density in $q\bar{q}g$ and $q\bar{q}\gamma$ events as a function of the scaled angle $x = \theta_+/\theta_{+-}$, where θ_{+-} is the angle between jets q and $\bar{q}$. Shown are data from JADE, MARK II and TPC [12].

inclusive characteristic it is possible to divide the essential coherent effects into two types: (i) accounts for the coherence effects in the intrajet cascades. These are reduced on average to the Markov process of particle multiplication into the sequentially shrinking angular cones $\theta_{n+1} \leq \theta_n$; (ii) gives an account of the interference effects in the total amplitude for production of the minimal number of jets (partons), whose configuration corresponds to the given experiment. Just this amplitude reflects the specificity of HP. Each of the produced jets evolves in an universal manner inside a fixed opening angle θ_0 , which size depends on the mutual location of jets from the ensemble.

The aforementioned division permits, in any concrete case, a classical probabilistic picture of parton branching to be retained, thus allowing event modeling .

2. The experimental evidence of such bright phenomena as the hump-backed plateau (coherence of the first kind) and the drag effect (coherence of the second kind) has shown quite convincingly that these interference effects

survive the hadronization stage. Therefore, one can say, that in spite of confinement the hadronic system reflects very delicate features of the colour field dynamics, which in turn stem from the nature of QCD as a gauge theory.

3. The observation of the colour interference between soft hadrons from, say, q- and g-jets reveals the QCD wave properties of hadronic flows. Thus, it can be considered as an experimental proof of the common bremsstrahlung nature of the hadroproduction mechanisms for both jets. The properties of drag interference phenomena are deeply rooted in the basic structure of non-Abelian gauge theory.

4. The relative smallness of the interference effects does not diminish their fundamental importance. This consequence of QCD radiophysics is a serious warning against continuing ideas about independently evolving jets.

5. Drag effects lead to a noticeable azimuthal asymmetry of particle flow relative to the 'jet axis'. The character of this asymmetry depends on the geometry of the whole event, see for details Subsec. 8.6.

8.2. Drag Phenomena in High $p_\perp$ Hadronic Reactions[7,68,69]

Jets or individual particles at high $p_\perp$ in hadron-hadron collisions originate from hard parton interaction at small distances. It is the colour dynamics of these quarks and/or gluons that determines the topology of the final state.

Because of the presence of coloured constituents in both the initial and final states, the study of high $p_\perp$ HPs has proved more complicated than in the case of e^+e^- annihilation. However, the nature of jets, basing on the dominant role of the QCD bremsstrahlung processes, is the same for both reactions. Therefore, the main physical phenomena and characteristics of final states are very

much alike. This puts jet physics on essentially the same footing as e^+e^- annihilation.

Let us enumerate the virtue of high $p_\perp$ processes.

1. A diversity of hard interactions at small distances; by varying the experimental conditions (triggers) one may extract the dominant subprocess and turn from one subprocess to another.

2. Dependence of length and height of the 'plateau' in the hadron spectra on the different parameters: the length is determined by the total energy of the collision, and the height and the plateau structure - by the process hardness (trigger $E_\perp$). Thus, information becomes available that is inaccessible in e^+e^- annihilation, where both the energy and the hardness are given by the same quantity W.

3. Unlike e^+e^- annihilation, where about half of the jets are generated by heavy quark pairs, subprocesses with heavy quarks Q are suppressed in hadronic collisions in a standard way.

4. Finally, there is the purely practical argument that just in high $p_\perp$ hadronic collisions the largest possible energies (hardness) will be reached in the near future. These reactions are also the best source of high energy gluon jets. Detailed studies of such processes are necessary for designing the future experiments and the analysis of their data, for finding new heavy objects. In particular, drag effects could provide a valuable additional tool, helping to extract and to study new physics.

The variety and complexity of colour antennae typical for high $p_\perp$ processes, complicate the picture of final hadronic distributions. However at very high energies, when particle multiplicities become large enough,

the interesting possibility arises of using a detailed analysis of hadron flows on an event by event basis to extract information about colour transfer at small distances. Of course, the question still persists, whether the colour coherence effects will be visible clearly enough above the normal soft scattering background.

In course of a hard interaction colour is transferred abruptly from one parton to another. For example, to leading order in $1/N_c$ the colliding quarks q_1 and q_2 are simply 'recharged':

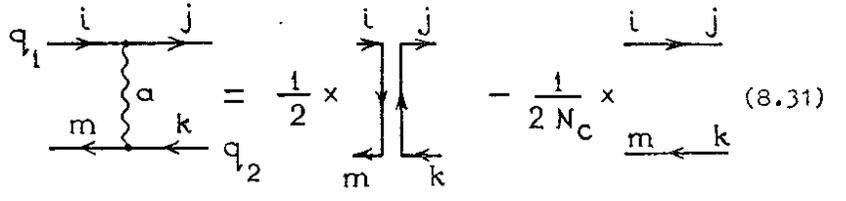

(8.31)

$$t^a_{ji}\, t^a_{mk} = \frac{1}{2}\,\delta_{im}\,\delta_{jk} - \frac{1}{2N_c}\,\delta_{ij}\,\delta_{mk}$$

The parton-parton scattering acts here as a colour antenna. Gluon bremsstrahlung associated with the incoming and the outgoing partons leads to the formation of jets of hadrons around the directions of these coloured emitters. It is the colour topology of the partons, participating in the scattering, that determines the radiation pattern.

To demonstrate, how the coherence of bremsstrahlung connectes the structure of hadronic accompaniment with the t-channel colour transfer, let us consider high $p_\perp$ scattering of energetic partons A and B ($E_A \sim E_B \sim \sqrt{s}$) at relatively small angles $\theta_s \approx p_\perp/E \ll 1$, as shown in Fig.24. The hardness of the process is determined by the momentum transfer $p_\perp \approx \sqrt{-\hat{t}}$, which naturally restricts the transverse momenta of the accompanying gluon bremsstrahlung $l_\perp < p_\perp$ and, so the development of partonic cascades.

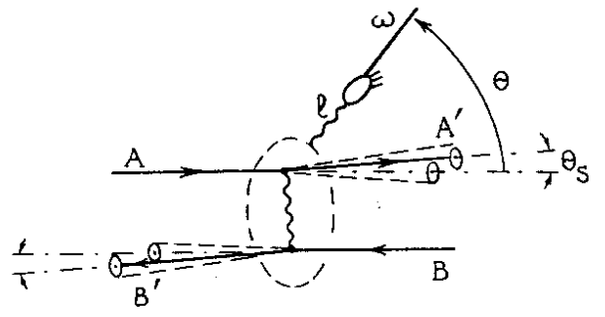

Fig.24. Soft gluon bremsstrahlung accompanying small angle scattering of partons A+B — A'+B' ($\theta_s \ll 1$ is the scattering angle).

In the structure of the final hadronic system three regions may be separated. Two of them adjoin the fragmentation regions of the colliding hadrons and occupy the intervals

$$\Delta\eta = \ln p_\perp/\Lambda \,, \qquad (8.32)$$

where η is the pseudorapidity

$$\eta = \frac{1}{2}\ln\frac{1+\cos\theta}{1-\cos\theta} \,.$$

The hadronic spectrum in each of these intervals ('extended fragmentation regions') is saturated with the particles from the bremsstrahlung cones of the incoming and the scattered partons, and so results from an incoherent sum of two jets with angular opening $\theta = \theta_s$. The height of the distribution is determined, roughly speaking, by the sum of parton'colour charges' $C_A+C'_A$ and $C_B+C'_B$ respectively.

In the central region

$$|\eta| < \eta(\theta_s) \simeq \ln\frac{\sqrt{s}}{p_\perp} \approx \ln\frac{E}{p_\perp} \qquad (8.33)$$

(final particle angles larger than the scattering angle θ_s) the incoming and the scattered partons radiate

coherently, and, as a result, the hadron density is determined by the colour charge C_t of the t-channel exchange. Since in the given kinematics ($-\hat{t} \ll \hat{s}$) gluon exchange dominates, we conclude that in the central region (8.33) hadronic spectrum is determined by the 'colour strength' of the gluon current C_g, and what is of importance, it becomes universal, independent of the nature of scattered partons (A, B = q or g).

As one can see from a not complicated analysis, the resulting spectrum, accounting for the parton branching effects, is independent of the energy (pseudorapidity) of the particle registered at angle $\theta > \theta_s$ at fixed transverse momentum $k_\perp$:

$$\frac{d\sigma}{\sigma d\eta\, dk_\perp} \simeq 4N_c \int_{k_\perp}^{P_\perp} \frac{d\ell_\perp}{\ell_\perp^2} \frac{\alpha_s(\ell_\perp^2)}{2\pi} \bar{\mathcal{D}}_g\left(\frac{k_\perp}{\ell_\perp}, \ln\frac{\ell_\perp}{\Lambda}\right) . \qquad (8.34)$$

In this expression $x\cdot\bar{D}_g$ (x,ln Q/Λ) is the standard distribution of particles with energy fraction x in a gluon jet, for which the product of energy and opening angle equals Q, see Sec. 6.

Integrating over $k_\perp$ of hadrons at fixed η, we obtain

$$f(\eta, \ln p_\perp) = \frac{d\sigma}{\sigma d\eta} = \int^{P_\perp} \frac{d\ell_\perp}{\ell_\perp} 4N_c \frac{\alpha_s(\ell_\perp^2)}{2\pi} \int_0^1 dx\, \bar{\mathcal{D}}_g(x, \ln\frac{\ell_\perp}{\Lambda}). \qquad (8.35)$$

Thus, the hadron yield in the interval $|\eta(\theta)| < \eta(\theta_s) \simeq \ln \frac{E}{P_\perp}$ does not depend on the rapidity, so a flat distribution emerges ('true plateau', see Fig. 25), whose height is determined by the hardness of the scattering process. This is given by the formula, familiar already from the discussion in the previous Subsec.,

$$f\ (\ln p_\perp) \simeq N_g'\ (\ln p_\perp/\Lambda). \qquad (8.36)$$

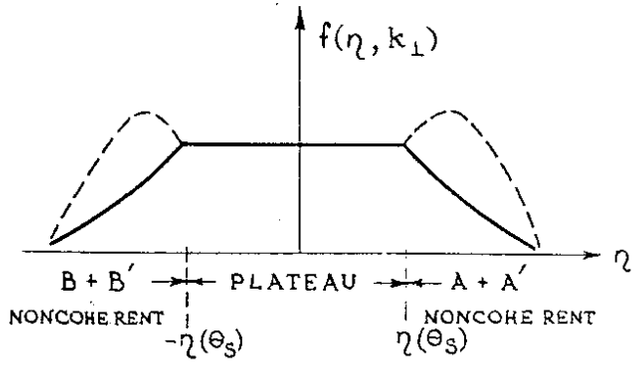

Fig.25. Universal rapidity plateau ($|\eta| < \ln 1/\theta_s$); the solid and dashed lines illustrate schematically the difference between $q\bar{q}$ and gg scattering.

A similar distribution appears in e^+e^- annihilation (the so-called truncated plateau [42]) when one considers a special kind of events, where at a given hardness of the process, E = W/2, all the hadron transverse momenta are bounded from above $p_\perp < p_{\perp\,max} \ll E$ ($p_\perp \gg \Lambda$). The asymptotic height of the rapidity plateau in high $p_\perp$ HPs should coincide with the doubled density of the interjet hadron flow in e^+e^-annihilation at $W \simeq 2p_\perp$.

Listed above conclusions about the structure of inelastic hadron scattering processes in the central region ($|\Delta\eta| < 1/2 \ln(\hat{s}/|\hat{t}|)$, $|\hat{t}| \ll \hat{s}$) are valid provided the one-gluon exchange dominates. To guarantee this, one should register in the final state of hadron-hadron collision at least one particle with transverse momentum $p_\perp$ exceeding some typical value $\langle p_\perp\rangle_{diffusion}$, characteristic for hadron processes at high energies. The latter emerges in the framework of QCD analysis of the total cross sections and grows very slowly as s

increases (see, e.g., Ref.[5]).

Colour interference between jets seems to become a phenomenon of large potential value as a new additional tool for discriminating between HPs. For example, reconstruction of antenna pattern by the effects of particle drag may help to visualize the production of new colourless heavy objects - the Higgs boson H, new quarks and leptons, supersymmetric particles, and so on. Most of these objects produce hadronic jets, and the configurations of interjet particles should differ from familiar QCD processes like parton scattering.

An instructive example comes from the study of the radiation pattern associated with the hadronic production of a heavy Higgs [7]. If H boson is produced via the g-g fusion of Fig.26a, then the similar plateau $f(\eta, \ln M_H/\Lambda)$ emerges in hadronic spectrum. However in the case of the W-W mechanism of Fig.26b the central region (8.33) should be

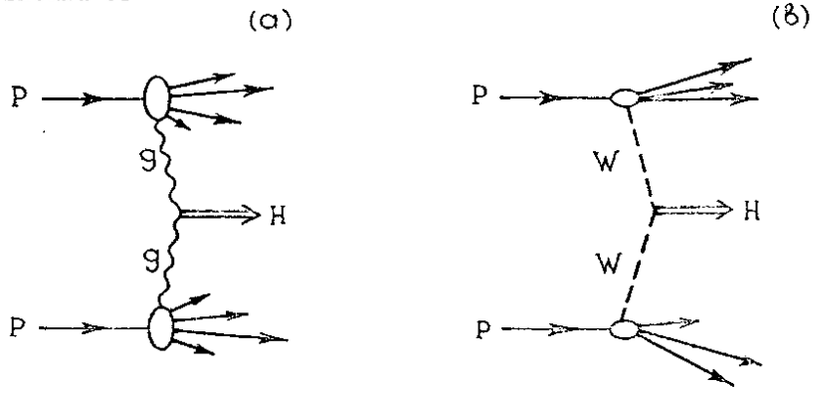

Fig.26. Hadronic Higgs boson production via a) gg fusion and b) WW fusion.

empty and the process looks as the quasi-diffractive one (the gluon emission by initial and final partons at large

angles cancel each other coherently because in t-channel colour is not transferred (see the discussion in Subsec. 3.1).

Another example is the comparison of the production of a colourless object via gg or $q\bar{q}$ collisions. Here, if the hard kinematics is the same, the heights of the accompanying plateau should differ approximately by a factor of two ($N_c/C_F = 9/4$).

High $p_\perp$ processes are rich in the drag effects. Let us consider, for example, the topology of events, resulting from the quark scattering *)

$$-\hat{t} \sim \hat{s} = x_1 x_2 s \quad (x_1, x_2 \sim 1).$$

In this case the two crossing processes shown in Fig. 27a and Fig.27b have approximately equal probabilities. However each of them has its own colour topology, and therefore specific particle flows, as seen in Fig.27c and Fig. 27d.

For the subprocess of Fig.27a, the soft particle radiation pattern is

$$\frac{4\pi dN^{q_1 q_2}}{d\Omega} = \Big[(\hat{14} + \hat{23}) + \frac{1}{2N_c C_F} \cdot (2(\hat{12} + \hat{34}) - (\hat{14} + \hat{23}) - (\hat{13} + \hat{24}))\Big] C_F/N_c \cdot N_g' \ (\ln E/\Lambda), \tag{8.37}$$

see for notations eqs. (3.13) and (7.20).

In full analogy with the discussion of string effect in the previous Subsec., one may say that the leading contribution (the first term in (8.37)) has the structure of the sum of two independent $q\bar{q}$-antennae $\hat{14}$ and $\hat{23}$. This fact also can be mimicked by means of the topological picture of the Lund model.

*) One can find a comprehensive study of the radiation associated with the different types of parton-parton scattering in ref. 69).

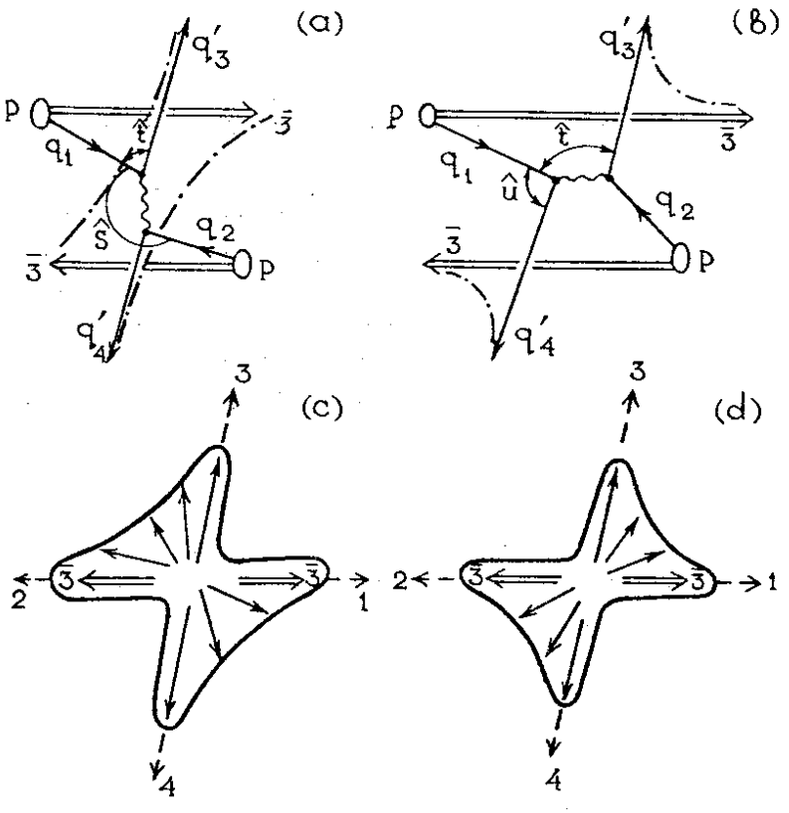

Fig.27. Colour antennae for two crossing high $p_\perp$ qq scattering processes and the corresponding particle flows.

It is important to emphasize, however, that here,unlike the Lund approach, to each contribution (single string) there corresponds not a phenomenological particle spectrum, connected with the standard plateau of the parton model, but a dynamical distribution which takes into account the effects of cascade multiplication.

The height of this distribution is determined by the hardness of the process. Furthermore, PT approach permits one to control not only the leading colour contributions, but also the $O(1/N_c)$ corrections. The interference between the subprocesses of Figs.27a and 27b also leads to the colour-suppressed effects.

Basing on the perturbative prediction for the distributions of the final particles, it may be possible to distinguish - on an event by event basis - the definite fluctuations in the angular structure of particle flows, corresponding to one of the two topologies of Fig. 27c or Fig. 27d.

As the first step, one can study the correlations of the multiplicity flows, e.g., their angular asymmetry, cf. ref. [70],

$$A = (N_{UR} + N_{LL} - N_{UL} - N_{LR}) / (N_{UR} + N_{LL} + N_{UL} + N_{LR}). \quad (8.38)$$

Here N_{ij} is the number of the final particles in the angular region ij on the scattering plane (i denotes the upper or the lower quadrant, j denotes the right ot the left quadrant).

As a more complicated example we shall discuss in Sec. 8.4 the characteristic features of the antenna pattern, associated with a subprocess $gq(\bar{q}) \longrightarrow gq(\bar{q})$.

Finally, let us briefly consider hard gluon-gluon scattering $g_1 + g_2 \to g_3' + g_4'$ at small angle $\theta_s \ll 1$, when one-gluon exchange dominates in t-channel. Here to leading order in $1/N_c$ the associated soft radiation is

$$\frac{8\pi dN^{g_1 g_2}}{d\Omega} \simeq \left[\hat{13} + \hat{24} + 1/2\cdot(\hat{12} + \hat{34} + \hat{14} + \hat{23})\right] N_g' \quad (8.39)$$

This formula shows that two colour configurations of the participating partons, as shown in Figs. 28a and 28b, contribute to the radiation pattern.

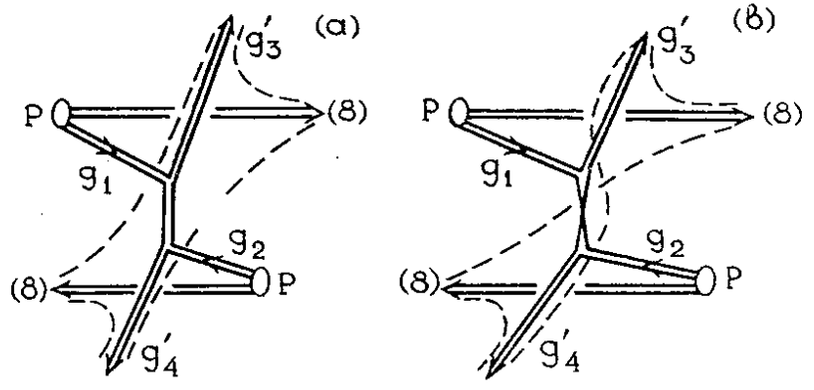

Fig.28. Colour antennae for hard scattering $g_1+g_2 \to g_3'+g_4'$ in the case when t-channel gluon exchange dominates ($\theta_s \ll 1$).

8.3. Prompt Production at Large $p_\perp$ [8)]

Drag effects, very similar to 3-jet events, can be studied in high $p_\perp$ processes, such as γ, $\mu^+\mu^-$ pair, W, Z, ... production, where a colourless object is used as a trigger [7,71)].

Consider the three jet production *)

$$p + \bar{p} \to \gamma(p_\perp) + \text{jet}_1 + \text{jet}_2 + \text{jet}_3. \qquad (8.40)$$

The basic graphs describing the process are shown in Fig. 29. We shall argue in a moment that $gq \to \gamma q$ dominates $q\bar{q} \to \gamma g$. Keeping only the hard Compton scattering process, the cross section for producing a hard photon of transverse momentum $p_\perp = E$, corresponding to 90° scattering in the center of mass system of the parton-parton scattering, is [72)]

*) The effects of colour coherence in the prompt W,Z production at high $p_\perp$ were studying in detail in refs.7,8,31).

$$\frac{d\sigma}{dp_\perp^2\, d\cos\theta} = \sum_q e_q^2 \int dy\; x_q\, D_p^q(x_q,p_\perp^2)\, x_g D_{\bar{p}}^g(x_g,p_\perp^2)\, \frac{d\sigma}{dp_\perp^2} + (P \leftrightarrow \bar{P}). \qquad (8.41)$$

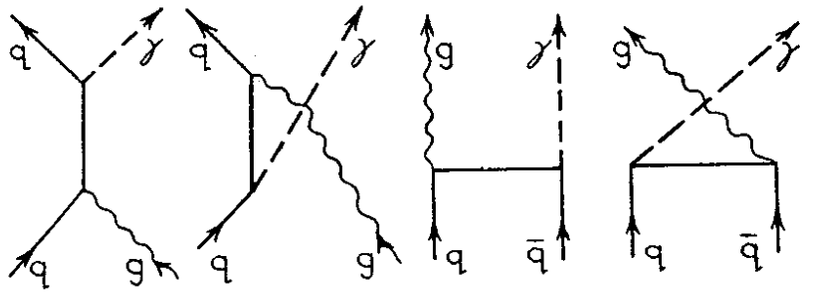

Fig.29. Hard scattering graphs leading to γ+ jet production.

In the above $x_g \cdot x_q \cdot s = 4p_\perp^2$ and $y = y_1+y_2$ with y_1 and y_2 the rapidities of the outgoing γ and gluon jet respectively. As usual e_q is the electric charge of the quark having flavour q. Then

$$d\sigma/(dp_\perp^2 dy\, d\cos\theta) = \sum_q e_q^2 \frac{5\pi\alpha\cdot\alpha_s}{9s\, p_\perp^4} x_q D_p^q(x_q,p_\perp^2)\, x_g D_{\bar{p}}^g(x_g,p_\perp^2) + (P \leftrightarrow \bar{P}). \qquad (8.42)$$

The corresponding formula for the hard process $q\bar{q} \to \gamma g$ is

$$d\sigma/(dp_\perp^2 dy\, d\cos\theta) = \sum_q e_q^2 \frac{\pi\alpha\cdot\alpha_s}{9p_\perp^4} x_q D_p^q(x_q,p_\perp^2)\, x_{\bar{q}} D_{\bar{p}}^{\bar{q}}(x_{\bar{q}},p_\perp^2) + (P \leftrightarrow \bar{P}). \qquad (8.43)$$

When $x_{\bar{q}}(x_g)$ is less than about 0.1 the Compton process dominates over annihilation and so we shall neglect the contribution given by eq.(8.43).

Now to the main point of this Subsec.. In addition to

the jet produced in the hard collision there are also soft gluon emissions associated with the incoming quark and gluon lines and with the final state quark which lead to an interference pattern (drag effect) almost exactly as in the process $e^+e^- \to q\bar{q}g$. The picture of the soft gluon emission is schematically illustrated in Fig. 30.

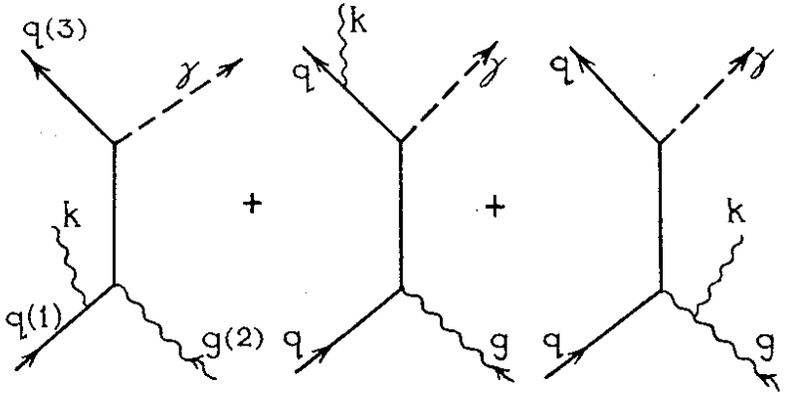

Fig.30. Soft gluon emission from the hard scattering graphs of Fig. 29.

The formula for radiation in direction $\vec{n}$, associated with the hard scattering has the same form as eq.(8.24),

$$8\pi \frac{dN}{d\vec{n}} = \left(\hat{(23)} + \hat{(21)} - \frac{1}{N_c^2} \hat{(13)} \right) \cdot N_g' (Y_m), \qquad (8.44)$$

where $\vec{n}_i$ is the direction of the parton i, as shown in Fig. 31. The variable $Y_m = \ln E\theta_m/\Lambda$ governes the evolution of a jet with energy E and opening angle θ_m. In the above $\theta_m = \min\{\theta_1, \theta_2, \theta_3\}$ with $\cos\theta_i = \vec{n}\vec{n}_i$.

As discussed in detail in refs. [41,42] (see also Sec. 6) a reasonable phenomenology can be done for $\pi^\pm$ production, taking the MLLA formulae for multiplicity of pions in a gluon jet, N_g (see eqs. (6.52),(6.53)).

To quantify the drag phenomena we shall evaluate

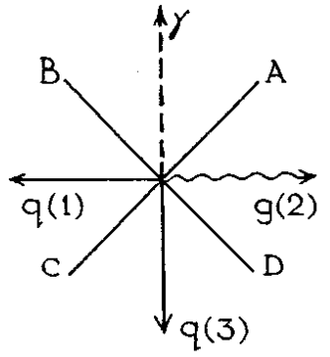

Fig.31. The kinematics of 90° scattering in the hard process for γ+jet production.

the radiation pattern for final state pions projected onto the plane of the hard scattering and at angles midway the between the partons involved in the HP, directions labelled by ABC and D in Fig.31. Thus, $dN^A/d\vec{n}$ corresponds to the number density of pions in the plane of the hard scattering and midway between the directions determined by the incoming gluon and the outgoing photon (note in Fig.31 that q_1 and g_2 are incoming while γ and g_3 are outgoing lines). For purposes of illustration we present in Table the values of pion multiplicities in the 30° sectors around the direction A, B, C and D respectively for different values of $E_\perp/\Lambda$ [73].

Table

The energy rise of pion multiplicities in the interjet 30° sectors

$E_\perp/\Lambda$	60	200	10^3	10^4
A	0.62	1.04	1.94	4.3
B	0.52	0.88	1.57	3.4
C	0.51	0.87	1.61	3.5
D	1.47	2.44	4.47	9.6

As is easily seen, the particle production is the largest

between the directions of the incoming gluon and the outgoing quark, but ~ 2.3 times smaller between the directions of the incoming quark and the outgoing quark. So, just as in the reaction $e^+e^- \to q\bar{q}g$, the drag of hadrons is predicted in the direction of the gluon jet. This drag effect leads to an azimuthal asymmetry of particles, which can be seen by looking end on at the struck q-jet, see for details Subsec. 8.6. The observation of such an asymmetry may indicate which of the incoming particles in a given event has shaken off the gluon.

Finally, notice that one can find in refs. [8,74] the discussion of the observability of the drag effects in prompt γ, W production at collider energies above the soft scattering background.

8.4. Two Jet Production at Large $p_\perp$ [8]

As it has been mentioned above coherence effects are more difficult to observe in the spectrum of hadrons associated with two jet production than in γ or W production. Nevertheless, there are some specific effects which should be observable. The only hard scattering process which has a large asymmetry in the spectrum of associated hadrons is $gq(\bar{q}) \to gq(\bar{q})$ for which subprocess the two jet cross section is

$$\frac{d\sigma}{dy_1 dy_2 dp_\perp^2} = x_q D_p^q(x_q,p_\perp^2) x_g D_{\bar{p}}^g(x_g,p_\perp^2) \frac{d\hat{\sigma}}{d\,p_\perp^2} + (P \leftrightarrow \bar{P}) \tag{8.45}$$

with $d\hat{\sigma}/d\,p_\perp^2$ referring to the fundamental hard process. In general, the process $gq \to gq$ does not dominate the competing hard processes such as $gg \to gg$, $q\bar{q} \to q\bar{q}$, etc. However, if one chooses x_g very small, say $x_g < 0.1$, and x_q not too small, then two jet cross sections will be dominated by eq. (8.45). As an example of a region where $gq \to gq$ should be the dominant subprocess we might

imagine the production of two jets having $p_\perp = 90$ GeV at the Tevatron $\bar{p}p$ collider and with $x_g = 0.03$ and $x_q = 0.3$. In what follows we assume an appropriate kinematic region has beeen chosen so that the QCD Compton process is the dominant hard scattering.

The spectrum of hadrons associated with the hard process eq.(8.45) is

$$8\pi \frac{dN}{d\eta} = \left[H^c(\hat{u},\hat{t},\hat{s})\right]^{-1} \cdot 2/N_c \cdot \Big\{ H^c(\hat{u},\hat{t},\hat{s}) \left[C_F(\hat{24}) + N_c(\hat{13})\right] - C_F\left[2\,(\hat{24}) + 2\,(\hat{13}) - (\hat{23}) - (\hat{12}) - (\hat{34}) - (\hat{14})\right] H_1^c(\hat{u},\hat{t},\hat{c}) + C_F\left[(\hat{12}) + (\hat{34}) - (\hat{23}) - (\hat{14})\right] H_2^c(\hat{u},\hat{t},\hat{s})\Big\} \cdot N_g'(Y_m), \tag{8.46}$$

where we use the notation of ref. [69] for the hard scattering amplitudes. The incoming gluon and quark lines are labelled by 1 and 2 while the outgoing gluon and quark lines are labelled by 3 and 4 as shown in Fig. 32. For $\hat{t} = \hat{u} = -\hat{s}/2$, 90° scattering in the partonic center of mass system, one finds

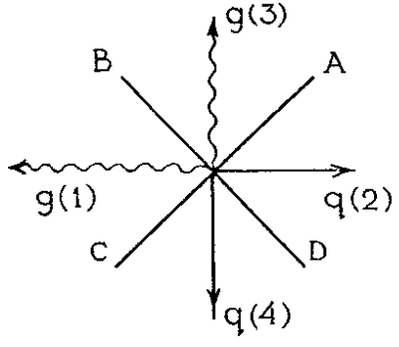

Fig. 32. The kinematics g 90° scattering in the hard process q(2)+g(1) $\to$ q(4) + g(3).

$$\frac{8\pi dN}{d\eta} = \frac{2}{N_c}\Big\{C_F(\hat{24}) + N_c(\hat{13}) - \frac{387}{704}C_F\left[2(\hat{24})+2(\hat{13})-(\hat{23}) - (\hat{12})-(\hat{34})-(\hat{14})\right] - \frac{243}{704}C_F\left[(\hat{12})+(\hat{34})-(\hat{23})-(\hat{14})\right]\Big\} N_g'(Y_m) \cdot \tag{8.47}$$

Evaluating eq. (8.47) in the plane of the scattering and midway between the direction of the parton momenta, in the partonic center of mass frame, one finds

$$\pi \frac{dN^A}{d\vec{n}} = \pi \frac{dN^C}{d\vec{n}} \approx 1.7\, N_g'(Y_m), \qquad (8.48a)$$

$$\pi \frac{dN^B}{d\vec{n}} \approx 2.1\, N_g'(Y_m), \qquad (8.48b)$$

$$\pi \frac{dN^D}{d\vec{n}} \approx 0.5\, N_g'(Y_m). \qquad (8.48c)$$

For pion production $d/dy\, N_g^{\pi}$ can be estimated to be $d/dy\, N_g^{\pi} \approx 9$ at $p_\perp = E = 90$ GeV. Thus, the asymmetry indicated in eqs. (8.48) may be observable above the normal soft hadronic background. However, the situation is quite different than in the case of hard γ or W production. There one had only a single outgoing jet. In the present situation there are two outgoing jets and it is not apparent which one is the gluon and which one is the quark jet. In fact, one must use the asymmetry indicated in eqs. (8.48) to decide which jet is the gluon and which is the quark. This, in principle, would give the possibility of comparing high $p_\perp$ quark and gluon jets in the same event.

8.5. Correlations of Interjet Particle Flows [61]

A new interesting manifestation of the QCD wave nature of hadronic flows arises from studying the double-inclusive correlations of the interjet flows in $e^+e^- \to q\bar{q}g$ events, as shown in Fig. 33. The point is that here, unlike the case of a single-inclusive distributions examined so far, one faces such tiny effects as the mutual influence of different $q\bar{q}$ antennae. These effects can not be mimicked by the orthodox Lund string model [45], which deals with the independently fragmenting string segments (antennae). To our understanding, only much more

sophisticated algorithm for the Lund Monte Carlo the so-called 'dipole formulation' [34,35] may reproduce them.

The double-inclusive correlation of Fig.33 bear the information on the colour shielding of $q\bar{q}g_1$ antenna by a field of gluon g_2, which has been produced in a cascade on the stage, preceding the emission of a soft gluon g_3. Just the latter initiates the registered flow of particles, so the energies are ordered

$$E_3 \ll E_2 \ll E_1 \sim E_+ \sim E_- \sim E = W/3. \qquad (8.49)$$

It is worth noting that for the single-inclusive multiplicity flows $dN(\vec{n}_3)/d\Omega_3$, examined so far, these shielding effects are asymptotically inessential since

$$\Delta\left(\frac{dN(\vec{n}_3)}{d\Omega_3}\right) = \int_{\left(\substack{\text{interjet}\\ \text{region}}\right)} \frac{d^2N_{23}}{d\Omega_2 d\Omega_3}\, d\Omega_2 \sim \int^{E} \frac{dE_2}{E_2} \frac{\alpha_s(E_2)}{2\pi} \int^{E_2} \frac{dE_3}{E_3} \frac{\alpha_s(E_3)}{2\pi} \times \qquad (8.50)$$

$$\times N_g\left(\ln \frac{E_3}{\Lambda}\right) \sim (\sqrt{\alpha_s})^2 N_g \sim \sqrt{\alpha_s}\, \frac{dN(\vec{n}_3)}{d\Omega_3}.$$

The double-inclusive correlation of the interjet flows, $d^2N / d\Omega_2 d\Omega_3$, is of the order of $(\sqrt{\alpha_s})^2 N_g^2$. Just as in the case of drag effect, one can neglect the weak dependence of the cascading factors N_g' on angles and the ratio of the correlation functions will be determined by the total lowest order amplitude for $e^+e^- \to q\bar{q}g_1g_2g_3$.

The angular distribution of particle flows in the directions of the secondary jets g_2 and g_3, whose energies are ordered according to eq.(8.49), is given by the sum of three terms having different structure:

$$\frac{d^2N}{d\Omega_2\, d\Omega_3} \sim B_I + B_{II} + B_{III}, \qquad (8.51)$$

where

$$B_I = N_c^2 [A_{21}^3 A_{1+}^2 + A_{2+}^3 A_{1+}^2 + A_{21}^3 A_{1-}^2 + A_{2-}^3 A_{1-}^2] +$$

$$+ N_c(2C_F-N_c)\left[A^3_{2+}A^2_{+-} + A^3_{2-}A^2_{+-}\right] ,$$

$$B_{II}=N_c^2\left[A^3_{1-}A^2_{1+}+A^3_{1+}A^2_{1-} + N_c(2C_F-N_c)\left[A^3_{+-}A^2_{1+}+A^3_{1+}A^2_{+-}+A^3_{+-}A^2_{1-} + A^3_{1-}A^2_{+-}\right],\right. \tag{8.52}$$

$$B_{III} = (2C_F - N_c)(2C_F-2N_c)A^3_{+-}A^2_{+-} .$$

In the above $A^i_{jk} = a_{jk}/(a_{ij}a_{ki})$, $a_{ij} = 1 - \vec{n}_i\vec{n}_j$ ($\vec{n}_i$ is the direction of a parton i; $i = +,-,1,2,3$).

The genetic link between the gluons g_3 and g_2, initiating the flow correlations, is encoded in the term B_I. The remaining terms B_{II} and B_{III} correspond to the independent emission of these gluons. In the large-N_c-limit expressions for B_I and B_{II} simplify and might be reproduced by the mentioned above 'dipole formulation' of the Lund MC.

To quantify the correlation effects we shall compare the ratio of the single-inclusive particle flows between jets,

$$r_1 = \frac{dN}{d\Omega_{(1+)}} \Big/ \frac{dN}{d\Omega_{(+-)}} , \tag{8.53a}$$

with the ratio of the double-inclusive ones,

$$r_2 = \frac{d^2N}{d\Omega_{(1+)}d\Omega_{(1-)}} \Big/ \frac{d^2N}{d\Omega_{(+-)}d\Omega_{(1-)}} . \tag{8.53b}$$

Here (ij) denotes the direction midway between the partons i and j.

In the picture of the independently emitting antennae (string segments) the additional registration of a particle flow in the region (1-) does not affect the ratio r_1, so one would expect $r_2 \simeq r_1$. The mutual influence of antennae leads to the numerically small difference between the ratios r_2 and r_1. For example, the ratios of flows, projected onto the event plane, in

the case of three-fold symmetric events are (see eqs. (8.24) and (8.51)-(8.53))

$$r_1 \simeq 2.42, \qquad r_2 \simeq 2.06.$$

The relative smallness of the colour shielding effects does not diminish their fundamental importance. This consequence of QCD radiophysics is a serious warning against ideas about independently fragmenting string segments.

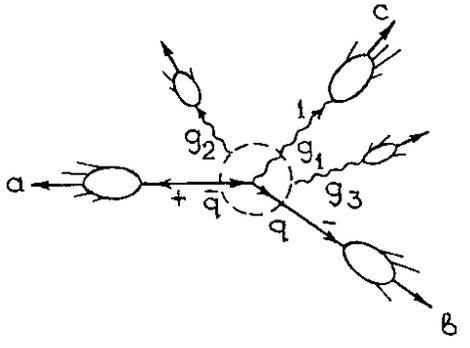

Fig.33. Double inclusive correlation of two multiplicity flows in $q\bar{q}g$ events.

8.6. Azimuthal Asymmetry of QCD Jets [7,73]

As we have already discussed, the treatment of the structure of final states given by the string picture qualitatively reproduces the QCD radiation pattern only up to $O(1/N_c^2)$ corrections (the large-N_c-limit). However, the $1/N_c$-expansion appears to be, as mathematician would say, nonuniform. Namely, under specific conditions $1/N_c$ terms become sizable or even dominating.

The simplest example is given by the study of the azimuthal asymmetry of a quark jet in $q\bar{q}g$ events. The radiation pattern is given here by eq.(8.24). When all the angles are large the third term in eq.(8.24)(negative colour-suppressed antenna ($+\hat{}-$) leads to a small ($\sim 10\%$)

correction to the Lund interpretation [67] of the drag effect.

The azimuthal distribution of particles produced inside a cone of the given opening half-angle θ_0 may be characterized by an asymmetry parameter (see Fig. 34).

$$A(\theta_0) = \frac{N_{\to g}(\theta<\theta_0) - N_{\to \bar{q}}(\theta<\theta_0)}{N_{tot}(\theta<\theta_0)} = \frac{(\Delta N)_{as}}{N_{tot}} \quad . \tag{8.54}$$

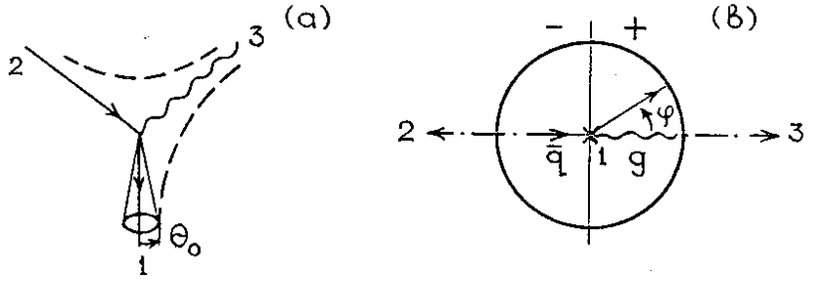

Fig.34. The azimuthal asymmetry of the quark jet in $e^+e^- \to q\bar{q}g$. (a) Geometry in the event plane, dashed lines show the topology of colour strings. (b) Scheme of azimuthal separation of particles from quark jet, see eqs. (8.54) and (8.55).

The azimuthal integration for $(\Delta N)_{as}$,

$$\left[\int_{-\frac{\pi}{2}}^{\frac{\pi}{2}} - \int_{\frac{\pi}{2}}^{\frac{3\pi}{2}}\right] \frac{d\varphi}{2\pi}\left(\frac{8\pi\, dN}{d\Omega}\right) \quad , \tag{8.55}$$

can be done explicitly (see ref. [73]). For parametrically small θ_0 values the contribution of the $(+\hat{}\,i)$-antenna $(i = -, 1)$ to $(\Delta N)_{as}$ is

$$\frac{1}{2}\int_0^{\theta_0} \frac{d\theta_+}{\theta_+}\left(\frac{2\theta_+}{\pi} ctg\, \frac{\theta_{+i}}{2}\right) N_g'(\ln E\theta_+) \simeq \tag{8.56}$$

$$\frac{1}{2}\frac{2\theta_0}{\pi} ctg\, \frac{\theta_{+i}}{2} \cdot N_g'(\ln E\theta_0)\cdot(1 + O(\sqrt{\alpha_s}))$$

while the nonsingular antenna $(-\hat{}\,1)$ produces negligible correction to $(\Delta N_{as}) \sim \theta_0^3$. The resulting asymmetry parameter reads

$$A(\theta_0) \simeq \frac{2\theta_0}{\pi} G \sqrt{4N_c \frac{\alpha_s(E\theta_0)}{2\pi}} \quad , \tag{8.57}$$

$$G = \frac{N_c}{2C_F} ctg\, \frac{\theta_{+1}}{2} + \frac{1}{2N_c C_F} ctg\, \frac{\theta_{+-}}{2} \quad ,$$

where we have substituted following eq. (7.20)

$$\frac{N_g'(\ln E\theta_0)}{N_g(\ln E\theta_0)} \simeq \sqrt{4N_c \frac{\alpha_s(E\theta_0)}{2\pi}}\cdot(1 + O(\sqrt{\alpha_s})) \quad . \tag{8.58}$$

G depends on the geometry of the jet ensemble.

The first colour-favoured term in (8.57) describes the Lund-motivated asymmetry due to the 'boosted string' connecting q- and g-directions. The corresponding asymmetry vanishes with increase of θ_{+1} as the string straightens. Here, however, the second term in eq.(8.57) enters the game, forcing the asymmetry to increase anew as shown in Fig.35a. This behaviour might be interpreted as an additional repulsion between particles from two neighbouring q- and $\bar{q}$-jets.

For symmetric configuration

$$\theta_{+1} = \theta_{-1} = \pi - \theta_{+-}/2$$

the colour-suppressed term in eq.(8.57) prevails when

$$\theta_{+-} \lesssim 2 \arctg\,(1/N_c) \approx 37^\circ. \tag{8.59}$$

To realize this effect one has to select $q\bar{q}g$-events with unnatural kinematics, when the hard gluon moves in opposite direction to the quasi-collinear $q\bar{q}$ pair.

Fig. 35b displays the predicted asymptotical asymmetry of the quark jet at finite values of θ_0 as a function of

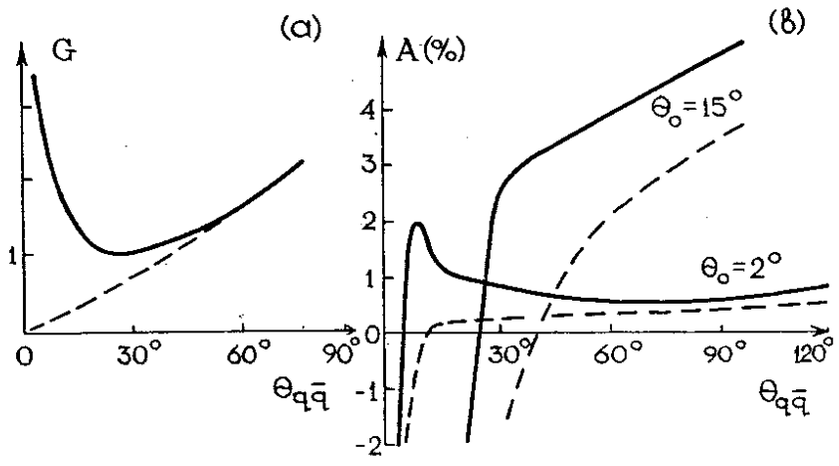

Fig.35. QCD (solid) versus 'string' (dashed) predictions for a) G-factor (see eq.(8.57)) and b)asymmetry parameter A in the symmetric $q\bar{q}g$ events.

the relative angle between the q-, $\bar{q}$-jets. The increase of A with decreasing $\Theta_{q\bar{q}}$ discussed above can be seen only for very small values of Θ_0. The reason is that for $\Theta_0 \gtrsim 5°$ the effect of repulsion is masked by the fragments of the neighbouring $\bar{q}$-jet which fill partially the Θ_0-cone, leading to drastically increasing negative contribution to A.

It would be important to observe the aforementioned phenomenon with the heavy quark (Q=c,b) jets identified.

The azimuthal asymmetry of produced jets is certainly not specific to 3-jet events. An analogous picture should be observed, e.g., in high $p_\perp$ processes. To elucidate the essence of the phenomenon, let us compare the angular pattern of the radiation accompanying high $p_\perp$ qq' and $\bar{q}q'$ scattering (where q and q' have different

flavours) in the quark cms, as shown in Fig. 27a and Fig. 36 respectively.

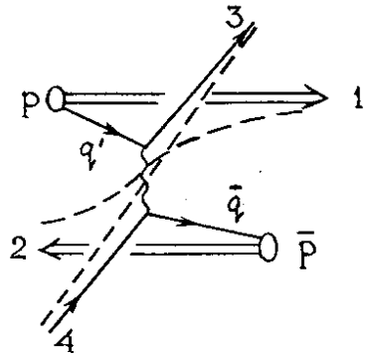

Fig.36. Colour antennae for high $p_\perp$ $\bar{q}q' \to \bar{q}q'$ scattering process.

The corresponding particle distributions are given by eq.(8.37) and by the analogous formula

$$\frac{4\pi dN^{\bar{q}q'}}{d\Omega} = \Big[(\hat{12}+\hat{34}) + \frac{1}{2N_c C_F}(2\cdot(\hat{14}+\hat{23})-(\hat{12}+\hat{34})-(\hat{13}+\hat{24}))\Big] \cdot C_F/N_c \cdot N'_g \ (\ln E/\Lambda) \ . \qquad (8.60)$$

Similarly to the discussed above $q\bar{q}g$ example, first colour-favoured terms in eqs.(8.37),(8.60) correspond topologically to Lund strings, as illustrated in Figs.27a and 36. 'Boosted' $\hat{14}$ and $\hat{23}$ antennae for the quark scattering lead to the certain drag phenomena and, in particular, to the azimuthal asymmetry of the jets . Unlike this case, for $\bar{q}q'$ scattering, following the Lund scenario, one should not expect such asymmetry since both $\hat{12}$ and $\hat{34}$ antennae appear to be straight (each strings is in its cms).

In the case of qq' scattering the colour-suppressed term in eq.(8.37) leads to some deviation from the Lund--motivated asymmetry. But for the $\bar{q}q'$ scattering such a term in eq.(8.60) determines the whole effect.

For illustration let us consider the azimuthal distribution of particles inside the jet-'3'. Determining the asymmetry parameter $A(\theta_0)$ analogously to eq. (8.54) (see Fig. 37)

$$A(\theta_0) = \frac{N_{\to 2}\ (\theta < \theta_0) - N_{\to 1}\ (\theta < \theta_0)}{N\ (\theta < \theta_0)}\ , \qquad (8.61)$$

one obtains for small opening half-angle θ_0 around the jet-'3' axis

$$A^{qq'}(\theta_0) = \frac{2\theta_0}{\pi}\left[\frac{N_c}{2C_F}\,tg\frac{\theta_s}{2} + \frac{1}{2N_cC_F}\left(ctg\frac{\theta_s}{2} - 2\,tg\frac{\theta_s}{2}\right)\right]\sqrt{4N_c\frac{\alpha_s(E\theta_0)}{2\pi}}\ , \qquad (8.62)$$

$$A^{\bar{q}q'}(\theta_0) = \frac{2\theta_0}{\pi}\left[\frac{1}{2N_cC_F}\left(2\,tg\frac{\theta_s}{2} + ctg\frac{\theta_s}{2}\right)\right]\sqrt{4N_c\frac{\alpha_s(E\theta_0)}{2\pi}}\ , \qquad (8.63)$$

where θ_s denotes the scattering angle :

$$\theta_{13} = \theta_{24} = \theta_s\ ,\quad \theta_{23} = \theta_{14} = \pi - \theta_s\ ;$$

E stands for a jet energy in the cms.

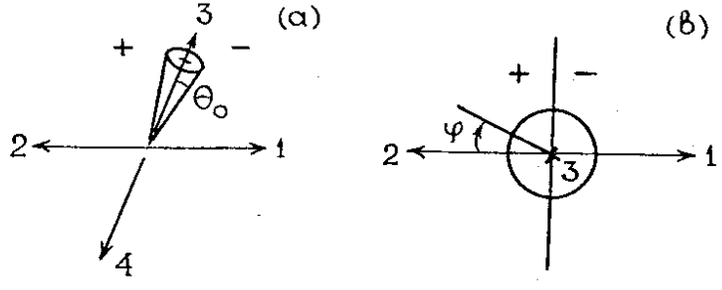

Fig.37. Definition of the azimuthal asymmetry $A(\theta_0)$ of the scattered jet-'3'.

Fig.38 demonstrates the comparison of event shape factors G (factors in square brackets in eqs.(8.62),(8.63) with their large-N_c-limits. $O(1/N_c^2)$ term in eq.(8.62) dominates for angles

$$\theta_s < 2\ \mathrm{arctg}\sqrt{1/(N_c^2+2)} \approx 33.6°. \qquad (8.64)$$

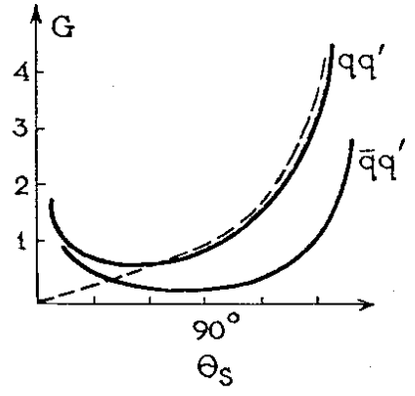

Fig.38. G-factor for qq' and $\bar{q}$q' scattering. Solid - QCD, dashed - large-N_c ('string')limit for qq' case ('string' prediction for $\bar{q}$q' case is G=0).

The predicted magnitude of the QCD asymmetry in $\bar{q}$q' scattering appears to be comparable with that of qq' case. For example, $A^{\bar{q}q'} \simeq A^{qq'}$ at small θ_s and $A^{qq'} = 3/8 \cdot A^{qq'}$ at $\theta_s = 90°$.

The absolute values of the asymmetry can be estimated using eqs. (8.37),(8.60). Then,

$$A^{qq'}\ (\theta_0 \simeq 10°,\ \theta_s \simeq 90°) \approx 5\%,$$
$$A^{\bar{q}q'}\ (\theta_0 \simeq 10°,\ \theta_s \simeq 90°) \approx 2\%, \qquad (8.65)$$
$$(\ \alpha_s \approx 0.12).$$

For small opening half-angles the effect grows linearly with θ_0. To increase the magnitude of the asymmetry one can take θ_0 larger and use the original eqs.(8.37),(8.60), accounting for the all contributions including terms, non-singular in the direction of the jet-'3'. Notice, that to study the azimuthal properties of jet-'3' the natural restriction $\theta_s > 2\theta_0$ has to be imposed.

For the interaction of identical quarks new effects arise leading to the complication of the antenna patterns.

(i) Modification of the qq scattering amplitude.

(ii) Opening of the annihilation channel for the $q\bar{q}$ case.

The associated soft gluon distribution is now given by for process $q(1) + q(2) \longrightarrow q(3) + q(4)$

$$\frac{4\pi dN}{d\Omega} = \Big[(\hat{14}+\hat{23})R_t + (\hat{13}+\hat{24})R_u + (\hat{12}+\hat{34})(1-R_t-R_u) + \frac{1}{2N_c C_F}\,(2(\hat{12}+\hat{34}) - (\hat{14}+\hat{23}) - (\hat{13}+\hat{24}))\Big] \cdot C_F/N_c \cdot N_g', \quad (8.66)$$

and for process $q(1) + \bar{q}(2) \longrightarrow q(3) + \bar{q}(4)$

$$\frac{4\pi dN}{d\Omega} = \Big[(\hat{12}+\hat{34})\tilde{R}_t + (\hat{13}+\hat{24})R_s + (\hat{14}+\hat{23})(1-\tilde{R}_t-R_s) + \frac{1}{2N_c C_F}\,(2(\hat{14}+\hat{23}) - (\hat{12}+\hat{34}) - (\hat{13}+\hat{24}))\Big] C_F/N_c \cdot N_g'. \quad (8.67)$$

Here

$$R_{t,u} = \frac{\sigma_{t,u}}{\sigma_{qq}}\ , \quad \tilde{R}_t = \frac{\sigma_t}{\sigma_{q\bar{q}}}\ , \quad R_s = \frac{\sigma_s}{\sigma_{q\bar{q}}}\ ;$$

$$1 - R_t - R_u = \frac{\Delta_s}{\sigma_{qq}}\ , \quad 1 - \tilde{R}_t - R_s = \frac{\Delta_u}{\sigma_{q\bar{q}}}\ ; \quad (8.68)$$

$$\sigma_s = \frac{C_F}{N_c}\cdot\frac{t^2+u^2}{s^2}\ , \quad \sigma_t = \frac{C_F}{N_c}\cdot\frac{u^2+s^2}{t^2}\ , \quad \sigma_u = \frac{C_F}{N_c}\cdot\frac{t^2+s^2}{u^2}\ ,$$

$$\Delta_s = -\frac{C_F}{N_c^2}\cdot\frac{2s^2}{tu}\ , \quad \Delta_u = -\frac{C_F}{N_c^2}\cdot\frac{2u^2}{st}\ ;$$

$$\sigma_{qq} = \sigma_t + \sigma_u + \Delta_s\ , \quad \sigma_{q\bar{q}} = \sigma_t + \sigma_s + \Delta_u\ .$$

Keeping in mind that the asymmetry of the jet-'3' comes mainly from $\hat{13}$ and $\hat{23}$ antennae, one can simply observe the following peculiarities. The inclusive asymmetry given by eq.(8.66) vanishes at $\theta_s = 90°$ ($R_t = R_u$) due to compensation between the antennae $\hat{23}$ (positive drag) and $\hat{13}$ (negative one). The eq.(8.67) leads to the asymmetry which, unlike the case of distinguishable quarks (see eq. (8.60)) contains also the colour-favoured term $\hat{13}\cdot R_s$ caused by the annihilation contribution.

Noteworthy to mention, this Lund motivated term

produces the negative asymmetry (Fig.39), opposite to the positive one due to remaining terms. Note, that the colour-favoured negative asymmetry occurs also for the cases of $q\bar{q} \longrightarrow q'\bar{q}'$ and $q\bar{q} \longrightarrow 2g$ subprocesses.

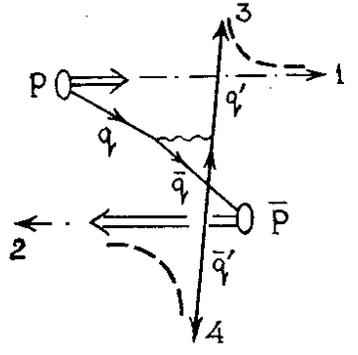

Fig.39. String topology for the $q\bar{q}$ annihilation subprocess.

Let us emphasize that just the colour-suppressed $O(1/N_c^2)$ term proves to govern the overall asymmetry owing to the numerical smallness of the annihilation cross section ($\sigma_s/\sigma_{q\bar{q}} \lesssim 1/10$ for $\theta_s \leq 90°$). One concludes, thus, that QCD differs here qualitatively from the Lund picture. In this point we at first time meet the situation when QCD and Lund model give opposite predictions.

To our understanding, this qualitative divergence should hold on for any string based hadronization scheme, even with QCD cascades built in.

The quark-quark scattering can be studied in pp collisions at high $p_\perp$. Here both qq and qq' scatterings occur with the relative weights $5/9\cdot(2u\cdot 2u + d\cdot d)$ and $4/9\cdot(2u\cdot d + 2d\cdot u)$ respectively. The resulting QCD asymmetry of the jet-'3' (at $\theta_s \leq 90°$), as depicted in Fig.40, differs noticeably from its large-N_c limit.

In the case of $p\bar{p}$ scattering the azimuthal distribution of particles inside the jet-'3' without identification its

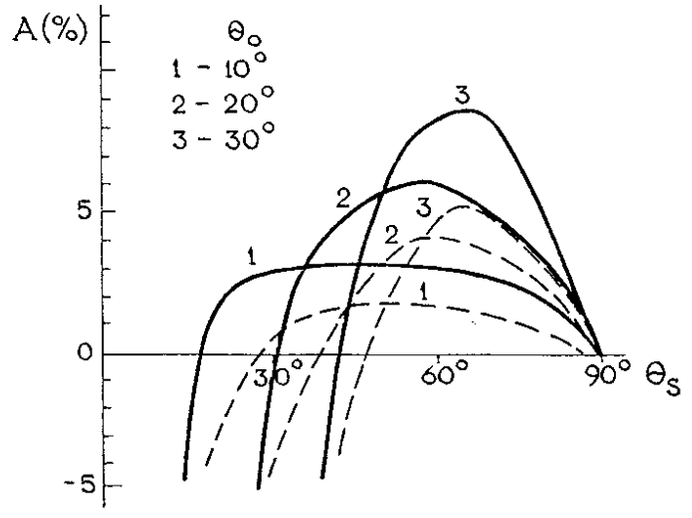

Fig.40. Asymmetry parameter $A(\theta_0)$ of the scattered (untagged) q-jet in pp collision as a function of the cms scattering angle θ_s. Solid: QCD prediction. Dashed: large-N_c ('string') limit.

species (q or $\bar{q}$ jet) may be characterized by an asymmetry pattern shown in Fig.41. The asymmetry here

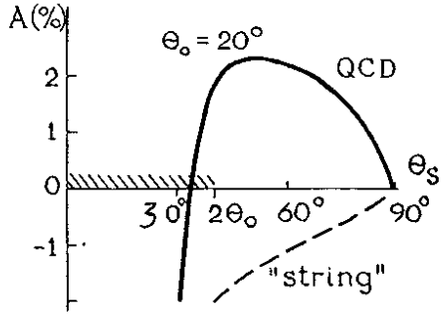

Fig.41. Different sign asymmetries $A(\theta_0=20°)$ of the scattered untagged (q or $\bar{q}$) jet-'3' in $p\bar{p}$ collisions as predicted by QCD (solid) and its large $-N_c$ limit ('string' - dashed).

proves to be considerably smaller than in pp case, but reveals the same sign of effect in contrast to the string picture.

Curves in Fig.41 correspond to $n_f = 3$. Account of the process $q\bar{q} \rightarrow gg$ works in the same direction as a rise of n_f, enhancing the colour-favouring negative asymmetry.

To make the qualitative difference between the predictions of QCD and its large-N_c limit (string) more spectacular it is necessary to identify scattered quark jet. The asymmetry, predicted for the case of tagged quark jet, is shown in Fig.42. As is easily seen, in the region of cms scattering angles $70° < \theta_s < 110°$ QCD predicts $A = +(4 \div 7)\%$ jet asymmetry at the half-angle $\theta_0 = 30°$ unlike the opposite sign effect

$$A = -(2.5 \div 1.5)\%,$$

originated from the large-N_c treatment of QCD formulae, here referred to as the 'string-motivated' approach.

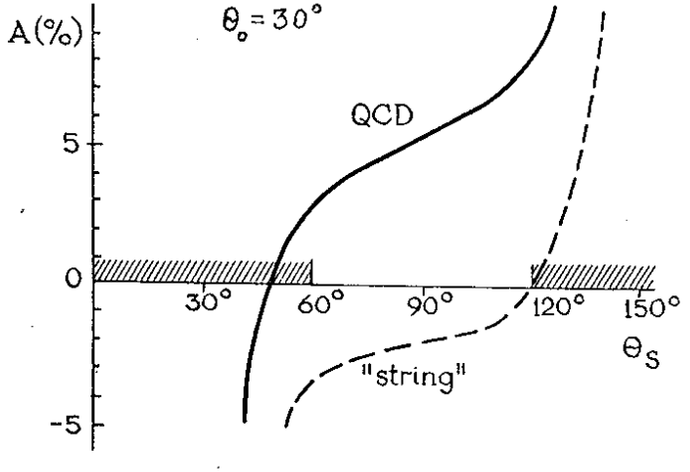

Fig.42. Asymmetry parameter $A(\theta_0=30°)$ of the scattered tagged q-jet in $p\bar{p}$-collisions.

9. COHERENCE AND FINAL STATES IN DEEPLY INELASTIC SCATTERING [20,75]

The parton model had its first great successes in explaining the scaling observed in deeply inelastic lepton -hadron scattering (DIS). Later, scaling violations were explained by the approach to asymptotic freedom dictated by QCD and became the first quantitative testing area of that theory. The spectrum of particles associated with a deeply inelastic scattering event has only recently begun [7,8,20,31,75-77] to receive serious theoretical treatment. In this Section we shall briefly summarize the present situation.

9.1. The Structure of Soft Radiation Associated with DIS

Hard lepton-hadron interaction with high $-q^2 = Q^2$ and fixed $x = Q^2/2Pq$ knocks the quark with longitudinal momentum $k = xP$ at virtuality level $k_\perp^2 \lesssim Q^2$ out of the initial partonic fluctuation which was prepared long before scattering.

The probability to find the appropriately prepared quark-parton inside target nucleon determines the DIS cross section (structure functions).

The structure of final state is governed by two main phenomena: dissociation of the initial parton system whose coherence was destroyed by removing the quark (target fragmentation) and evolution of the struck quark (current fragmentation).

These fragmentation regions are best separated kinematically in the Breit frame ($q_0 = 0$, $2x\vec{P} = -\vec{q}$). Here, similar to e^+e^--annihilation, the process looks like abrupt spatial spreading of two colour states 3 (the struck q) and $\bar{3}$ (the disturbed proton) moving in the opposite directions.

The current jet (time-like cascades) should be identical to that produced in e^+e^- annihilation at $W^2=Q^2$. One again finds a hump in the energy distribution with the dip occurring for particles with finite energies in the Breit frame.

In the target fragmentation region situation proves to be much more complicated, especially for $x \ll 1$. The DIS occurs in this case on a 'sea' quark coming from brems-strahlung of soft $(q\bar{q})_g$ pairs in colour octet state (gluon exchange in t-channel). The dominant structure of the appropriate fluctuation can be characterized in terms of the multirung ladders of Fig. 43 determining the small -x behaviour of $D_p^q(x,Q^2)$. However, in order to calculate the single particle spectrum in the target jet it is not enough to consider those graphs shown in Fig.43 even

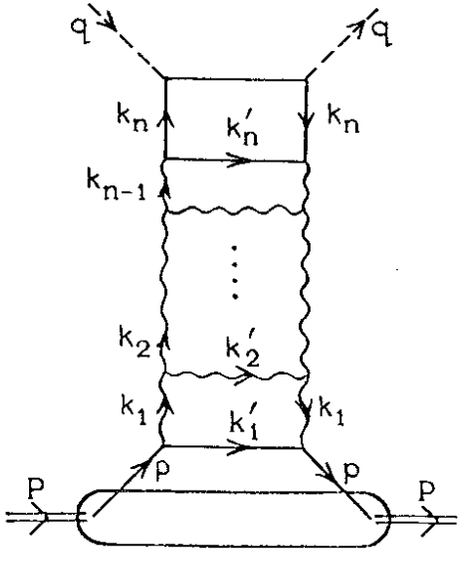

Fig.43. Ladder graphs, with transverse momentum ordering, dominating in structure functions at small x.

allowing that the horizontal parton lines may fragment. Sets of graphs which cancel in the structure function no longer cancel in the inclusive spectrum.

In addition to the offsprings of decaying subjects - remnants of the ordered 'ladders' (structural contribution), the collective coherent accompaniment arises, which is determined by the overall colour topology of partonic system (soft t-channel contribution).

9.2. Angular Ordering for Space-Like Cascades

Similar to the time-like case, the PT-analysis has proved the AO of the radiation of soft gluons 'ℓ' associated with the space-like fluctuations shown in Fig. 43 [75] (see also ref. [76]).

The character of 'soft' radiation associated in the hard scattering can be understood, to a large extent, by considering radiation from the elementary vertex $p \to k_1' + k_1$ appearing in Fig.43 [7]. Suppose an addition gluon, ℓ is radiated from this vertex as shown in Fig.44. Call $\ell_+ = \beta_\ell P_+$, $p_+ = \beta_p P_+$, $k_{1+} = \beta_{k_1} P_+$, etc. We suppose $\beta_{k_1} \ll \beta_{k_1'} \approx \beta_p$, the usual strong ordering appropriate to small-x processes. Then there are two cases to consider. (i) $\beta_\ell < \beta_{k_1}$ and (ii) $\beta_\ell > \beta_{k_1}$.

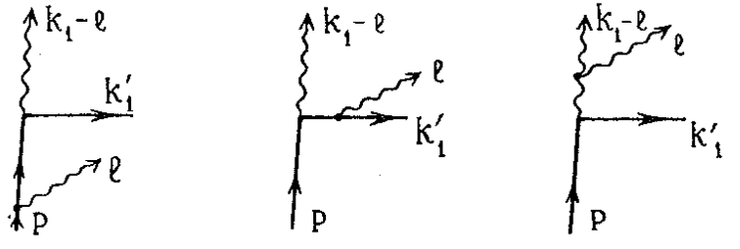

Fig.44. Additional soft gluon, ℓ, radiated from lower vertex of the graph shown in Fig. 43.

(i) When $\beta_\ell < \beta_{k_1}$ there is of course radiation off $p(k_1')$ when $\theta_{p\ell}$ ($\theta_{k_1'\ell}$) is less than $\theta' = \theta_{pk_1'}$, in the usual manner. The interesting region is $\theta_\ell \approx \theta_{\ell k_1'} \approx \theta_{\ell p} \gg \theta'$. Now when $2(k_1\cdot\ell) < k_{1\perp}^2$, that is when

$$\theta' < \theta_\ell < \frac{\beta_p}{\sqrt{\beta_{k_1}\beta_\ell}}\,\theta' \quad , \tag{9.1}$$

the ℓ - line can be emitted off the p and k_1' lines coherently. When $2(k_1\cdot\ell) > k_{1\perp}^2$ only the graph of Fig.44c is effective and here one covers the angular region

$$\theta' \frac{\beta_p}{\sqrt{\beta_{k_1}\beta_\ell}} < \theta_\ell \quad . \tag{9.2}$$

However, the coherent emission of Figs.44a and 44b give the same answer in the region (9.1) as does the emission corresponding to Fig.44c in region (9.2).

(ii) When $\beta_\ell > \beta_{k_1}$ it does not make sense to route the momenta as shown in Fig.44. Rather, we should write the momenta for graphs (a) and (b) as shown in Fig.45. Then so long as $\ell_\perp \ll k_{1\perp} \approx k_{1\perp}'$ these two graphs add coherently, that is in the region

$$\theta_\ell < \frac{\beta_p}{\beta_\ell}\,\theta' \quad . \tag{9.3}$$

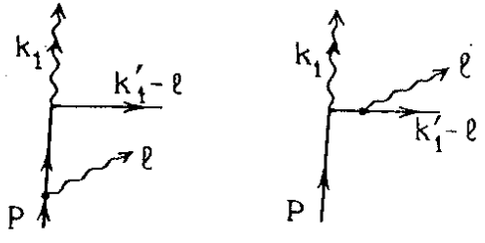

Fig.45. Graphs which add coherently in region $\ell \gg k_1$.

The graph analogous to Fig.44c is already included in Fig.43 since here k_1 is the soft emission off ℓ .

9.3. The Structure of Inclusive Spectrum in Target Fragmentation

As a result in the target region there also arises the hump-backed energy particle distribution with predictable shape, evolving with $\ln Q^2$ and $\ln 1/x$.

The resulting inclusive spectrum of hadron h in the target fragmentation can be represented conveniently as a sum of three terms.

The contribution I related to the upper quark cell in Fig.43 comes from the soft emission $\ell < xP$ off the line k_n', when $\theta_{\ell k_n'} < \theta_{P k_n'}$, and off the line k_n when $\theta_{\ell k_n'} > \theta_{P k_n'}$:

$$\left(\frac{d\sigma}{\sigma dy}\right)_{\underline{I}} = \frac{C_F}{N_c}\left[\frac{\omega}{xP}\,\bar{\mathcal{D}}_g^h\left(\frac{\omega}{xP}, \ln\frac{Q}{\Lambda}\right)\right] , \qquad (9.4)$$

where $y = \ln \omega/\Lambda$; ω being the energy of hadron h.

The contribution II also accounts for $\ell < xP$ coming from effective emissions off the vertical gluon lines of Fig.43 up to angles $\theta_{\ell P} < \theta_{P k_n'}$:

$$\left(\frac{d\sigma}{\sigma dy}\right)_{\underline{II}} = \frac{1}{\mathcal{D}_p^q(x,Q^2)} \int_0^{\ln\frac{Q}{\Lambda}} d\ln\frac{k_\perp}{\Lambda}\;\frac{\partial}{\partial \ln\frac{k_\perp}{\Lambda}}\,\mathcal{D}_p^q(x,k_\perp^2)$$

$$\times\left[\frac{\omega}{xP}\,\bar{\mathcal{D}}_g^h\left(\frac{\omega}{xP}, \ln\frac{k_\perp}{\Lambda}\right)\right] , \qquad (9.5)$$

where D_p^q is the sea quark distribution.

The contribution III combines relatively soft gluons ($xP < \ell < P$) off the lower part of the ladder with fragments of ladder rungs:

$$\left(\frac{d\sigma}{\sigma dy}\right)_{\underline{III}} = \frac{1}{\mathcal{D}_p^q(x,Q^2)} \int_{xP}^{P}\frac{d\ell}{\ell}\int_0^{\xi_Q} d\xi_k\,\mathcal{D}_p^g\left(\frac{\ell}{P}, k_\perp^2\right)\frac{\partial^2}{\partial\xi_k^2}\,\mathcal{D}_g^q\left(\frac{xP}{\ell}, Q^2, k_\perp^2\right)$$

$$\times\int_\Lambda^{k_\perp}\frac{d\ell_\perp}{\ell_\perp}\,\frac{\alpha_s(\ell_\perp^2)}{2\pi}\left[\frac{\omega}{\ell}\,\bar{\mathcal{D}}_g^h\left(\frac{\omega}{\ell}, \ln\frac{\ell_\perp}{\Lambda}\right)\right] , \qquad (9.6)$$

where $\xi_k = \frac{1}{b}\ln\ln\frac{k_\perp}{\Lambda}$.

Fig.46 demonstrates contributions I, II and III. Contributions II and III, being negligible at $x \sim 1$, rise with x decreasing.

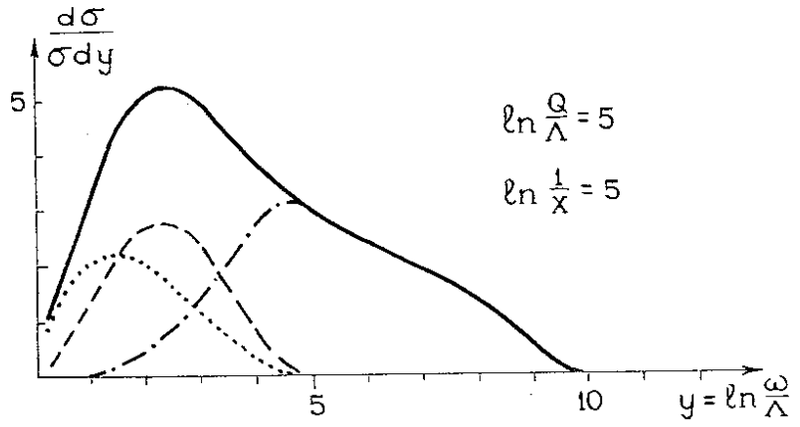

Fig.46. Contributions to the energy particle spectrum in DIS target fragmentation region at $\ln Q/\Lambda = 5$, $\ln 1/x = 5$. I - quark box contribution (dotted line), II - coherent 't-channel' colour radiation (dashed), III - fragmentation of ladder rungs (dash-dotted); solid line - total sum.

The relative magnitude of II versus I depends on the characteristic value of the 'sea' quark k_n' emission angle which becomes larger with increase of number of cells in

-the ladder, i.e. with $\ln 1/x$ increasing.

Angular structure of the basic ladder is responsible for the shape of the curve III as well. The most energetic particles with $\omega \lesssim P$ can originate only from the very bottom of the ladder where emission angles of partons, and thus the opening angles of fragmenting subjets, are comparatively small. This damps the parton cascades, leading to a smooth increase of the particle yield with decreasing ω .

Evolution of resulting hadron energy spectra with q^2 and x is shown in Fig.47. The left wings correspond to the current fragmentation, the right ones - to the hadrons from target fragmentation.

Similarly to the e^+e^- annihilation case, coherence in DIS stiffens energy spectra. The yield of 'slow' particles ($\ln\omega/m \lesssim 1$) should be independent of Q^2.

9.4. On the QCD Solution of Feynman-Gribov Puzzle

It is important to note that the fragmentation of the ladder rungs (the contribution III, see eq.(9.6) and Fig. 46) does not populate the energy interval $\omega < xP$. This coherent phenomenon has been predicted long ago in the framework of the parton picture suggested by Feynman. From the general physical arguments based on quantum-mechanical coherence V.N.Gribov has shown [78] that the DIS on a quark with the momentum $x\vec{P} \simeq -\vec{Q}/2$ (in the Breit system) did not affect the development of the soft part of the partonic fluctuation. The undisturbed upper part of the partonic fluctuation in Fig.48 results just in a single final hadron, thus, leading to the back of particles within the rapidity $y = \ln\omega/\Lambda$ interval $0 < y < \ln Q/\Lambda$ (the so-called Gribov gap).

Later on the experimental observation of the continuous

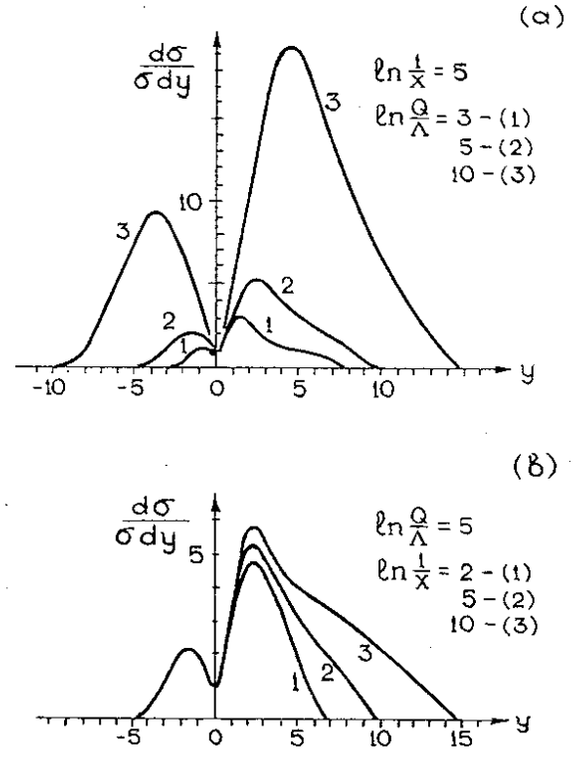

Fig.47. Evolution of DIS energy hadron distribution in the Breit system with a) Q^2 : $\ln Q/\Lambda = 3, 5, 10$ at $\ln 1/x = 5$, and b) x: $\ln 1/x = 2, 5, 10$ at $\ln Q/\Lambda = 5$.

plateau (without the gap) was interpreted as an evidence in favour of the Feynman conjecture about the identity of partons with fractionally charged quarks. This fact did not remove the puzzle however. Moreover, establishing QCD has only sharpened it, since QCD maintains both the partonic concept and the physics of coherence which provided the base for Gribov conclusion about the rapidity gap.

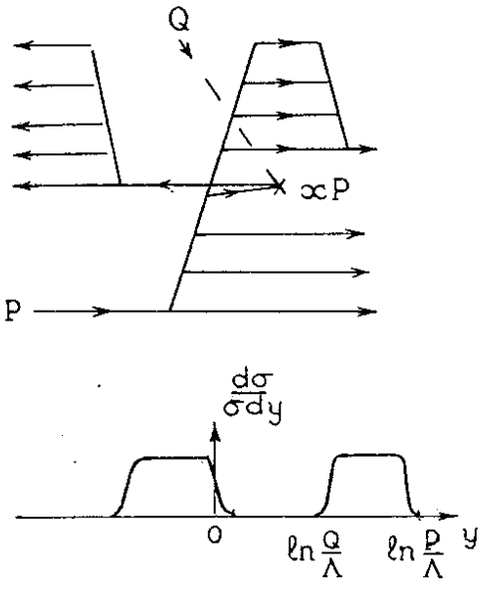

Fig.48. Development of partonic fluctuation in DIS and rapidity distribution of final particles.

As is clear now it is the coherent soft bremsstrahlung caused by the t-channel colour transfer that fills partially this gap, being insensitive to the details of the target wave function.

10. CONCLUSIONS

The perturbative approach represents a model independent scheme for the quantitative predictions of hadronic properties of hard processes. So far no experimental fact exists which endangers this endeavour. This means that the QCD parton bremsstrahlung can be thought as the main source of multiple hadroproduction in hard processes.

Looking for manifestations of the nonperturbative

dynamics one may conclude that the confinement acts as if a coloured parton was substituted promptly by a hadron at the large-distance stage of the evolution.

Finally, we list the main lessons from the above discussions.

1. It is time to critically revise the experimental approach to the analysis of the jet structure of hard processes. One should abandon any attempt to attribute each particle in the event to a certain jet. That is, the notion of isolated jet should be rejected. Purely inclusive studies of jet characteristics (calorimetric and many-particle $E^{\alpha}M^{\beta}$ correlation measurements) are probably the best way to make sharp connection between theory and experiment.

2. A theoretically substantiated scheme exists (MLLA + + LPHD) for making quantitative predictions for jet characteristics without invoking any phenomenological hadronization model. Such a scheme maintains the probabilistic picture of parton branching and could be simulated by Monte Carlo technique.

3. The hump in the energy spectra - one of the brightest consequences of the intrajet coherence - evolves with the hardness of the process in a predictable way. Valuable information on the confinement mechanism may be obtained from a comparison of spectra of different hadron species and from the studies of the fine structure of distributions varying independently the pairs of parameters: s and t in large $p_{\perp}$ processes, and x and q^2 in DIS.

4. The drag effects, reflecting the interjet coherence strongly support the LPHD concept. The collective nature of multiple hadroproduction reveals itself here via QCD wave properties of multiplicity flows. The drag phenomena should be valuable in helping to distinguish New Physics

signals from the conventional QCD background.

5. Hadroproduction studies within the perturbative approach are far from being exhausted. The MLLA - LPHD approach accomodates the attractive features of the current fragmentation models being free however from their shortcomings. Moreover the evolution of the phenomenological models seems to lead to some convergence between them. In particular the most successful schemes incorporate nowadays the concept of the well developed coherent parton cascade as the basic ingredient necessary to withstand the pressure of the experiment.

ACKNOWLEDGEMENTS

We wish to thank Ya. Azimov, V.Fadin and Al.Mueller for a nice collaboration and sharing with us the belief in power of the perturbative approach to hadron jet physics. We are indebted to S.Bethke, M.Derrick, W.Hofmann, B.Ioffe, E.Levin, L.Lipatov and T.Sjöstrand for fruitful discussions. We would like to express our heartfelt gratitude to V.Gribov for the constructive criticism and stimulating discussions.
One of us (V. Khoze) would like to thank DESY for the hospitality during his visit.

R E F E R E N C E S

1. Dokshitzer Yu.L., Dyakonov D.I. and Troyan S.I., Phys. Rep., 58, 270 (1980).
2. Mueller A.H., Phys.Rep., 73, 237 (1981).
3. Altarelli G., Phys.Rep., 81, 1 (1982).
4. Bassetto A., Ciafaloni M. and Marchesini G., Phys. Rep., 100, 201 (1983).
5. Gribov L.V., Levin E.M. and Ryskin M.G., Phys.Rep., 100, 1 (1983).
6. Mueller A.H., in: Proceedings of the 1985 Int. Symposium on Lepton and Photon Interactions at High Energies, eds. M.Konuma, K.Takahashi, Kyoto, 162 (1986).
7. Dokshitzer Yu.L., Khoze V.A. and Troyan S.I., in: Proceedings of the 6th Int.Conference on Physics in Collisions, ed. M.Derrick (World Scientific, Singapore) 365 (1987).
8. Dokshitzer Yu.L., Khoze V.A., Mueller A.H. and Troyan S.I., Columbia Preprint CU-TP-374 (1987), to be published in Rev.Mod.Phys.
9. Yamamoto H., in: Proceedings of the 1985 Int.Symposium on Lepton and Photon Interactions at High Energies, eds. M.Konuma, K.Takahashi, Kyoto, 50 (1986).
10. Mättig P., Preprint DESY 86-161 (1986); Preprint CERN-EP/88-59 (1988).
11. Dorfan J., Preprint SLAC-PUB-4287 (1987).
12. Hofmann W., Preprint LBL-23922 (Talk at the 1987 Int. Symposium on Lepton and Photon Interactions at High Energies, Hamburg, July 1987);
Hofmann W., Preprint LBL-24897, to be published in Ann.Rev.Nucl.Part.Sci.
13. Sugano K., in: Proceedings of the 6th Int.Conference on Physics in Collisions, ed. M.Derrick (World Scientific, Singapore) 365 (1987).

14. Bethke S., in: Proceedings of the XXIII Int.Conference on High Energy Physics, ed. S.C.Loken (World Scientific, Singapore) 1079 (1987).
15. Saxon D.H., Rutherford Preprint RAL-86-057 (1986).
16. Azimov Ya.I., Dokshitzer Yu.L. and Khoze V.A., in: Proceedings of the XVII Winter School of the LNPI, v.I, 162 (1982).
17. Dokshitzer Yu.L. and Troyan S.I., in: Proceedings of the XIX Winter School of the LNPI, v.I, 144 (1984); Preprint LNPI-922 (1984).
18. Azimov Ya.I., Dokshitzer Yu.L., Khoze V.A. and Troyan S.I., in: Proceedings of the XX Winter School of the LNPI, v.I, 82 (1985); Preprint LNPI-1051 (1985).
19. Dokshitzer Yu.L., Khoze V.A. and Troyan S.I., in: Proceedings of the XXII Winter School of the LNPI, v.II, 3 (1987).
20. Gribov L.V., Dokshitzer Yu.L., Khoze V.A. and Troyan S.I., in: Proceedings of the XXII Winter School of the LNPI, v.II, 61 (1987).
21. Lipatov L.N., Yad.Fiz., 20, 181 (1974).
22. Konishi K., Ukawa A. and Veneziano G., Nucl.Phys., B157 , 45 (1979).
23. Furmanski W., Petronzio R. and Pokorski S., Nucl.Phys. B155, 253 (1979);
Bassetto A., Ciafaloni M. and Marchesini G., Nucl. Phys., B163, 477 (1980).
24. Fadin V.S., Yad.Fiz., 37, 408 (1983).
25. Dokshitzer Yu.L., Fadin V.S. and Khoze V.A., Z.Phys., C15, 325 (1982).
26. Dokshitzer Yu.L., Fadin V.S. and Khoze V.A., Z.Phys., C18, 37 (1983).
27. Mueller A.H., Nucl.Phys., B228, 351 (1983).
28. Mueller A.H., Nucl.Phys., B213, 85 (1983) and Erratum quoted in Nucl.Phys., B241, 141 (1984).
29. Marchesini G.and Webber B.R.,Nucl.Phys.,B238, 1 (1984);

Webber B.R., Nucl.Phys., B238, 492 (1984).
30. Webber B.R., Ann.Rev.Nucl.Part.Sci.,36, 253 (1986); Cavendish Preprint HEP-87/4 (1987).
31. Marchesini G., Webber B.R., Cavendish Preprint HEP--87/ 8 (1987), to be published in Nucl.Phys.
32. Sjöstrand T., in: Proceedings of the XXIII Int.Conf. on High Energy Physics, ed. S.C.Loken (World Scientific, Singapore) v.II, 1157 (1987);
Sjöstrand T., Lund Preprint LU TP 87-18, to be published in Int.J.Mod.Phys.A.
33. Gottschalk T.D., Preprint Calt-68-1075 (1987).
34. Gustafson G., Phys.Lett., 178B, 453 (1985).
35. Gustafson G. and Pettersson U., Lund Preprints LU TP 87-9 and 87-19 (1987).
36. Ermolayev B.I. and Fadin V.S., JETP Lett., 33, 285 (1981).
37. Mueller A.H., Phys.Lett., 104B, 161 (1981).
38. Azimov Ya.I., Dokshitzer Yu.L. and Khoze V.A., JETP Lett., 35, 390 (1982).
39. Bassetto A., Ciafaloni M., Marchesini G. and Mueller A.H., Nucl.Phys., B207, 189 (1982).
40. Dokshitzer Yu.L., Fadin V.S. and Khoze V.A., Phys. Lett., 115B, 242 (1982).
41. Azimov Ya.I., Dokshitzer Yu.L., Khoze V.A. and Troyan S.I., Z.Phys. C27, 65 (1985).
42. Azimov Ya.I., Dokshitzer Yu.L., Khoze V.A. and Troyan S.I., Z.Phys. C31, 213 (1986).
43. Azimov Ya.I., Dokshitzer Yu.L., Khoze V.A. and Troyan S.I., Phys.Lett., 165B, 147 (1985); Yad.Fiz.43, 149 (1986).
44. Amati D. and Veneziano G., Phys.Lett.,83B, 87 (1979).
45. Andersson B., Gustafson G., Ingelman G. and Sjöstrand T., Phys.Rep., 97, 31 (1983).
46. Bigi I., Dokshitzer Yu., Khoze V., Kühn J. and Zerwas P., Phys.Lett., 181B, 157 (1986).

47. Gribov V.N., Budapest Preprint (1986).
48. Chudakov A.E., Izv.Akad.Nauk SSSR, Ser.Fiz., 19, 650 (1955).
49. Webber B.R. in: Proceedings of the XVI Int.Symposium on Multiparticle Dynamics, Kiryat Anavim, p.41 (1985).
50. Frenkel J. and Taylor J.C., Nucl.Phys.,B116,185(1976); Cornwall J.M. and Tiktopoulos G., Phys.Rev., D13,3370 (1976).
51. Ermolayev B.I., Fadin V.S. and Lipatov L.N., Yad.Fiz., 45, 817 (1987).
52. Gribov V.N., Sov.J.Nucl.Phys., 5, 280 (1967).
53. Kirschner R. and Lipatov L.N., Sov.Phys.JETP, 54 266 (1982).
54. Koba Z., Nielsen H.B. and Olesen P., Nucl.Phys., B40, 317 (1972).
55. Azimov Ya.I., Dokshitzer Yu.L. and Khoze V.A., Yad. Fiz., 37, 703 (1983).
56. Yung A.V., Yad.Fiz., 33, 1660 (1981).
57. Kalinowski J. et al., Nucl.Phys., B181, 253 (1981); Furmanski W. and Petronzio R. Z.Phys., C11, 293 (1982).
58. Mueller A.H., Nucl.Phys., B241, 141 (1984).
59. Malaza E.D. and Webber B.R., Phys.Lett.,149B, 501 (1984).
60. Derrick M. et al. (HRS Collab.), Phys.Lett., 165B, 449 (1985).
61. Dokshitzer Yu.L., Khoze V.A. and Troyan S.I., Yad. Fiz., 47, 1384 (1988).
62. Aichara H. et al. (TPC Collab.), Phys.Rev.Lett., 52, 577 (1984).
63. Dokshitzer Yu.L., Dyakonov D.I. and Troyan S.I.,Phys. Lett., 78B, 290 (1978).
64. Basham C., Brown L., Ellis S. and Love S., Phys.Rev. Lett., 41, 1585 (1978).
65. Webber B.R. and Rakow P., Nucl.Phys.,B187, 254 (1981).

66. Dokshitzer Yu.L., Khoze V.A. and Troyan S.I., Yad. Fiz., 47, 238 (1988).
67. Andersson B., Gustafson G., and Sjöstrand T., Phys. Lett., 94B, 211 (1980).
68. Dokshitzer Yu.L., Khoze V.A. and Troyan S.I., Yad. Fiz. 46, 1220 (1987).
69. Ellis R.K., Marchesini G. and Webber B.R., Nucl.Phys. B286, 643 (1987); Erratum - ibid, B294, 1180 (1987).
70. Andersson B., Bengtsson H.-U., Gustafson G. and Nilsson-Almqvist B., Lund Preprint LU TP 84-11 (1984).
71. Andersson B., Bengtsson M. and Gustafson G., Lund Preprint LU TP-82-10 (1982).
72. Eichten E., Hinchliffe I., Lane K. and Quigg C., Rev.Mod.Phys., 58 579 (1984).
73. Dokshitzer Yu.L., Khoze V.A. and Troyan S.I., Preprint LNPI-1372 (1988).
74. Ellis R.K., FERMILAB-Conf.-87/108-T (1987).
75. Gribov L.V., Dokshitzer Yu.L., Khoze V.A. and Troyan S.I., JETP Lett., 45, 405 (1987); Phys.Lett., 202B 276 (1988); JETP, 94, 12 (1988).
76. Ciafaloni M., Preprint CERN-TH 4672/87 (1987); Nucl. Phys., B296, 249 (1987).
77. Ciafaloni M., Report at the XXIII Int.Conference on High Energy Physics, Berkeley (1986).
78. Gribov V.N., in: Proceedings of the VIII Winter School of the LNPI, v. II, 5 (1973).